NASA Contractor Report 159382

(NASA-CR-159382) FULL SCALE VISUALIZATION OF THE WING TIP VORTICES GENERATED BY A TYPICAL AGRICULTURAL AIRCRAFT Final Report (Mississippi State Univ., Mississippi State.) 103 p HC A06/MF A01 CSCL 01A G3/02

N81-12019

Unclas 29433

FULL SCALE VISUALIZATION OF THE WING TIP VORTICES GENERATED BY A TYPICAL AGRICULTURAL AIRCRAFT

Ernest J. Cross, Jr., Philip D. Bridges,
Joe A. Brownlee, and W. Wayne Livingston

MISSISSIPPI STATE UNIVERSITY
Mississippi State, Mississippi 39762

NASA Grant NSG-1511
November 1980

National Aeronautics and
Space Administration

Langley Research Center
Hampton, Virginia 23665

Abstract

The trajectories of the wing tip vortices of a typical agricultural aircraft were experimentally determined by flight test. A flow visualization method, similar to the vapor screen method used in wind tunnels, was used to obtain trajectory data for a range of flight speeds, airplane configurations, and wing loadings. Detailed measurements of the spanwise surface pressure distribution were made for all test points. Further, a powered 1/8 scale model of the aircraft was designed, built, and used to obtain tip vortex trajectory data under conditions similar to that of the full scale test. The effects of light wind on the vortices were demonstrated, and the interaction of the flap vortex and the tip vortex was clearly shown in photographs and plotted trajectory data.

TABLE OF CONTENTS

DISCLAIMER

The use of brand names in this report is for the purpose of identifying the particular airplane used to conduct this research. This use does not constitute endorsement of any product, either explicitly or implicitly.

CONVERSION CONSTANTS

The primary units used in this report are U.S. Customary. The constants listed below can be used to convert to SI units.

To convert from	to	multiply by
Foot	Meter	.3048
Horsepower	WATT	745.69987
Pound/FT^2	Newton/M^2	47.88026
Slug/FT^3	Kg/M^3	515.379

LIST OF FIGURES

LIST OF FIGURES (continued)

LIST OF TABLES

LIST OF SYMBOLS

AR	Aspect Ratio
b	Wing Span
C_L	Coefficient of Lift
C_{L_α}	Slope of Lift Curve = $\frac{dC_L}{d\alpha}$
C_p	Coefficient of Pressure
c_r	Wing Root Chord
c_t	Wing Tip Chord
D	Drag
L	Lift
P_s	Local Static Pressure
$P_{\infty s}$	Free Stream Static Pressure
q	Free Stream Dynamic Pressure
S	Wing Surface Area
V	Velocity
W	Weight
α	Geometric Angle of Attack
α_i	Induced Angle of Attack
Γ	Circulation
ρ	Mass Density
θ	Pitch Angle

Subscripts

A	Aircraft
M	Model
S	Stall

I. INTRODUCTION

During the past decade, the use of aircraft for the application of a wide variety of chemicals to crop and forest lands has increased to significant proportions. The agricultural aircraft has become an essential element for the high level of farm productivity realized in the United States. The world-wide demand for food has in turn provided the U.S. with a market of such magnitude that this productivity can become one of our most valuable resources. Thus, the agplane and its associated technology have taken on a measurable national level of importance. This has led to a renewed interest by the government in advancing the state of this technology through the establishment of a research program at NASA Langley Research Center (NASA-LRC).

There are many technical problems associated with agricultural aviation that influence productivity and effectiveness and involve important environmental factors. These problems can be categorized as those which pertain separately to the aircraft, the dispensing equipment, and the integration of this and other special equipment with the aircraft. The strong technology base needed for the next generation of agricultural aircraft will require an intensive coordinated theoretical and experimental program. Heavy emphasis must be put on an experimental program because of the extremely complicated nature of the physical processes involved. The interaction that occurs between the aircraft, dispersal equipment and dispersant, and the performance influence that each has on the others must be investigated as a total system.

Such a program is presently underway at NASA-LRC and, in part, utilizes small scale model testing in the Vortex Research Facility (1). Flow visualization and, subsequently, laser Doppler velocimeter studies of the model

aircraft wake constitute the experimental method. The use of small scale testing for investigations of this type is essential because of the large amount of configuration-dependent information which can be obtained for relatively low cost. However, the validity of this information rests upon the degree to which correlation can be developed with full scale data.

The Raspet Flight Research Laboratory at Mississippi State University (MSU) has developed a full scale flow visualization method with which such a correlation investigation can be performed (2). The visual data is in a format similar to that being used at the Vortex Research Facility and a direct comparison can be made on this basis.

This report presents the results of an investigation of the wing tip vortex trajectory of a full scale Cessna A188 Agwagon and a 1/8 scale model of the Agwagon. Also, effect of the ground plane and surface winds on the behavior of the trailing vortices near the ground was briefly investigated. The scope of the program was limited to acquiring the test data and did not allow a significant amount of analysis to be performed. The discussion presented in this report is intended to provide sufficient information to define the pertinent test conditions and to provide those observations that were noted during the performance of the test program and the subsequent efforts to present the test data in its most representative form.

II. FULL SCALE FLIGHT TESTS

Wing span-wise pressure distributions and wing tip vortex trajectories were experimentally determined by full scale flight test of the laboratory Agwagon. The test aircraft is shown in Figure 1. Wing tip configuration and the strut-wing fairing arrangement were varied to provide three combinations which were tested in a range of flight conditions to simulate typical agchemical delivery conditions. Aircraft geometry was essentially standard with only minor changes to accommodate special systems and instrumentation for purposes of this test sequence. The following values were used, as required, in the data reduction:

S = 202 square feet

b = 40.71 feet

c_r = 5.33 feet

c_t = 3.71 feet

Aspect Ratio = 8.2

The wing airfoil section used was a NACA 2412 from the wing root to eighteen inches from the tip, with a NACA 0009 from there to the tip. Wing incidence was +1.5° at the root and -1.5° at the tip; however, there was zero twist in the constant chord segment of the wing. Wing dihedral was 6°. A Teledyne-Continental IO-520-D fuel injection engine rated at 300 HP drove an 86-inch constant speed 2-blade propeller. The aircraft chemical hopper was used to vary airplane gross weight by addition of approximately 1400 lbs of water ballast. Two takeoff gross weights were flown--2600 lbs and 4000 lbs.

Test Equipment and Instrumentation

The aircraft was equipped with self-aligning sensor probes mounted on a rigid flight test boom (see Figure 2). The sensor probes were for measuring static and total pressures, and they were calibrated with a trailing cone static source. The position error at the boom was considered negligible for flight conditions out of ground effect and within the test envelope. A spot calibration of the airplane pitot-static system was conducted at test altitudes within the ground effect region using a police doppler-radar speed unit. The radar unit had a built-in calibration that provided accuracy within the resolution of the aircraft airspeed indicator. Position error in the test pitot-static system within ground effect was also considered negligible over the speed range of testing.

Wing span-wise pressure distribution was measured for several configurations. Brass tubing, .035 inch i.d., was installed internally and mounted flush and normal to the wing surface at 11 span-wise stations along the quarter-chord line. Pressure lines were routed from the surface taps to a scannivalve and pressure transducer which was used to measure the pressure values. Each pressure tap was manifolded to four positions on the scannivalve such that local pressures were sampled every 2.5 seconds on the scannivalve cycle period of 10 seconds. The transducer output was recorded on magnetic tape with a Lockheed Electronics Model 417, 7-track recorder. Recorded values were digitized and averages calculated as part of the automatic data reduction process.

The test aircraft was equipped with a dust system which ejected controlled amounts of dust from the wing tips for use in the vortex visualization tests. The dust system consisted of a high-pressure nitrogen bottle which supplied ejection pressure through a pressure regulator and a dust

reservoir, a 2100-cubic inch, low-pressure, aircraft oxygen bottle. The dust was then routed through a 0.5-inch pressure line to a hand-operated control valve taken from a dry-chemical fire extinguisher which was mounted in the cockpit. After passing through the valve, the dust was routed to the wing tips through a Y-fitting and a 0.75-inch steel tubing mounted inside the wings. The outlet in each wing tip-fairing which is shown in Figure 3 was formed by extending the tubing about one inch out of the lower surface of the fairing. Several arrangements of exit position and nozzle geometry were tried, but no significant change in the dust pattern was noted. The best vortex visualization was obtained with a nitrogen pressure of 1500 psig at the regulator and approximately 200 psig in the dust reservoir. Ten to fifteen test runs were obtained with this procedure using an S-type bottle initially pressurized to 2200 psig, before the nitrogen bottle was depleted. The dust was pink in color and was identified as a "dilvent blend" used as a filler in certain chemicals used in aerial application work. Other types of dust were not investigated as the dust that was used was available and provided satisfactory results. Three aircraft configurations were investigated in which the wing-strut fairing and wing-tip were modified. Two types of wing-strut fairings were investigated. Each type was molded fiberglass and provided by Cessna Aircraft. The first type (Type I), shown in Figure 4, was an early design and is no longer in production. Type II, Figure 5, incorporates a full chord wing fence and is the current production fairing. Type I wing-tip, Figure 6, is the standard Cessna Ag-series aircraft configuration, and Type II, Figure 7, is the optional Cessna-type drooped tip. Table 1 identifies each of the combinations evaluated during these flight tests.

Table 1

Agwagon Wing Tip and Strut Fairing Configurations

Configuration	1	2	3
Wing Tips	I	II	II
Strut Fairing	I	I	II

These configuration numbers will be used subsequently to identify tip-fairing arrangements in connection with the discussion of results.

Test Methods and Data

Span-wise Pressure Distribution

The strength of the rolled-up trailing vortex is determined not only by the coefficient of lift but also by the span loading of the aircraft (4). For example, on conventional aircraft, the span loading is a maximum at the wing root and decreases to zero at the tip. Since the strength of the trailing vortex is approximately equal to the circulation at the wing root, the vortex strength is higher than if the wing were uniformly loaded.

The spanwise pressure distribution of the Agwagon was determined for various flight conditions and weights. A matrix of the test conditions (Table 2) lists values of test variables--airspeed, flap setting, gross weight, ground effect, and aircraft configuration.

All of the airspeed, flap, gross weight, and aircraft configuration points were flown out of ground effect. A series of test points in ground effect were flown with the aircraft in the standard configuration, but results showed the span-wise pressure distribution was not affected by the ground plane. Therefore, flights in ground effect were discontinued and

Table 2

Flight Test Matrix--Full Scale

Configuration	Airspeed (mph)	Flaps	GWT	Ground Effect
Standard (1)	80	0°	2600 lbs	Out
Drooped Tips (2)	100	20°	4000 lbs	
Wing Cuffs and (3) Drooped Tips	120			

all others were conducted at relatively high altitude.

To obtain the pressure distribution, the left wing was fitted with eleven flush pressure taps along the quarter chord of the airfoil. A ng planview showing the location of these surface orifices is illustrated in Figure 8. The eleven taps and the free stream static pressure were connected to a 1/2 psi scannivalve box located in the baggage compartment of the Agwagon. The scannivalve cycled through these twelve pressures at 5 readings per second and measured the pressure difference between the surface orifice and the free stream total pressure. This ΔP was converted to an electrical signal and stored on magnetic tape. The 5 Hz sampling continued for one minute at each test point. After the flight the data on the magnetic tape was processed through an analog-to-digital converter and minicomputer and stored on a 9-track digital tape. Converted data was processed on a UNIVAC 1108 to calculate the average coefficient of pressure for each wing tap. The average airspeed over the one-minute run was also computed. The results for each test point were plotted to obtain a span-wise pressure distribution for the wing. A schematic of this process is shown in Figure 9.

The data was plotted as coefficients of pressure vs. span-wise distance along the wing line of quarter chords in inches from the aircraft center-line. The coefficient of pressure was defined as:

$$C_p = \frac{P_s - P_{\infty s}}{q}$$

where P_s is the local, measured static pressure, $P_{\infty s}$ is the free stream static pressure, and q is the free stream dynamic pressure. Since the scannivalve measured the difference between local static and free stream total pressure, it was possible to define C_p as:

$$C_p = 1 + \frac{\Delta P}{q}$$

where ΔP is the pressure difference across the scannivalve.

The results of the flight tests are shown in Figures 10-21. Three air-speeds were plotted on each graph to show the effects of increasing dynamic pressure. All of the plots show a roughly elliptical lift distribution with a deviation at the midpoint for the wings with the early type cuff installed and an increase in lift near the tip for all the configurations except at 4000 lbs. gross weight with standard wing tips. These variations will be discussed in detail later in the report.

Full scale flow visualization was possible by means of an adaptation of the well-known wind tunnel vapor screen flow visualization method. The experimental arrangement for this purpose is shown schematically in Figure 22. The camera was located slightly to the side of the measurement station centerline which was the runway centerline. A Nikon 35mm single lens reflex camera was used with a 135mm lens for photographing the vortex trajectories. Black and white photos were obtained using Tri-X film pushed to an equivalent ASA 1000, exposed at 1/8 second shutter speed and f2.8. Photo sequences were taken at 1 second intervals for the first 10-12 seconds after

the vortices formed. Flights were conducted at night and the vortices were made visible by illuminating entrained dust particles in the wing wake by a 'light-plane' created by a pair of light boxes located on either side of the runway. The result is a time varying section view of the wake which produces a highly visible display of the tip vortices. Dimensional reference poles, or grid poles, were placed on both sides of the runway. Reflective panels were attached to these poles and provided reference points for a large measurement grid when illuminated by light sources. This measurement grid was available on all photographic records and established a network within which resulting vortex motion was referenced. A binary clock light panel was used to provide a time reference on the data photographs. Also, a recording wind station, shown in Figure 23, was located in the area of the measurement plane to provide wind velocity data. Altitude guidance to the pilot was provided by three poles erected beyond the light screen. Each pole had a single light mounted at the desired altitude. By keeping the three lights aligned as he flew down the runway, the pilot was able to maintain the desired altitude.

An example of the vortex trajectories is shown in Figure 24. The reduced data from the trajectories is shown in Figures 25 through 39. The data represents the position of the vortices as if the airplane were approaching the observer. The position of the left and right vortices are plotted as non-dimensional distances above the ground plane and lateral distances from the aircraft longitudinal axis. Distances were non-dimensionalized with the wing semispan. The time tick with each vortex point represented the downstream distance from the generating aircraft in wing semispans. The wind direction was referenced to the direction of flight of the aircraft.

III. ONE-EIGHTH SCALE MODEL FLIGHT TESTS

A one-eighth scale model was constructed for purposes of comparing small scale and full scale tip vortex trajectory data. The model was designed with the use of standard Cessna aircraft preliminary design drawings which were the best available design information. Conventional model airplane construction methods and materials and off-the-shelf engine and hardware were used to keep costs and development problems at low levels. The original intent was to fly the model as a 4-wire U-control model utilizing essentially the same experimental methods as the full scale airplane. A combination of model weight, stall speed, and controllability made night flying impractical and this was abandoned as a useful experimental method. Subsequently, the model was mounted to a large boom-strut arrangement on an automobile chassis, and the small scale data was obtained by driving the car at desired speeds similar to the powered carriage used in the NASA Langley Vortex Research Facility.

Test Equipment and Instrumentation

Three view and section geometry of the Agwagon were carefully scaled to 1/8 and the model constructed to these dimensions in essentially exact scale (Figure 40). The model was constructed of readily available model materials to provide sufficient strength and light weight for use in tests at Mississippi State University and possible use in the NASA Langley Vortex Test Facility. The fuselage construction was of built-up balsa stringers and formers with heavy balsa plank skins. All joints were cemented and the interior painted with a high-strength epoxy cement. The top of the fuselage was removable for easy access. The interior of the fuselage with installed engine is shown in Figure 41. This fuselage design includes provision for

easy conversion to the Vortex Test Facility support system and test practices at that facility. There are machined aluminum blocks which bolt to the fuselage and provide an adaptation to the facility sting support and internal 6-component force balance, and replacement of the piston engine with a Tech Development Model 845A pneumatic motor. These are shown in Figure 42.

The wing construction utilized standard model airplane construction methods but because of geometry complications it was made in several sections. The basic materials were high density styrofoam core and balsa or .064 inch plywood skin with hardwood leading and trailing edges. The styrofoam core material was cut with a hot wire and a template jig to provide good scale dimensional fidelity. This construction technique and a typical wing section are shown in Figure 43. Wing flaps are hinged to provide Fowler action in addition to deflection to 30°. The hinges were machined from drawings which were produced by photographically reducing full scale drawings to model scale. The flaps are ground adjustable and pinned to provide 0° and 20° deflection. Figure 44 shows the flaps extended 20°.

Test Methods and Data

Flight speeds were computed for the model which would produce the same lift coefficient as the full scale Agwagon. The lift coefficient is defined as:

$$C_L = \frac{2W_A}{\rho V_A^2 S_A} = \frac{2W_m}{\rho V_M^2 S_M}$$

Scale flight speeds can be calculated which will produce identical lift coefficients by solving for V_M. Thus:

$$V_M = 8V_A\left(\frac{W_M}{W_A}\right)^{1/2}$$

where the subscripts M and A indicate model and full scale airplane values, respectively. A table of values can be computed for V_M which corresponds to the full scale airplane test conditions for a specified airplane weight and flight speed. Then, for a model weight W_M = 10 lbs, and airplane gross weight W_A = 4000 lbs, the following tabulated values for V_M and C_L correspond to each of the full scale flight speeds.

Table 3

Equivalent Scale Model Test Speeds

V_A (mph)	C_L	V_M (mph)
80	1.21	30
100	0.77	37.5
120	0.54	45

It was not practical to fly the model at night as a 4-wire control line model as designed because of very poor handling qualities at low speeds which caused extremely difficult control problems. Further, the model stall speed was relatively high at V_{MS} = 28 mph due in part to a relatively high wing loading of 3.14 LB/FT^2 and it was not possible to maintain the lower scale test speeds. Therefore, the model flight test program was abandoned and an alternative test method was developed which would permit testing at

conditions nearly the same as those listed in Table 3.

The model was supported on a 4 ft vertical strut which was attached to a 20 ft tubular-steel truss boom which extended horizontally from the front of the ground test vehicle. This arrangement is shown in Figure 45. The support strut included a mechanism for manually changing the model pitch angle. The boom strut combination was such that the model wing tip was approximately 10 ft above the ground and nearly 20 ft in front of the ground test vehicle chassis. The test vehicle is a 1956 Buick chassis, engine, and drive-train which provides the propulsive power necessary to sustain the desired test speeds. This test vehicle is capable of stable test speeds up to 70 mph. The apparatus necessary to eject chalk dust in controlled amounts at the wing tips, similar to the full scale system, was mounted on the chassis close to the driver's position for easy control. This included a S-size bottle of dry nitrogen, chalk dust reservoir, plumbing, and the control valve. All of the major components were removed from the Agwagon for use in this series of tests. Dust was routed through the model fuselage and ducts interior to the wings and ejected from nozzles near each wing tip on the lower surface of the wing.

The ground equipment for the model tests is shown in Figure 46. The equipment configuration was similar to the full scale system, but some changes were necessary to account for scale effect. Only one light box was needed to adequately illuminate both vortices since they were initially close together and dissipated relatively quickly. The binary coded digital clock was modified to run in 0.1 second intervals, and a motion picture camera running at 8 frames/second was used to photograph the vortices. Also, the dimensional grid poles were marked in the 12-inch increments to provide better resolution in tracking the vortices.

It was essentially impossible to test under "no wind" conditions. Winds of 3 ft/sec were found to have a significant effect on the trajectories of the tip vortices and natural conditions are never completely still where variations in surface thermal conditions exist. Small differences in the cooling rate of varying surface types result in light and variable thermally induced convection which is apparent as a very light wind. All model tests were conducted at late night when the conditions were "apparently calm." However, it is obvious from observations of the data that significant wind did exist for most of the tests. The wind velocity in each case was less than the minimum wind speed which could be measured with available equipment. Thus, no wind corrections are possible for the model data.

Table 4 is a listing of the model test conditions. The model configuration was identical to full scale configuration 1, listed in Table 1. No attempt was made to fabricate and install drooped tips or wing cuffs as was done on the full scale aircraft.

Table 4
Flight Test Matrix--1/8 Scale

V_M	θ	C_L	Flaps
30	12°	1.21	0°
37.5	8°	0.77	20°
45	4°	0.54	

The lift coefficients which are listed are only approximate since there is some uncertainty in the calculation of wing angle of attack and the slope of the lift curve, C_{L_α}. The pitch angle, θ, was measured from the fuselage

reference line. Each of the three speeds listed in the table was "flown" for each of the pitch angles, i.e., 4°, 8°, and 12°. This provided a good range of lift conditions which bracketed the full scale flight tests and can be easily duplicated in the Vortex Test Facility.

The model developed well-defined tip vortices which were readily discernible using the test apparatus as described. A sequence of photographs showing a typical time history of the model vortices is provided in Figure 47. The trajectories data are shown in Figures 48 through 65 plotted in the same way as the full scale data. The horizontal axis is the distance from the aircraft centerline in wing semispans and the vertical axis is the height above ground in semispans. Time ticks on the trajectories indicate the location of paired vortices downstream from the aircraft in semispans.

Discussion of Results

Influence on Ground Effect

The effect of the ground plane on aircraft drag is well known. As an aircraft approaches the ground, the induced drag is decreased due to a reduction in the downwash of the wing. The reduction in downwash is due to the interference of the ground plane with the flow field induced by the trailing vortex sheet. It seemed, initially, that since the downwash was significantly changing, the lift distribution along the wing might also be altered and this could be demonstrated. However, for an airplane in free flight the span-wise pressure distribution is not changed by ground effect sufficiently to measure with standard instrumentation.

Consider a finite wing in straight and level flight out of ground effect (Figure 66). Because of the downwash velocity, w, the free stream velocity, V_∞, is changed so that the wing sees not V_∞ but V. Thus the lift vector $\bar{L}$ is inclined rearward by an amount equal to the induced angle

of attack α_i. Since the wing must support the aircraft weight, $\overline{W}$, with the vertical component of the lift, the aircraft is flown at some angle of attack, α, so that level flight can be maintained. Typical values of these numbers for the Agwagon will illustrate how the lift vector changes as the aircraft goes in and out of ground effect. Assume the aircraft weighs 4000 lbs, has an elliptical lift distribution along the wing, and is flying at 80 mph at standard sea-level conditions. These represent a worst-case condition for induced drag (low velocity, high weight). The aircraft coefficient of lift for this condition is $C_L = 1.21$. The induced angle of attack at the aircraft centerline can be calculated (3) as:

$$\alpha_i = -\frac{C_L}{\pi AR}$$

or $$\alpha_i = -\frac{1.21}{\pi \times 8.20} = .047\text{rad} = 2.69°$$

Since the vertical component of lift is 4000 lbs, the magnitude of the lift vector is:

$$L = \frac{4000}{\cos 2.69°} = 4004.4 \text{ lbs}$$

and the induced drag is:

$$D_i = L \sin \alpha_i = 187.7 \text{ lbs}$$

Consider the ideal case in ground effect where the downwash goes to zero. Then induced drag is zero and the lift vector, L, is equal to the weight, W. Since W = 4000 lbs, the lift vector is 4000 lbs. Note that this is only 4.4 lbs of lift less than the worst case for out-of-ground effect. Thus, the wing pressure distribution has only changed approximately 1/10 of

1%. This change was too small to see on the instrumentation. The major influence of ground plane proximity is to rotate the lift vector forward by an amount equal to the induced angle of attack, α_i, and the pressure distribution changes are negligible.

Influence of Strut Fairing

Plots of the experimental pressure distributions for configurations 1 and 2 show a large drop in the magnitude of C_p at the point where the wing strut is faired into the wing. This corresponds to a significant decrease in lift and would result in a larger angle of attack required to maintain level flight and thus would result in a stronger trailing vortex. The strut fairing was tufted (Figure 67) to observe the airflow around the strut at various flight conditions in an effort to determine the characteristics of the flow. It was found that on the fairing and fanning out behind the fairing there was a region of very turbulent flow. Outside this area the flow was attached and well-behaved. As the aircraft approached stall, the region behind the strut separated fully well before the rest of the wing. Obviously, the fairing was not smoothing the airflow around the strut-wing junction effectively. Configuration 3 had a large wing cuff and fence combination installed which improved the lift distribution significantly. These wing cuffs are now standard equipment on all Cessna Agwagons. They were developed to improve the stall characteristics of the Agwagon, but they also smooth the lift distribution and ultimately reduce the strength of the trailing wing-tip vortex.

Influence of Tip Configurations

The span-wise pressure distribution near the tip varied depending upon the aircraft configuration and weight. The pressure distribution generated

by the standard wing tip configuration with a 4000 lb gross weight decreased smoothly and to zero at the tip. This is a typical pressure distribution and is nearly elliptical. However, at light weights (2600 lbs), the pressure at the two points furthest outboard (Figures 10-11) were nearly equal at 80 mph, and at higher flight speeds the pressure coefficient at the tip was higher than the one inboard. Since the airfoil section changes from NACA 2412 to NACA 0009 between these two points, it was initially thought that this might be the cause of the rise in lift near the tip. However, an examination of the twist distribution and the lift curve slopes showed that the lift should be decreasing instead of increasing. The same phenomena was shown more clearly when the drooped tips were added. At all flight test points, the lift distribution goes down, up, and back down at the tip. The decrease in lift inboard of the tip was even more pronounced with the large wing cuffs installed. In each configuration, an increase in the gross weight produced a corresponding increase in the deviation in the C_p curve.

Unfortunately, there is no clear explanation for this behavior; however, there are three possible reasons why the lift could decrease near the tip. These are decreased dynamic pressure, decreased angle of attack, and instrument error. A decreased local dynamic pressure would normally be associated with a flow separation forward of the measurement point. Therefore, the wing tip area was tufted and flight tested at the different airspeeds and flap settings. There was no evidence of turbulence or separation along the tip section. Thus decreased dynamic pressure is probably not a factor.

The second possible reason is an effective decrease in local angle of attack at the section involved. Examination of the geometric and aerodynamic twist of the wing, however, shows that this is unlikely. There is increased aerodynamic washout when the section changes from 2412 to 0009 and

the last 18 inches of the tip has a significant (1.5°) geometric washout in addition to the section change. This would cause a decrease in lift along the tip section. Further, there is no evidence of any strong local downwash that would alter the angle of attack of the section inboard of the tip.

Instrumentation error or problems related to instrumentation were considered the most probable source of the apparent deviation and thus were examined closely. A decrease in the lift (i.e., higher pressure than expected) is usually caused by a leak in the plumbing from the static port to the scannivalve. All of the tubes were vacuum checked after installation by an aircraft static pressure tester and were found to be secure. After the flight tests showed the anamoly near the tip, the pressure taps were rechecked and still showed no leaks. It was possible that if there were a leak present, it may have been fixed while the tubes were being checked to insure proper connections. Therefore, the flight test sequence with a gross weight of 2600 lbs in the standard configuration was repeated to check the span-wise pressure distribution of the wing. As before, the pressure distribution at the tip showed the same characteristic rise. Apparently, a line leak was not the cause. Scannivalve errors were eliminated as a possible cause by switching leads such that the pressure sensed at station 9 was measured on a different set of four scannivalve positions and no change in indicated pressure was noted. Another argument against the possibility of a leak was the consistent behavior. Experience with the static pressure system has shown that in the presence of a system leak the static pressure as seen by the scannivalve was relatively insensitive to dynamic changes. However, in this case, the static pressure near the tip varied in proportion to the rest of the wing, depending upon the flight configuration and dynamic

pressure. The consistency of the measured pressure seemed to say "no leak."

Thus, the tip region pressure distribution as measured seems to be valid, but no acceptable physical explanation for the unusual distribution has been developed.

Wind Effects on Vortex Trajectories

The initial flight tests were conducted at wing tip heights of 5, 10, and 20 feet above the ground for the purpose of observing the behavior of the wing tip vortices in ground effect. A special effort was made to fly only during zero wind conditions since no method was available to correct the tip vortex trajectory data for wind effects. It was found, however, that even light winds of 1 mph or less had large effects on the motion of the vortices. Light and variable winds caused by local variations in surface cooling rates and the convective motion of the air induced by these temperature gradients caused significant variations in the trajectory maps. The available wind velocity instrumentation system simply was not sufficiently sensitive to measure wind speed and direction within the sensitivity range required by the nature of the experiment. This very sensitive behavior of the tip vortices to wind effects was not anticipated.

An inviscid analytical model consisting of two vortices descending in ground effect was used to investigate the sensitivity of the trajectories to a crosswind (Figure 68). The vortices descend until they approach the ground plane, then level off and separate depending upon the velocity of the crosswind. In a no wind condition ($V_\infty = 0$), the trajectories describe a hyperbola. As the vortices separate and approach a level altitude above the ground, it can be shown (4) that the horizontal velocity approaches a value of:

$$\dot{y} = V_\infty \pm \frac{\Gamma}{4\pi z}$$

where $\dot{y}$ is the horizontal velocity, V_∞ is the velocity of the crosswind, Γ is the magnitude of the strength of the vortex, and z is the altitude of the vortex above the ground plane. The value of Γ for an arbitrary planform can be estimated by the procedures in reference 5. For the special case of an elliptic lift distribution, the strength of the trailing vortex is:

$$\Gamma = \frac{4L}{\pi \rho V b}$$

where L is the lift of the aircraft, ρ is the mass density of the air, V is the free stream velocity of the aircraft, and b is the wingspan. For the flight conditions of the Agwagon, assuming no crosswind and an average height of 10 feet for the vortices, the velocities of the wing tip vortices were found to be as listed in Table 5.

Table 5

Lateral Velocity of Tip Vortices in Ground Effect

Gross WT	V (mph)	Γ (ft^2/sec)	$\dot{y}$ (ft/sec)
2600	80	296.6	2.36
	100	237.3	1.89
	120	197.7	1.57
4000	80	456.3	3.63
	100	365.1	2.91
	120	304.2	2.42

Since $\dot{y}$ represents the maximum horizontal velocity in the no-wind case, it is apparent that any wind at all will substantially change the vortex trajectory. For example a crosswind of 1 ft/sec would change the velocity of

the strongest vortex (80 mph, 4000 lbs) by 28%. Note that this is for the case where the vortex has leveled off. As the vortex descends vertically, the wind would have a much greater effect on its horizontal component of velocity.

An analytical model which would account for the viscous interaction of the vortex and surface boundary layer could possibly be used to correct the observed vortex trajectories for wind effects so that "zero-wind" data could be calculated. This is a difficult calculation and impractical for the purposes of this study. Thus, it was decided to conduct all of the data flights at 20 ft to minimize ground effects and allow a simpler calculation of wind effects. The tip vortices were tracked for the first 10-15 seconds and it was expected that the wind velocity integrated over the test time would allow a simple wind correction. However, this method was unsatisfactory. The anemometer system had a start threshold of 1.1 ft/sec which is well above a "significant" wind, and wind variations in direction and speed which occurred during the 10-15 sec test period were not measurable. Thus, it was not possible to correct trajectory data for the effects of crosswind. Here, crosswind is taken to mean the lateral component of the wind velocity vector.

A similar and equally difficult problem was caused by the influence of the headwind or tailwind component of the prevailing wind. Since the experimental method consisted of photographing time sequences of the airplane wake cross-section and relating the tip vortex location to the generating aircraft flight speed, a wind component along the flight path will produce an apparent change in the observed vortex trajectory. No satisfactory method was developed to correct for this wind effect either.

The influence of the wind on the behavior of the tip vortices is very

significant and unpredictable for even very light winds (less than 1 ft/sec). Consequently, the drift of agro-chemicals entrained in the tip vortices is also affected in a very significant way and would be apparent on irregular surface distribution of the chemicals.

Effects of Flaps on Wing-Tip Vortices

The wing-tip vortices are affected in two ways by deployment of wing flaps. The strength of the tip vortex is altered (decreased) and the tip vortex trajectory is changed due to the influence of the shed trailing vortex of the flap. The effective angle of attack of the flapped section of a wing is increased as the flaps are extended and the wing section lift is correspondingly increased. To maintain level flight, the overall lift of the wing must be maintained constant at its original value. This is done by decreasing the pitch angle of the airplane at a given airspeed until equilibrium is achieved. The lower pitch angle of the airplane results in a lower angle of attack for the unflapped outboard section of the wing, thus decreasing the strength of the wing-tip vortex while increasing the strength of the flap vortex.

The wing flaps, however, now generate their own vortex system. Each flap segment has two trailing vortices associated with it, one on the inboard side and one on the outboard side (Figure 69). The outboard vortex has a significant effect on the wing-tip trailing vortex. As the trailing vortices are shed, the tip vortex and outboard flap vortex will move laterally outward due to the influence of the ground plane. The inboard flap vortex moves inward and is destroyed by the propeller wake and/or the opposite inboard trailing flap vortex. However, the outboard flap vortex and tip vortex will also mutually influence each other as seen in Figure 69. The mutual interference which occurs between the flap-induced vortex and

the wing-tip vortex is such that initially the flap vortex moves rapidly outward and beneath the tip vortex forcing the tip vortex upward. As the flap vortex moves outboard of the wing-tip vortex, the induced velocities cause the wing-tip vortex to move downward and the flap vortex upward in a generally circular motion. In this manner, they rotate about one another in a windup until they finally merge in a single trailing vortex. This is shown in the sequence of photographs in Figure 70. Airplane gross weight was 4000 lbs for this test point, airspeed was 100 mph, and the wing flaps were positioned at 20°. The wing-tip height was 23 ft above the runway. At time t = 0, the Agwagon had just passed through the light plane. The white dust marks the tip vortices. At t = 2 seconds, the core of the tip vortex is visible in each dust cloud, but now the flap vortex is also outlined as it moves beneath the tip vortex and begins to entrain chalk dust. At t = 5 seconds, the right flap vortex is now clearly visible. It is moving up and to the left, while the wing tip vortex is moving down and to the right starting the windup motion. In the photo labeled t = 7 seconds, the vortex system for the right wing is rotating about one another as they begin to merge into one trailing vortex. The left wing vortex system is also doing this, but is not shown as clearly as the right one. At t = 9 seconds, there is one well-defined vortex trailing the right wing with a vague outline of a weak vortex above it. By t = 17 seconds, the vortex roll-up is complete and there is only one trailing vortex.

V. CONCLUDING REMARKS

The sensitivity of the tip vortices to drift in light winds was demonstrated by both theoretical analysis and flight test data. From a practical standpoint this is important to the aerial applicator, since even on a supposedly calm day there could be significant vortex drift. Because the vortices can contain a high concentration of the chemicals being sprayed, this drifting may result in uneven application on the desired field or unintentional drift to a neighboring field. It also means that future flight testing on the interaction of tip vortices and agri-chemicals must have provisions for accurate measurement of local air currents.

No direct correlation of full scale and 1/8 scale data was done. However, certain qualitative observations were possible for the vortex behavior. The tip vortices formed symmetrically above the wing and slightly inboard of the wing tip. As they descended out of ground effect, they tended to drift toward the aircraft centerline. This may be due to the propeller/fuselage wake. At approximately 0.75 semispans, the separation distance started to increase as the vortices entered ground effect. They then moved laterally apart and often rose again to a higher altitude. The duration of the vortices ranged from a few seconds to over a minute, depending upon the aircraft configuration and atmospheric conditions.

At the completion of the tests the model was sent to the NASA Vortex Test Facility at Langley, Virginia. By duplicating the model flight test conditions, it should be possible to determine the extent of wall effect in the Facility tunnel. And with a careful analysis of the full scale data with the model test data, it may be possible to determine the scale effects on the model data.

REFERENCES

1. Frank L. Jordan, Jr., H. Clyde McLemore, and Michael B. Bragg, "Status of Aerial Applications Research in the Langley Vortex Research Facility and the Langley Full Scale Wind Tunnel," NASA Technical Memorandum 78760, August 1978.

2. Lawrence J. Mertaugh and Rustam B. Damania, "An Investigation of the Trailing Vorticity Behind a STOL Aircraft," AFFDL-TR-73-138, December 1973.

3. Arnold M. Kuethe and C. Y. Chow, "Foundations of Aerodynamics," 3rd edition, John Wiley & Sons, 1976.

4. Hallock, J. N. and W. R. Eberle, "Aircraft Wake Vortices, A State of the Art Review of U.S. R&D Program," FAA-RD-77-23, February 1977.

5. Razak, Kenneth, "Computation of Spanwise Distribution of Circulation and Lift Coefficient for Flapped Wings of Arbitrary Planform," NASA CR159329, August 1980.

Figure 1. Cessna A188 Agwagon

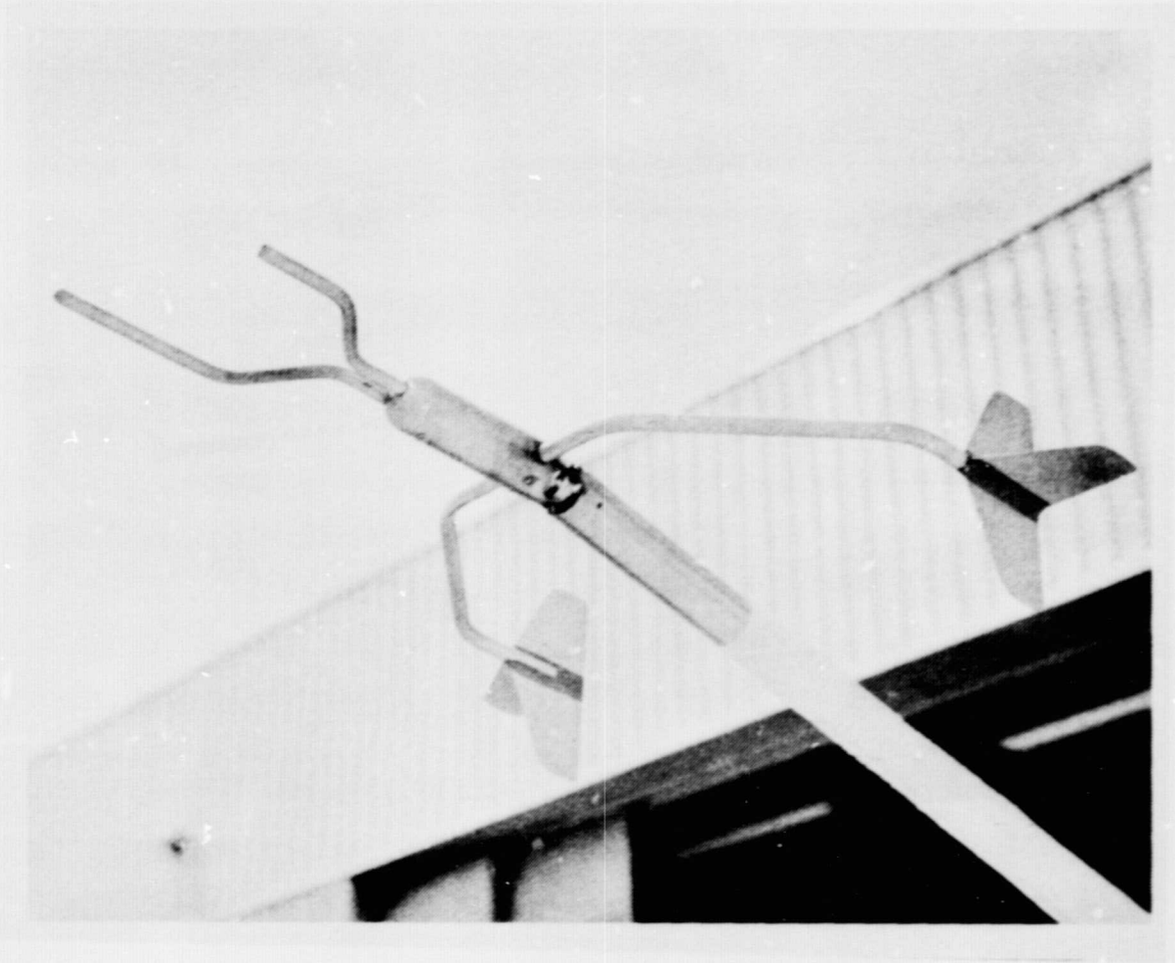

Figure 2. Flight Test Boom

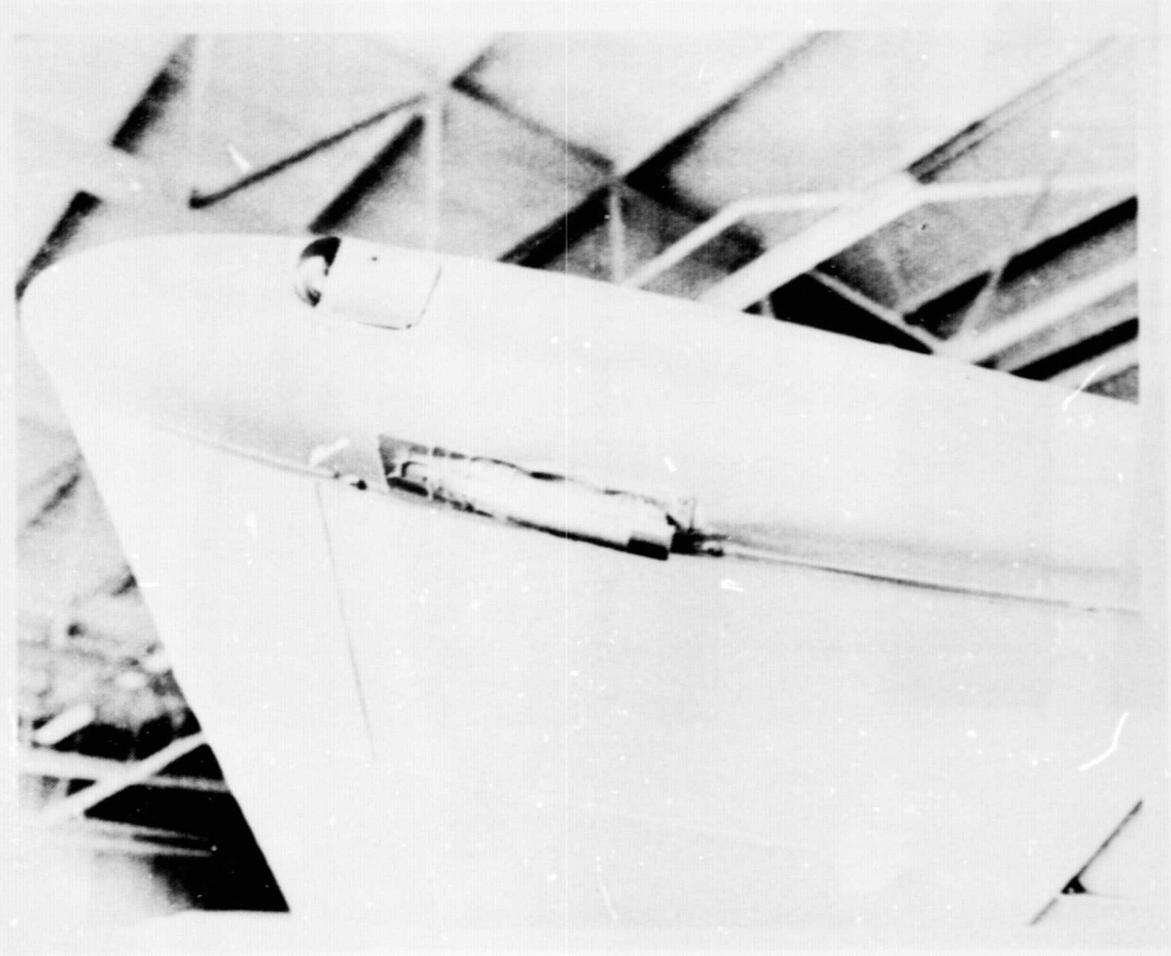

Figure 3. Wing Tip Dust Nozzle

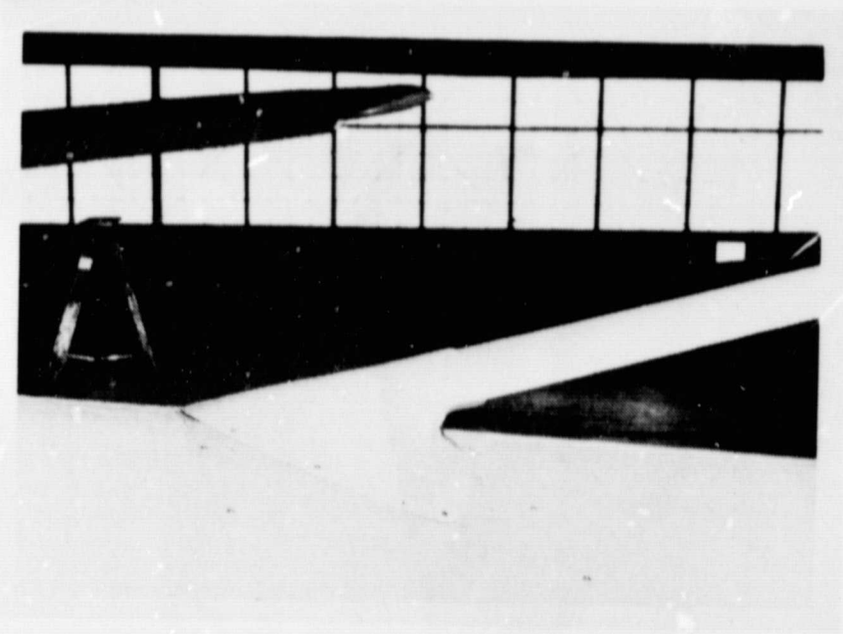

Figure 4. Type I Wing Strut Fairing

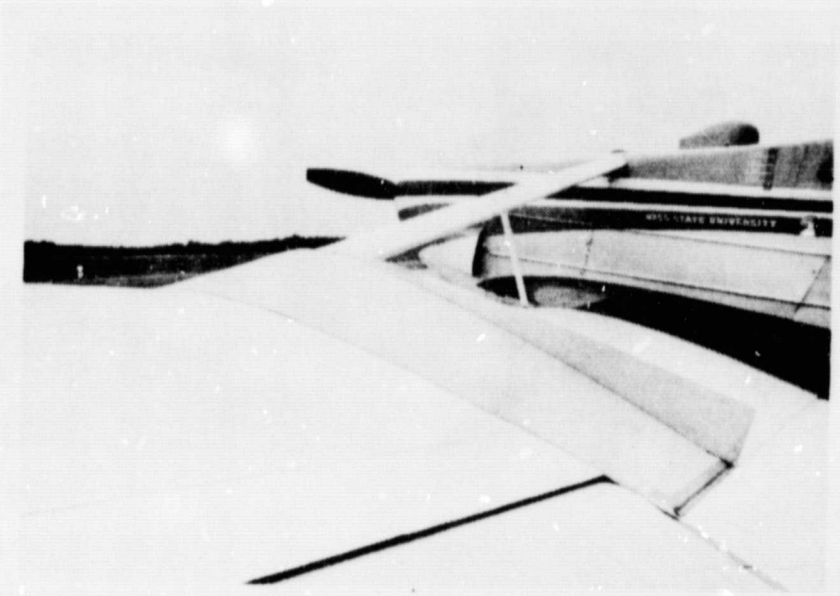

Figure 5. Type II Wing Strut Fairing

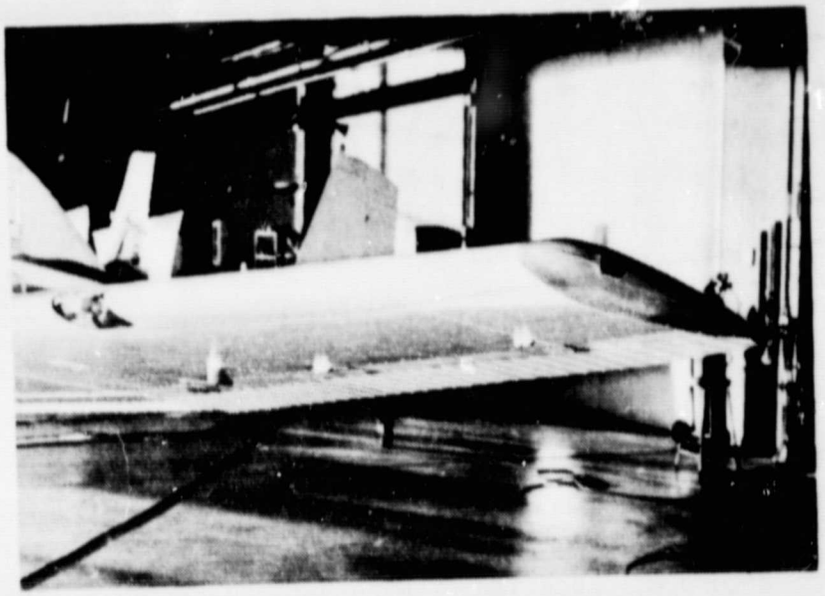

Figure 6. Type I Wing Tip

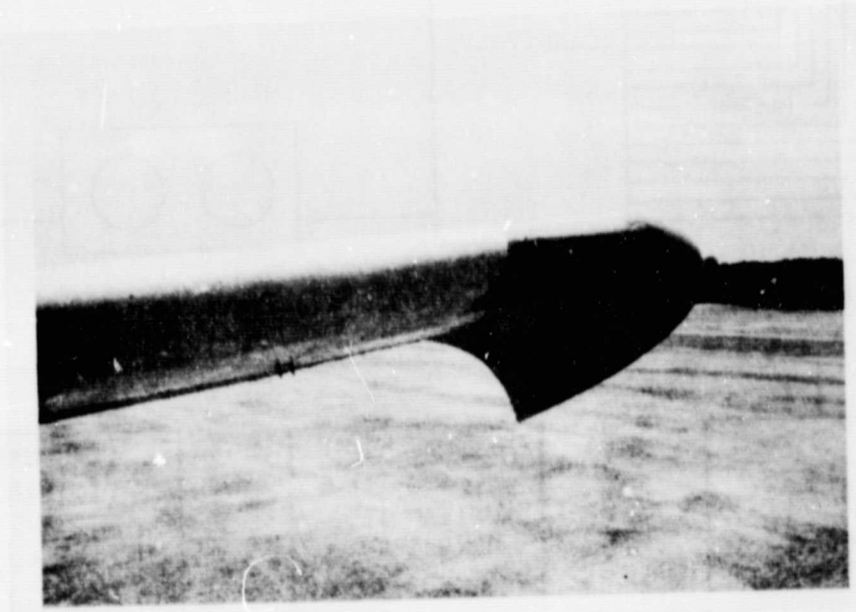

Figure 7. Type II Wing Tip

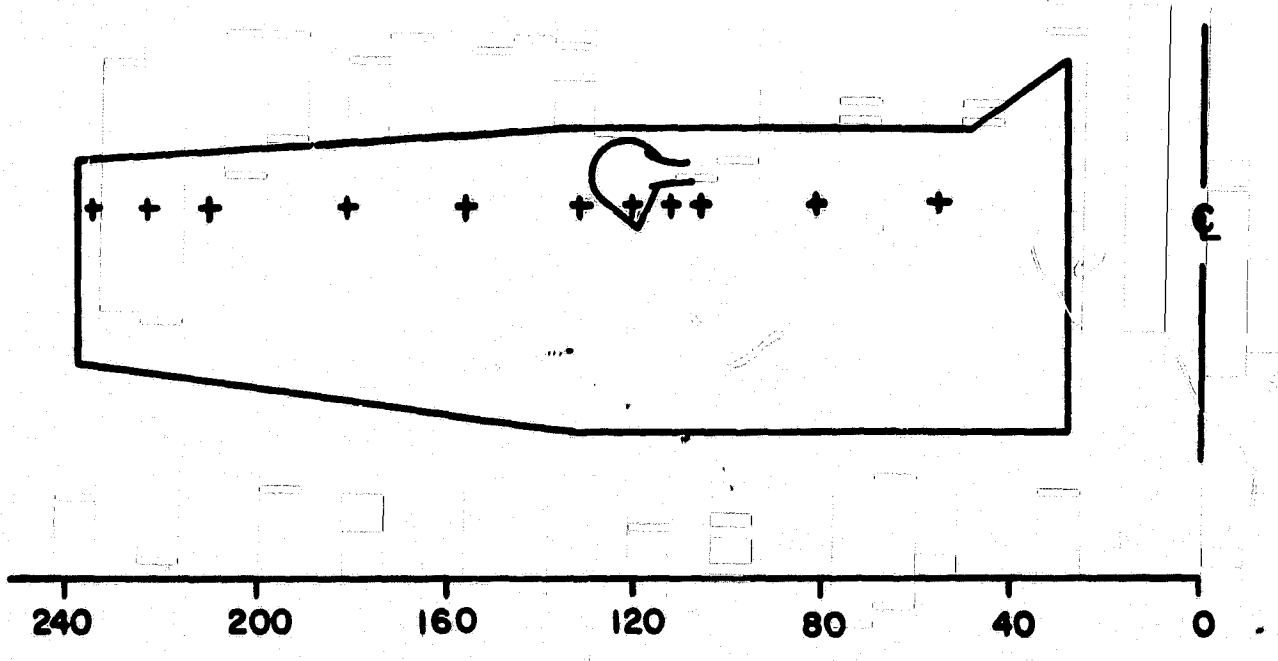

Figure 8. Location of Wing Surface Pressure Taps

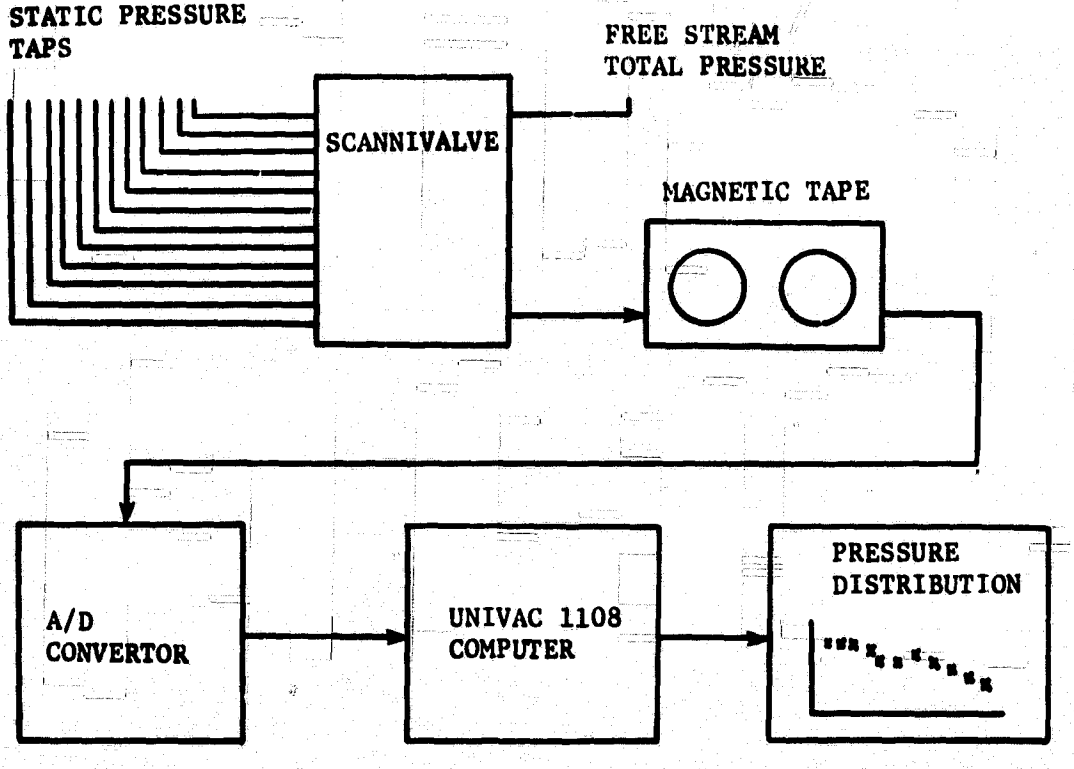

Figure 9. Schematic of Data System

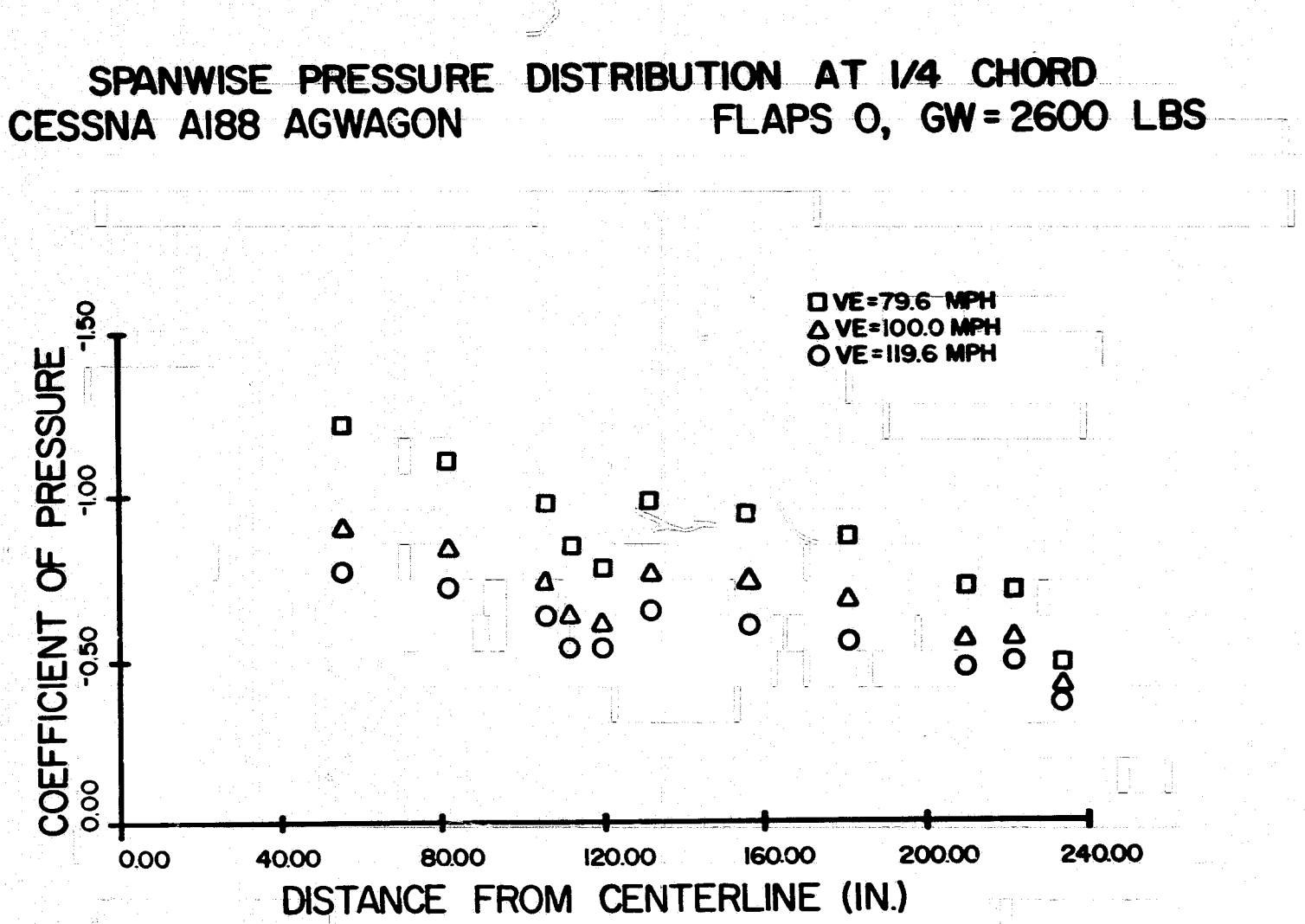

Figure 10. Spanwise Pressure Distribution

SPANWISE PRESSURE DISTRIBUTION AT 1/4 CHORD
CESSNA A188 AGWAGON FLAPS 20, GW = 2600 LBS

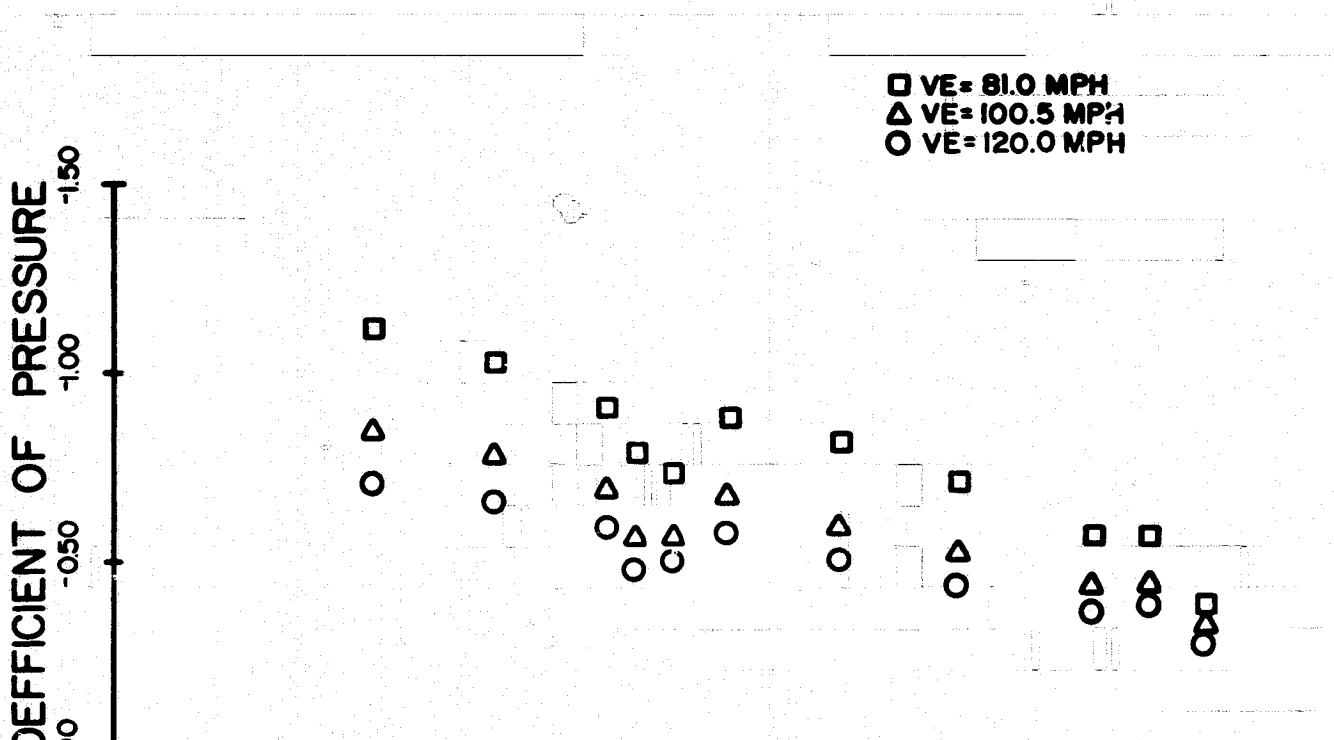

Figure 11. Spanwise Pressure Distribution

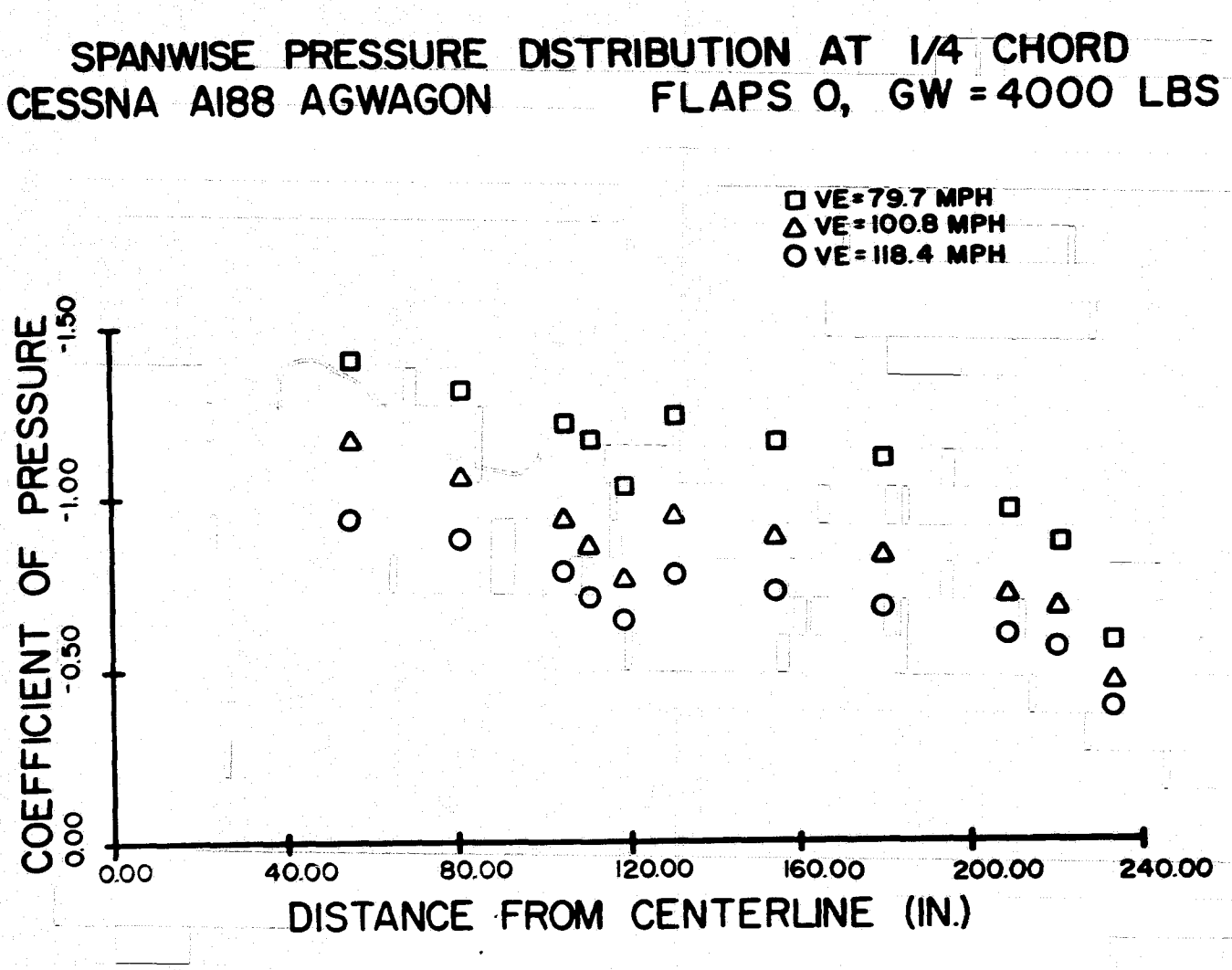

Figure 12. Spanwise Pressure Distribution

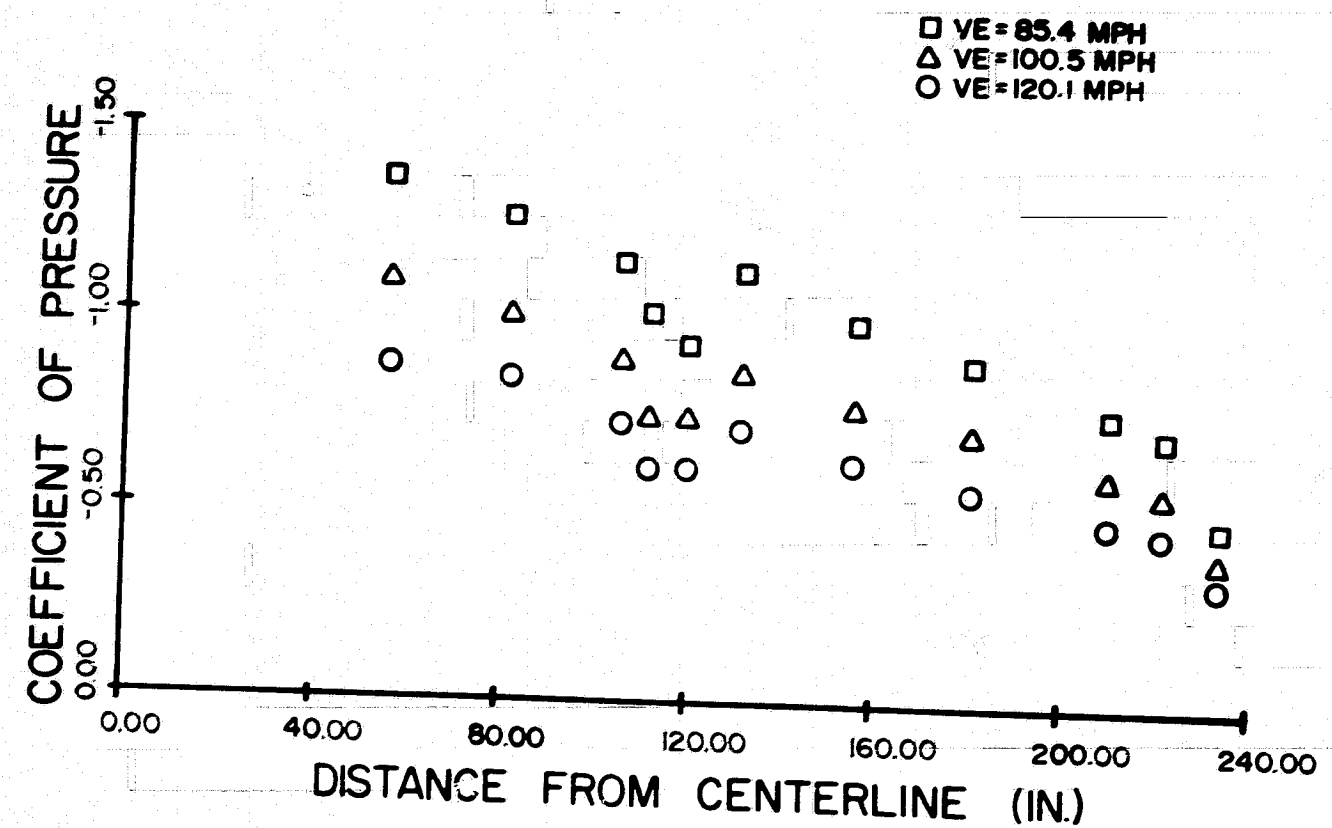

Figure 13. Spanwise Pressure Distribution

SPANWISE PRESSURE DISTRIBUTION AT 1/4 CHORD
CESSNA A188 AGWAGON WITH DROOP TIPS
FLAPS 0, GW=2600 LBS

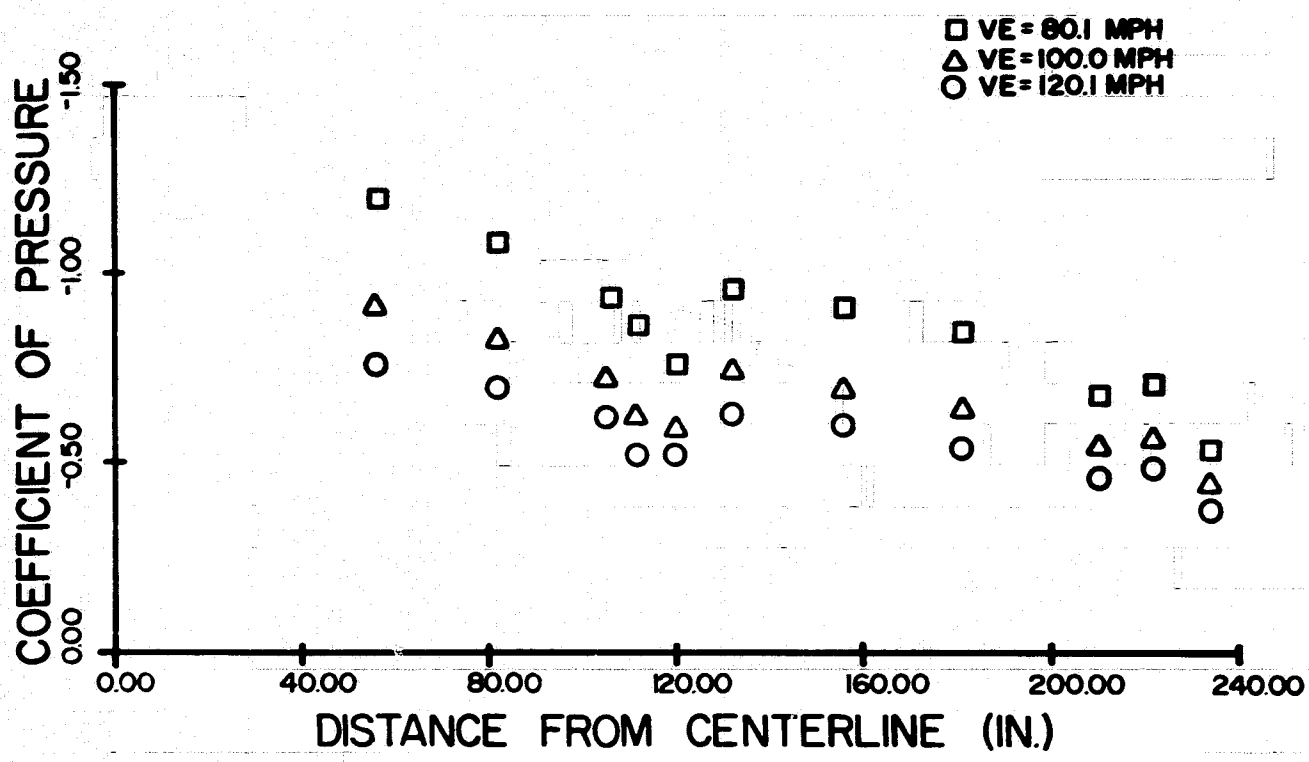

Figure 14. Spanwise Pressure Distribution

SPANWISE PRESSURE DISTRIBUTION AT 1/4 CHORD
CESSNA A188 AGWAGON WITH DROOP TIPS
FLAPS 20, GW = 2600 LBS

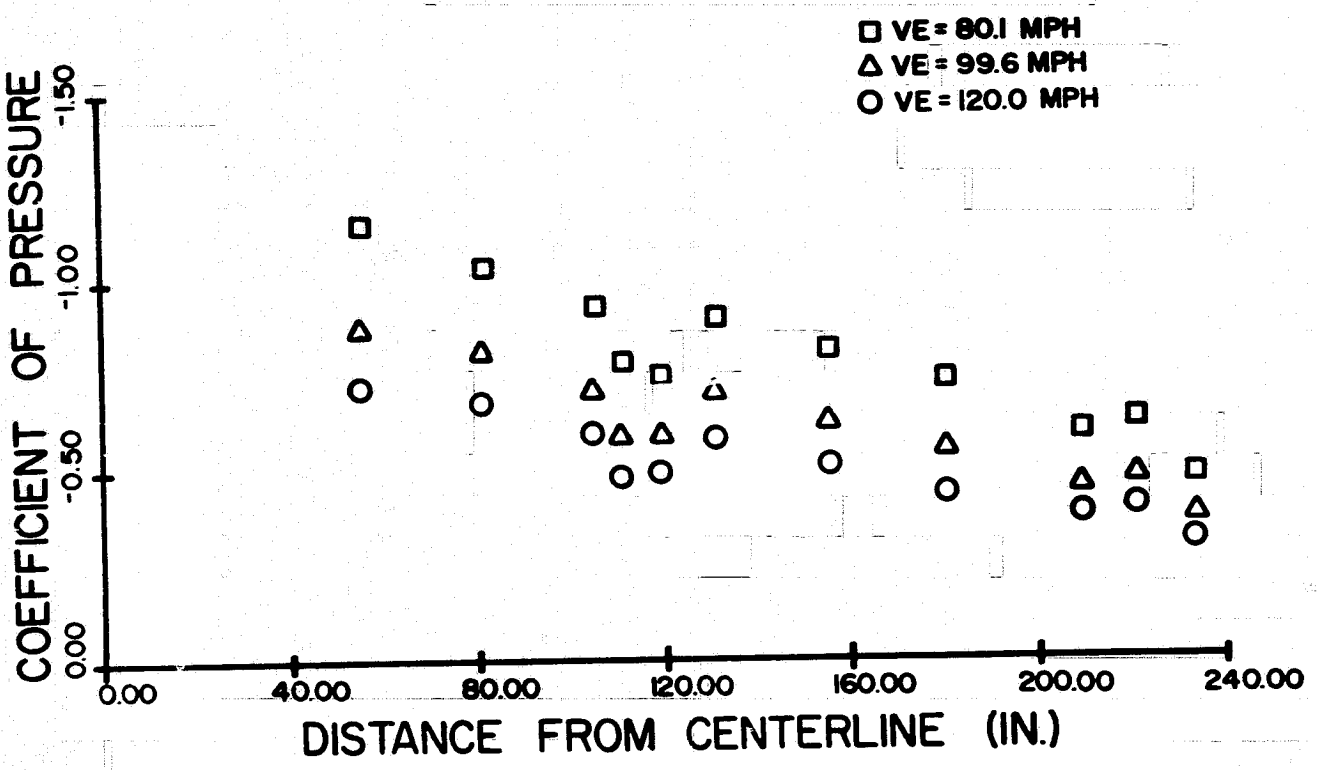

Figure 15. Spanwise Pressure Distribution

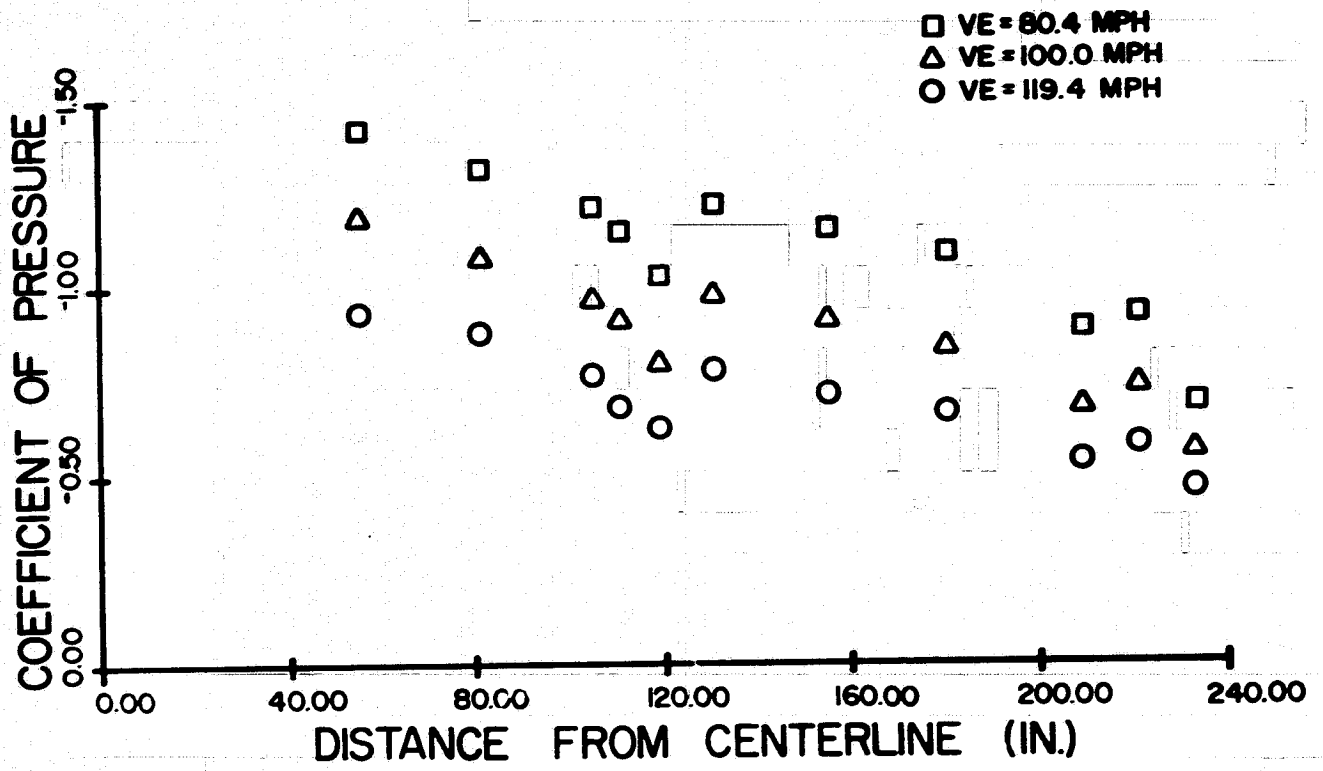

Figure 16. Spanwise Pressure Distribution

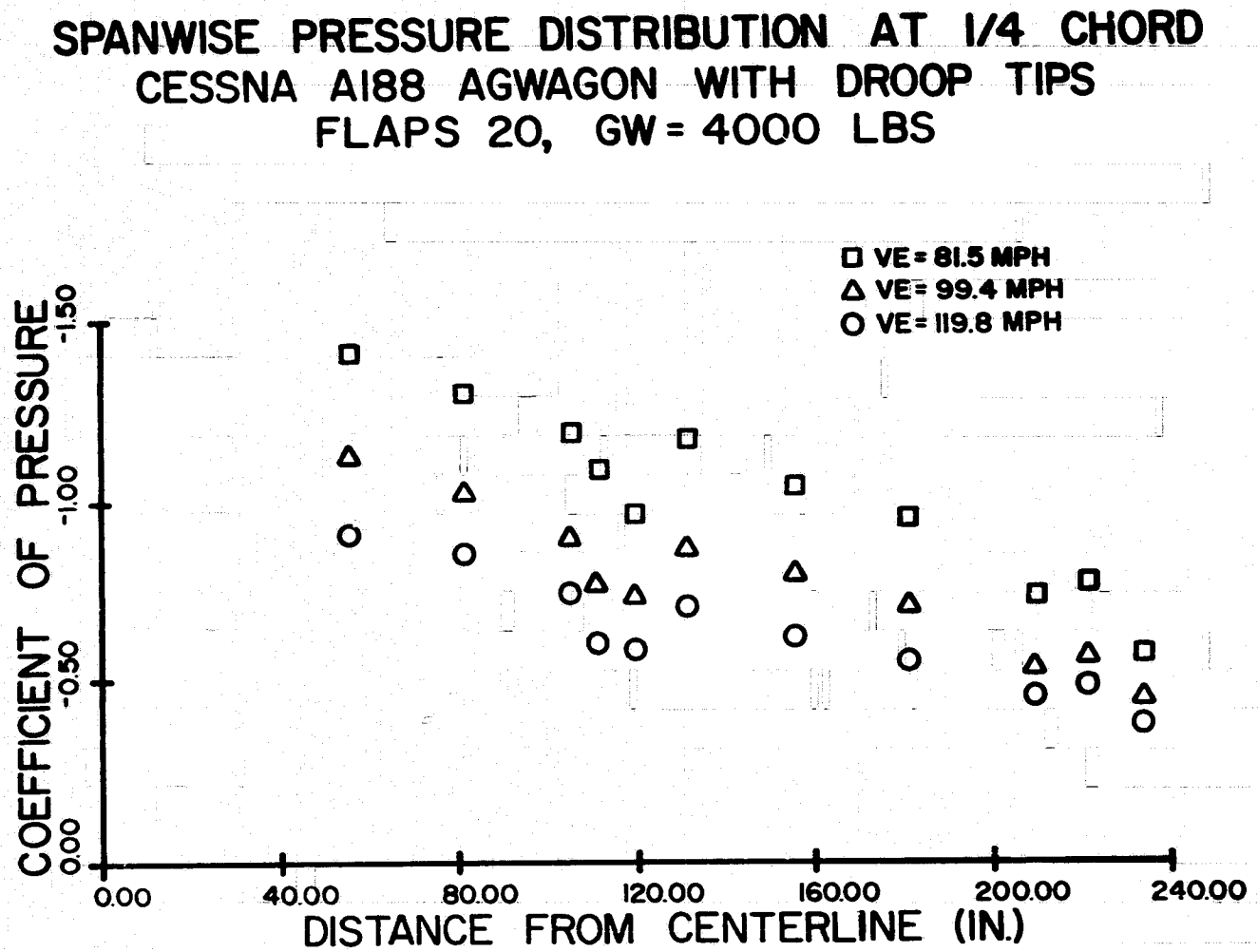

Figure 17. Spanwise Pressure Distribution

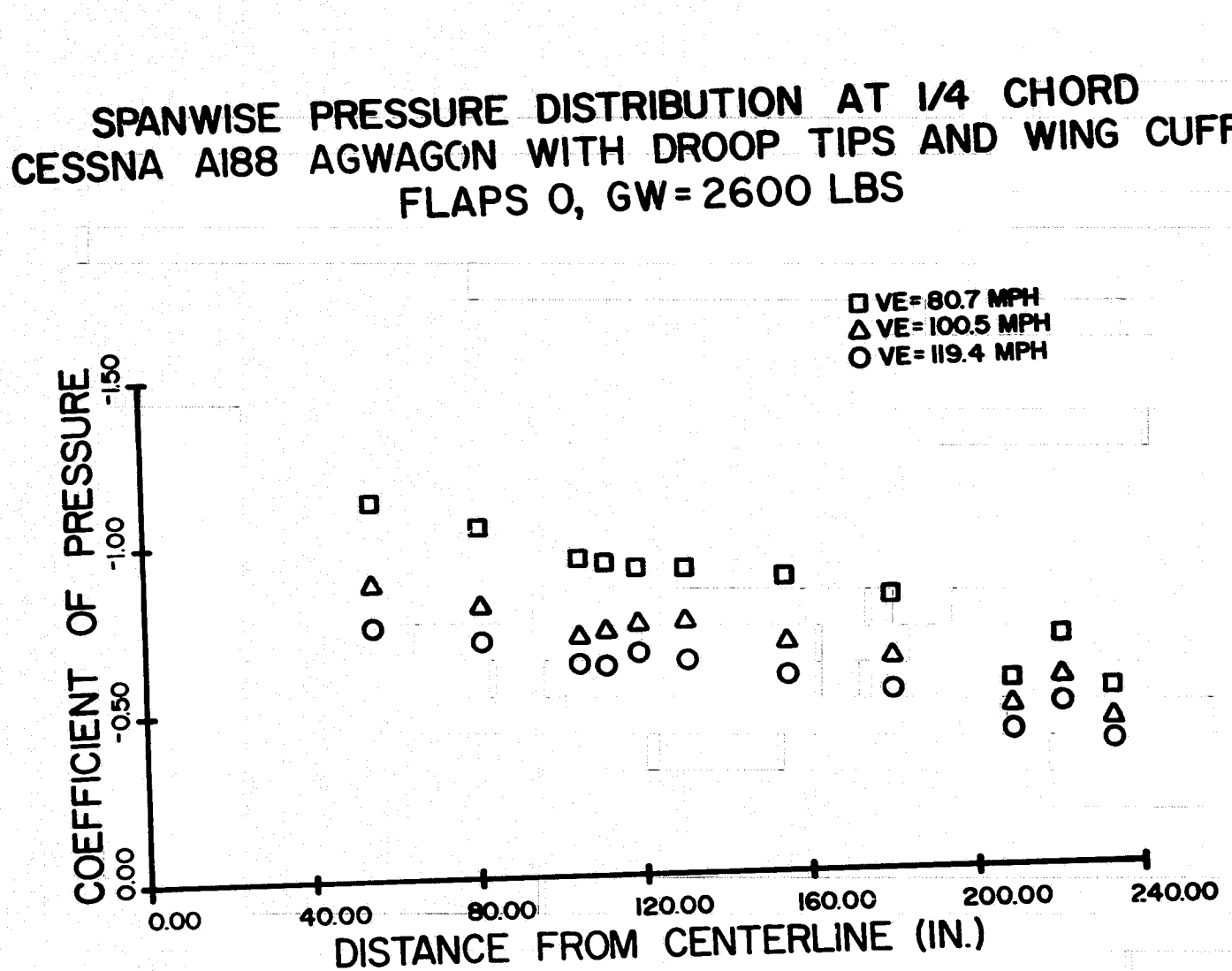

Figure 18. Spanwise Pressure Distribution

SPANWISE PRESSURE DISTRIBUTION AT 1/4 CHORD
CESSNA A188 AGWAGON WITH DROOP TIPS AND WING CUFFS
FLAPS 20, GW = 2600 LBS

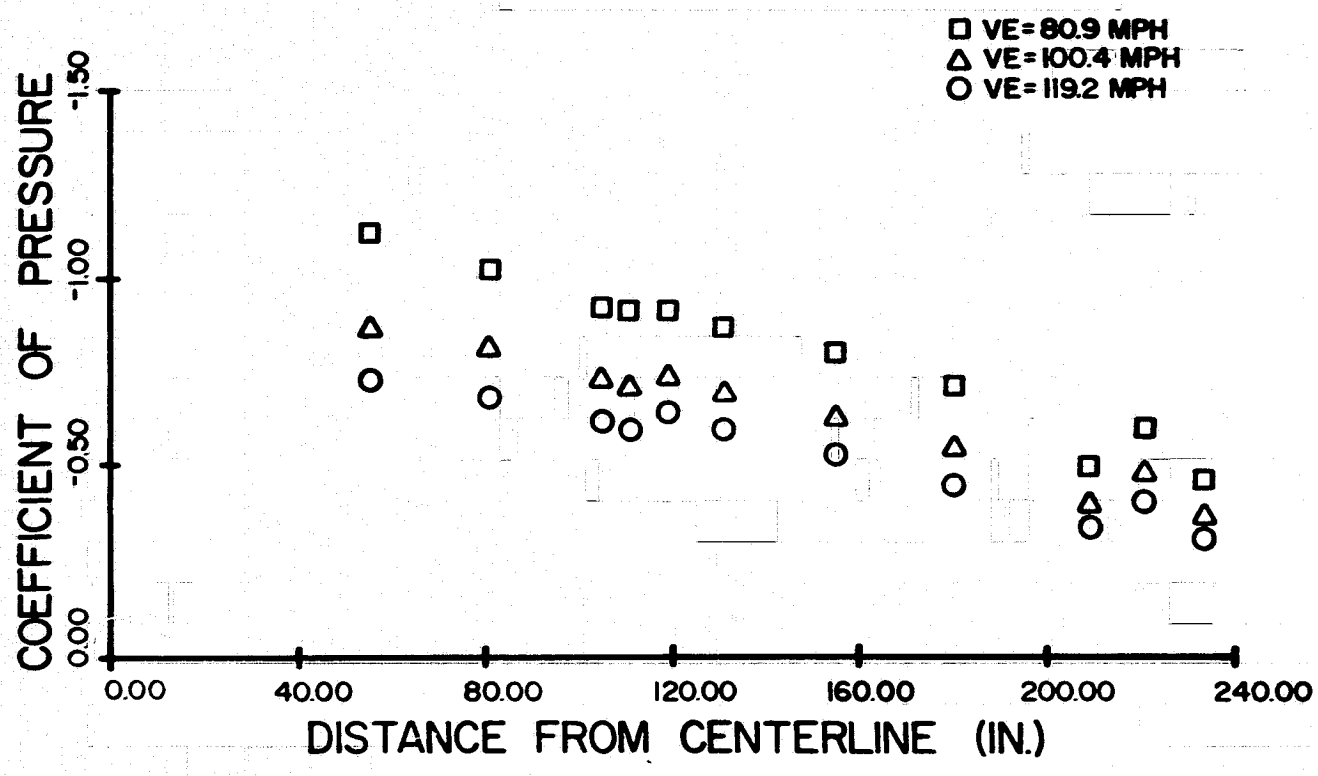

Figure 19. Spanwise Pressure Distribution

SPANWISE PRESSURE DISTRIBUTION AT 1/4 CHORD
CESSNA A188 AGWAGON WITH DROOP TIPS AND WING CUFFS
FLAPS 0, GW = 4000 LBS

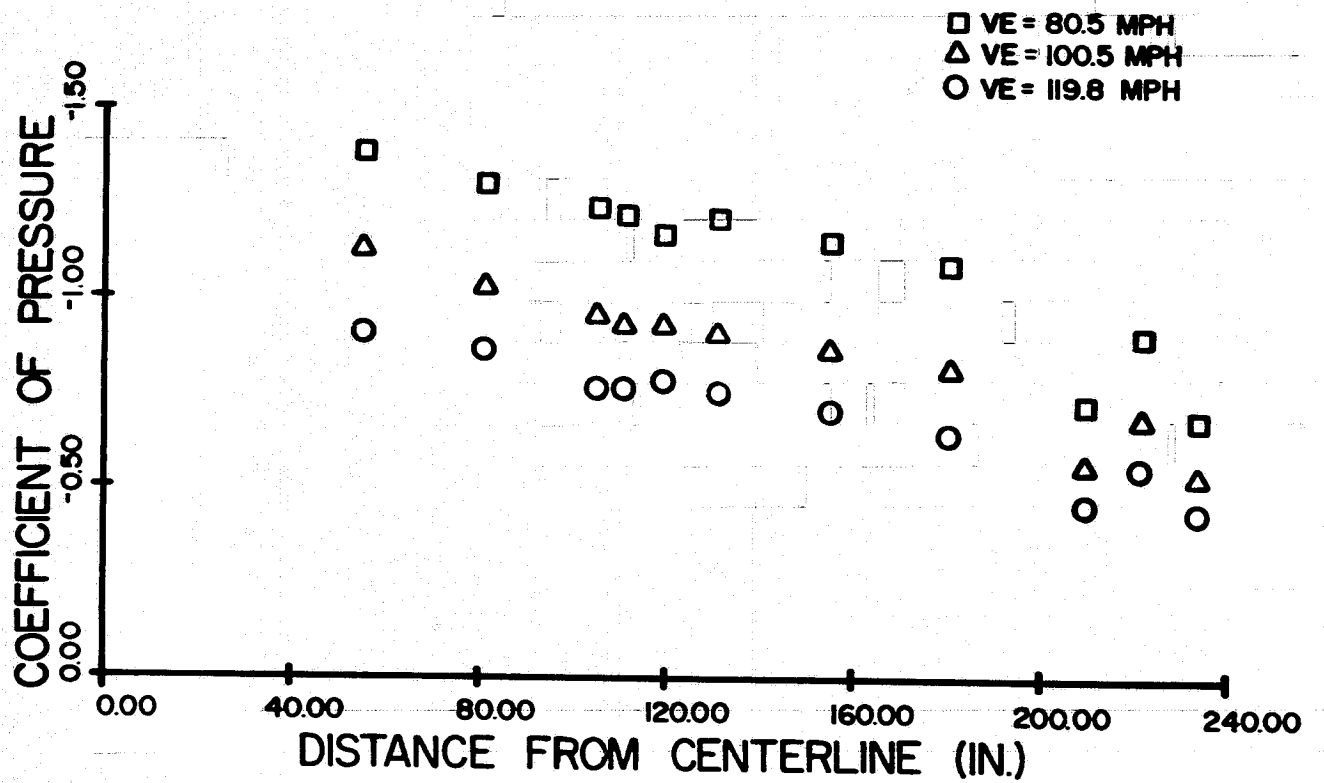

Figure 20. Spanwise Pressure Distribution

SPANWISE PRESSURE DISTRIBUTION AT 1/4 CHORD
CESSNA A188 AGWAGON WITH DROOP TIPS AND WING CUFFS
FLAPS 20, GW = 4000 LBS

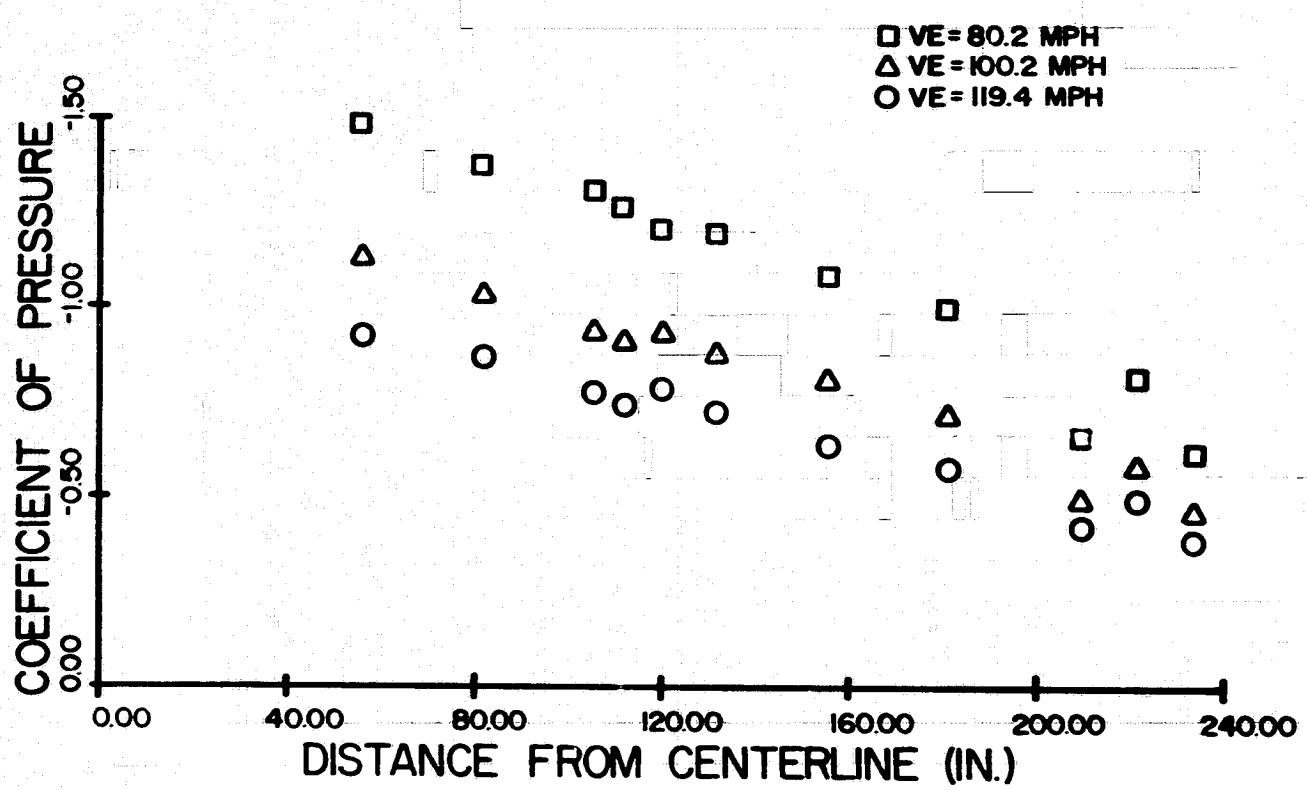

Figure 21. Spanwise Pressure Distribution

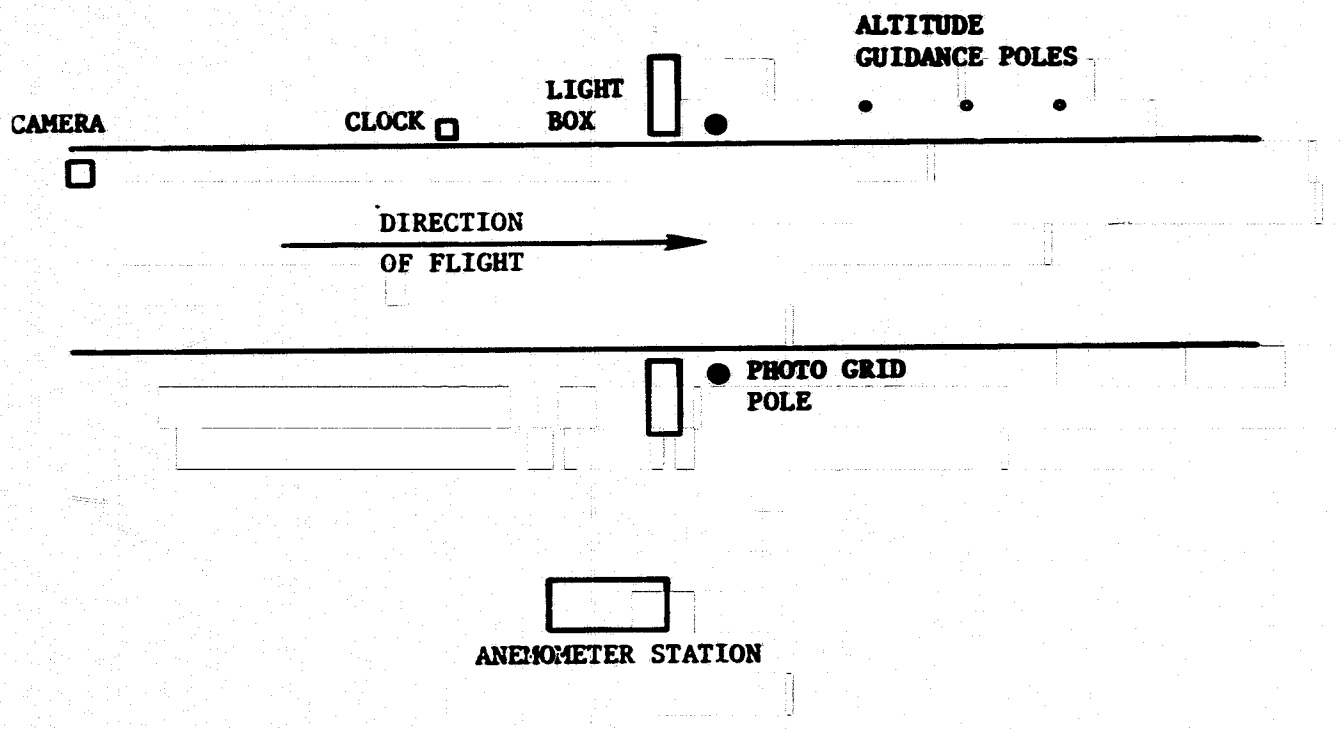

Figure 22. Schematic of Flow Visualization Method

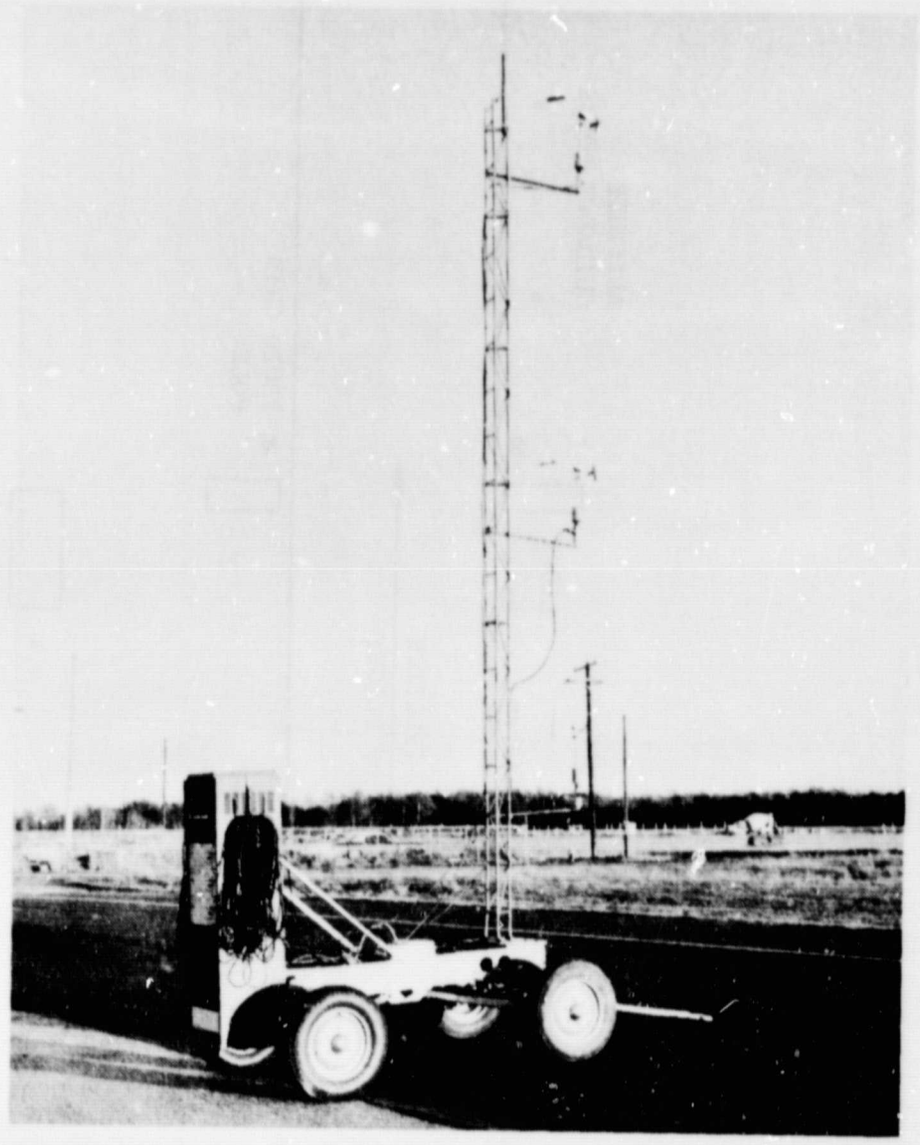

Figure 23. Wind Anemometers

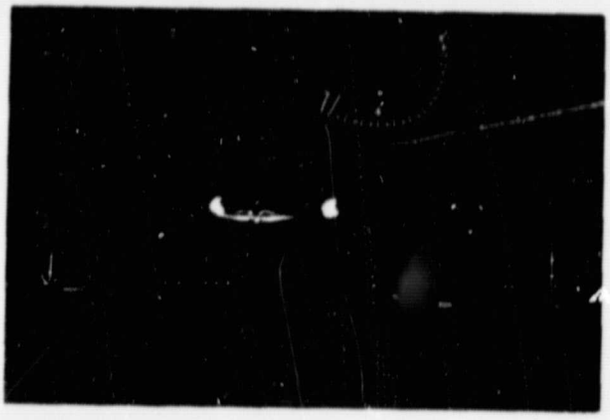

t = 1 sec.

t = 5 sec.

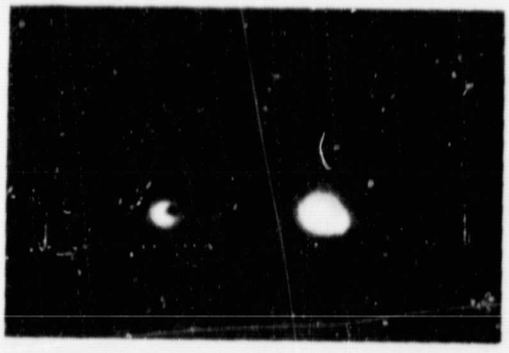

t = 8 sec.

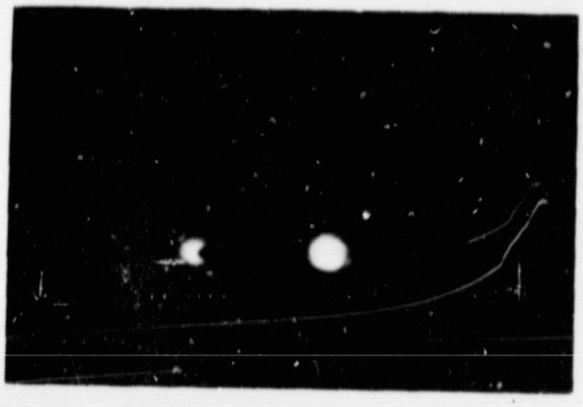

t = 12 sec.

t = 15 sec.

t = 19 sec.

Figure 24. Tip Vortex Trajectory Photos

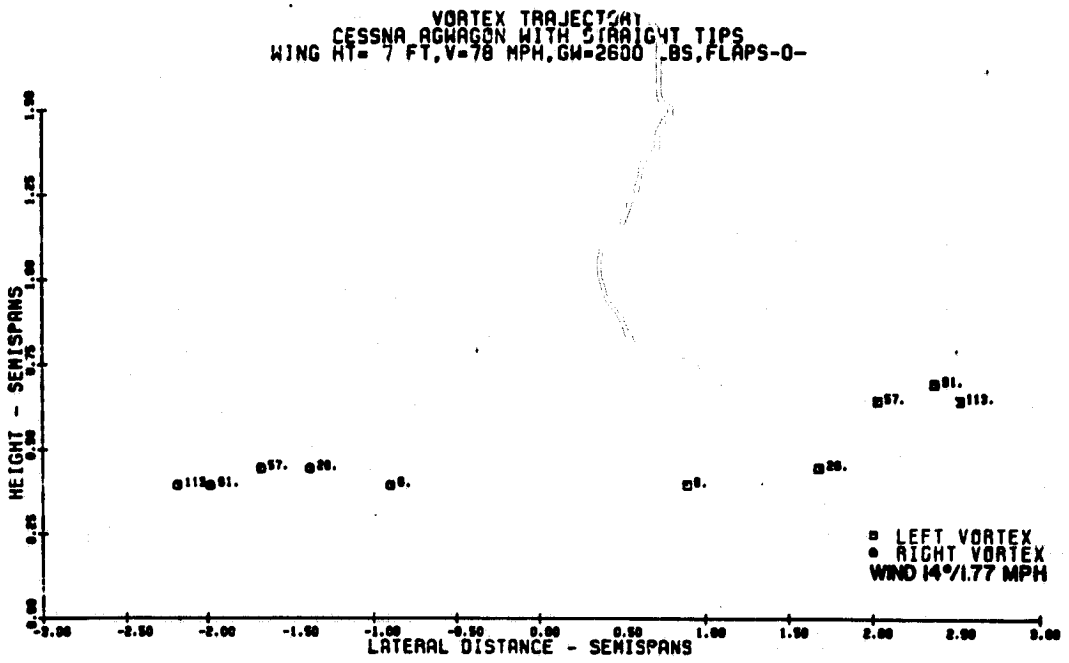

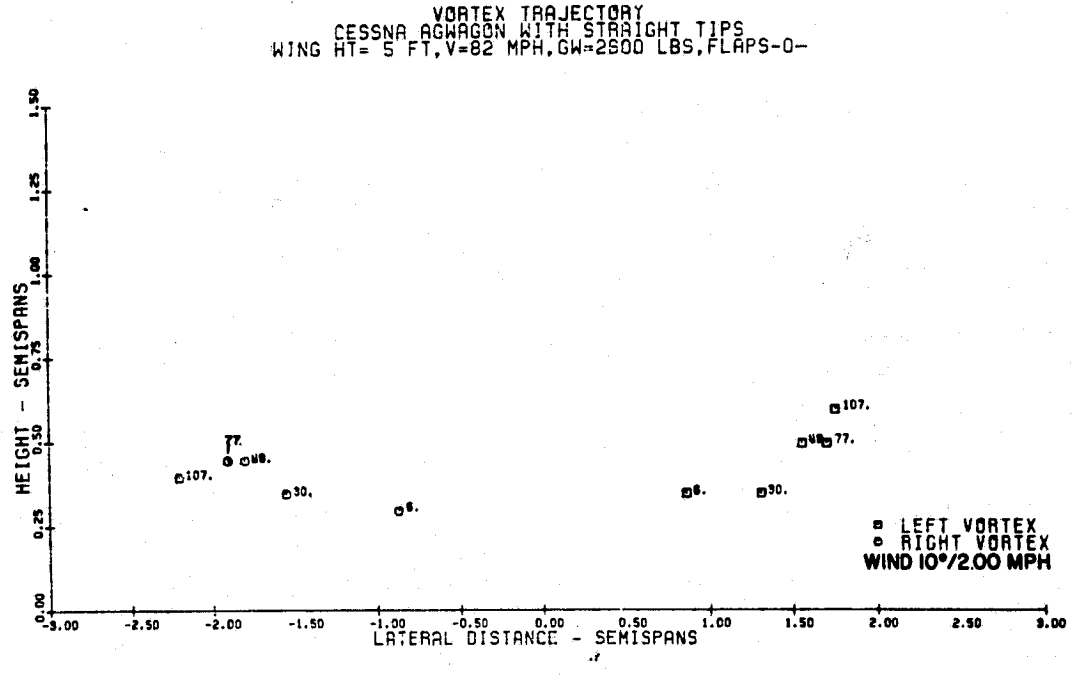

Figure 25. Tip Vortex Trajectory--Full Scale

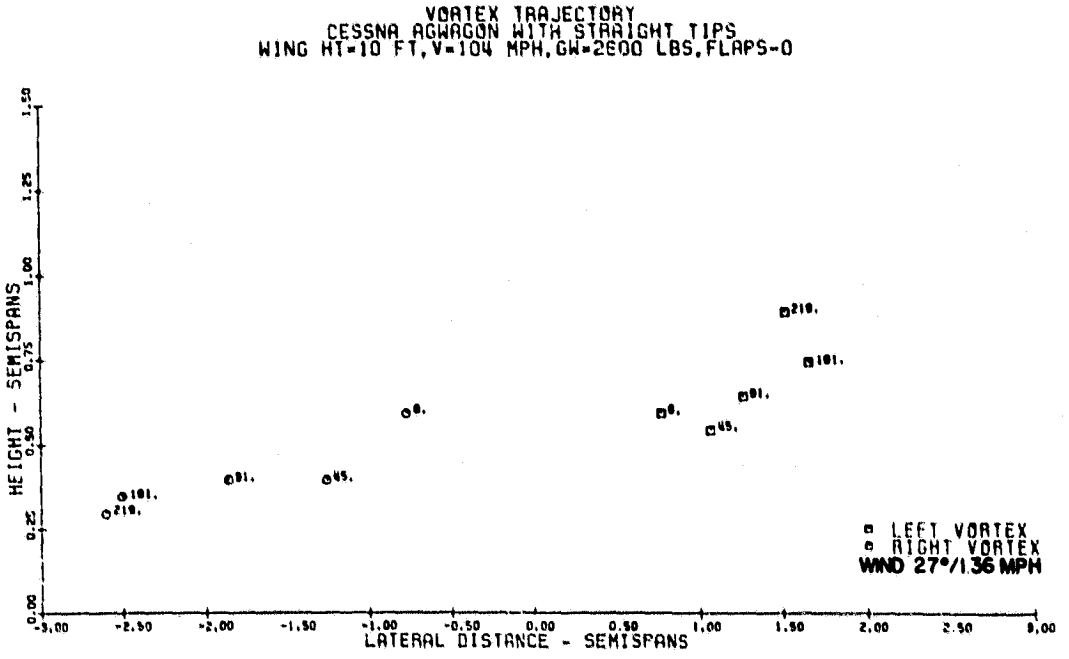

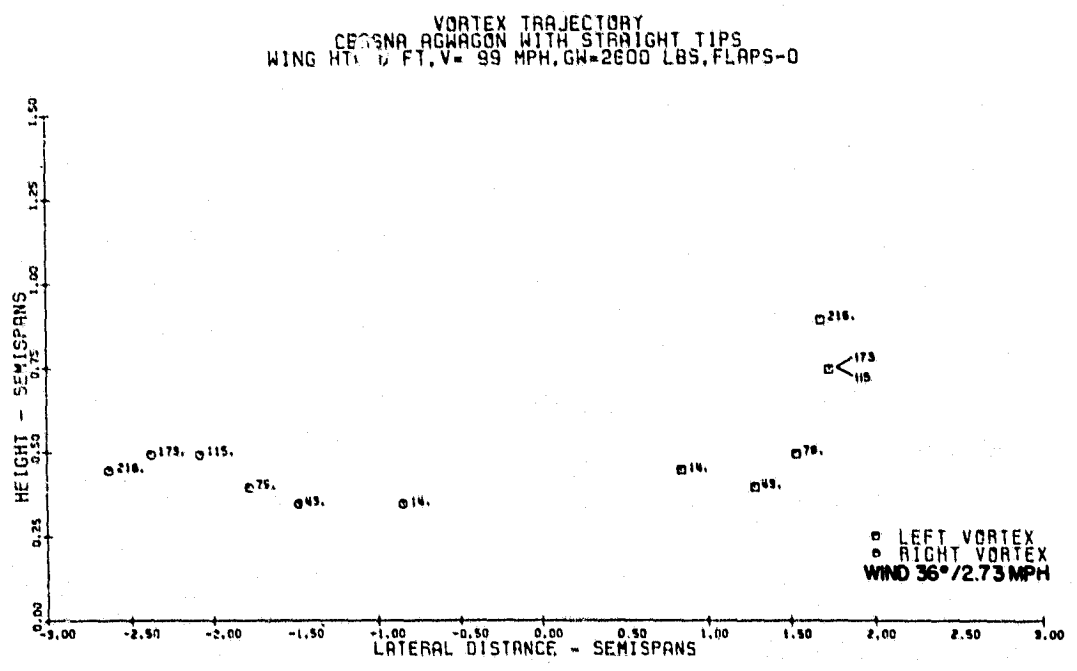

Figure 26. Tip Vortex Trajectory--Full Scale

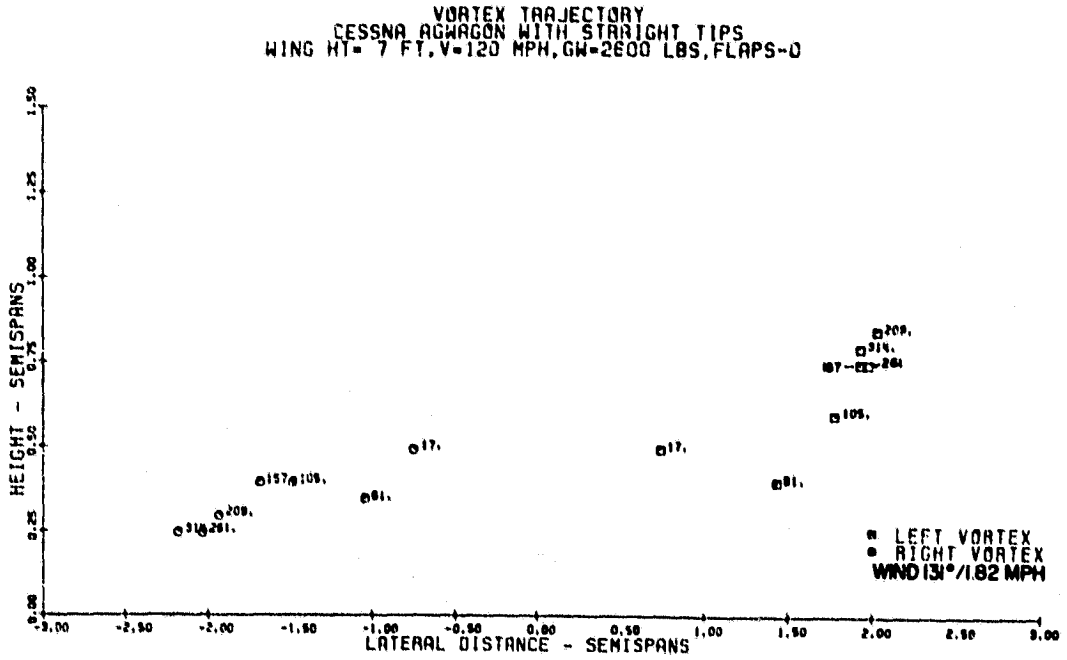

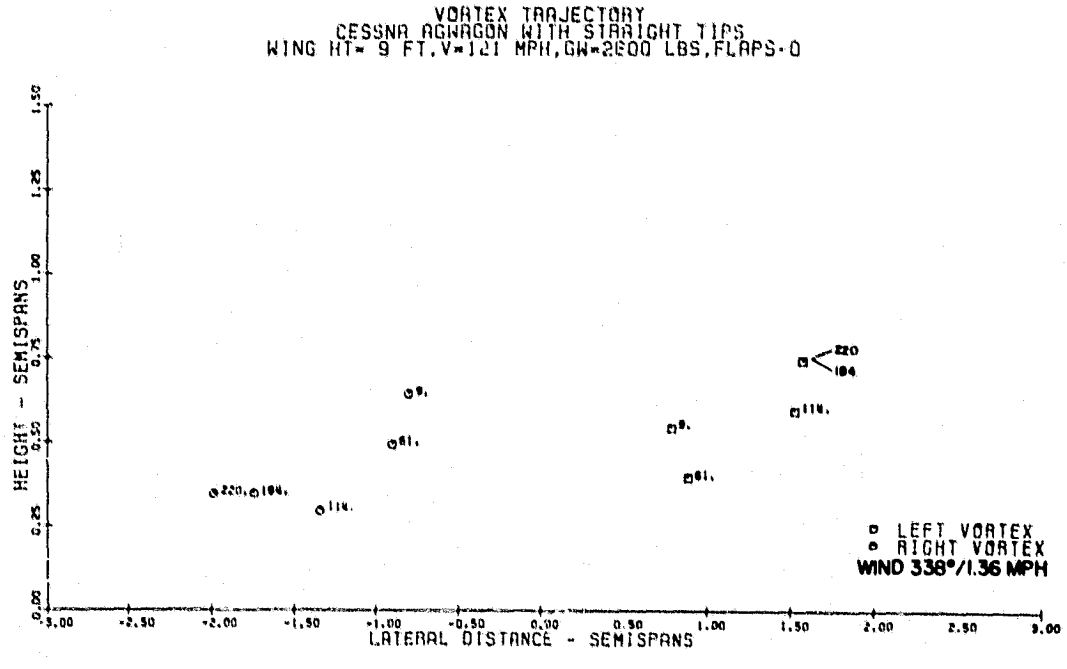

Figure 27. Tip Vortex Trajectory--Full Scale

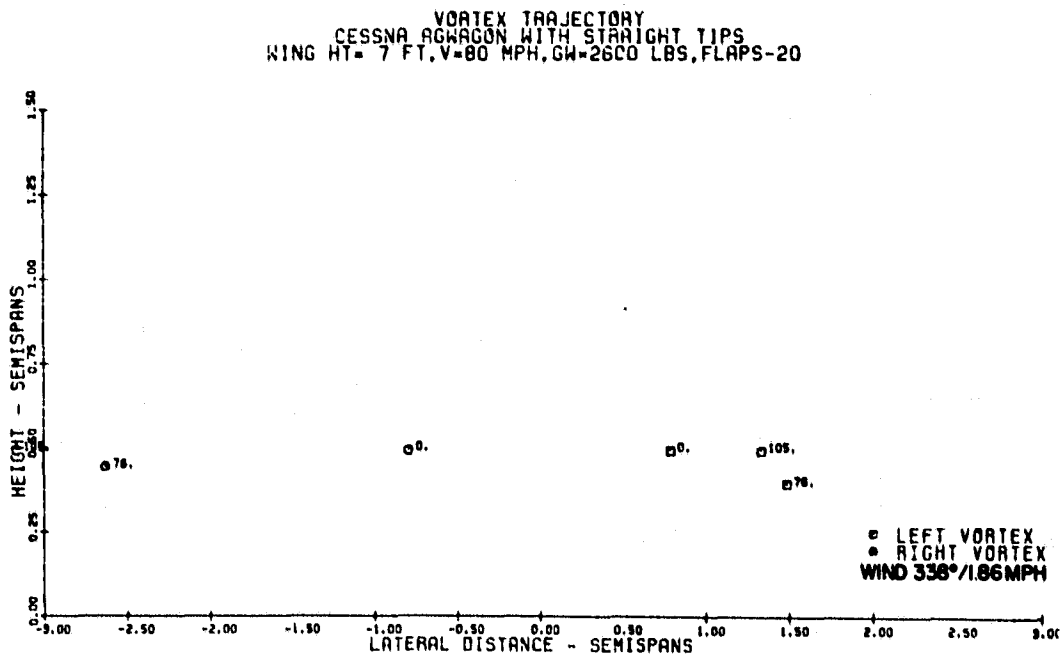

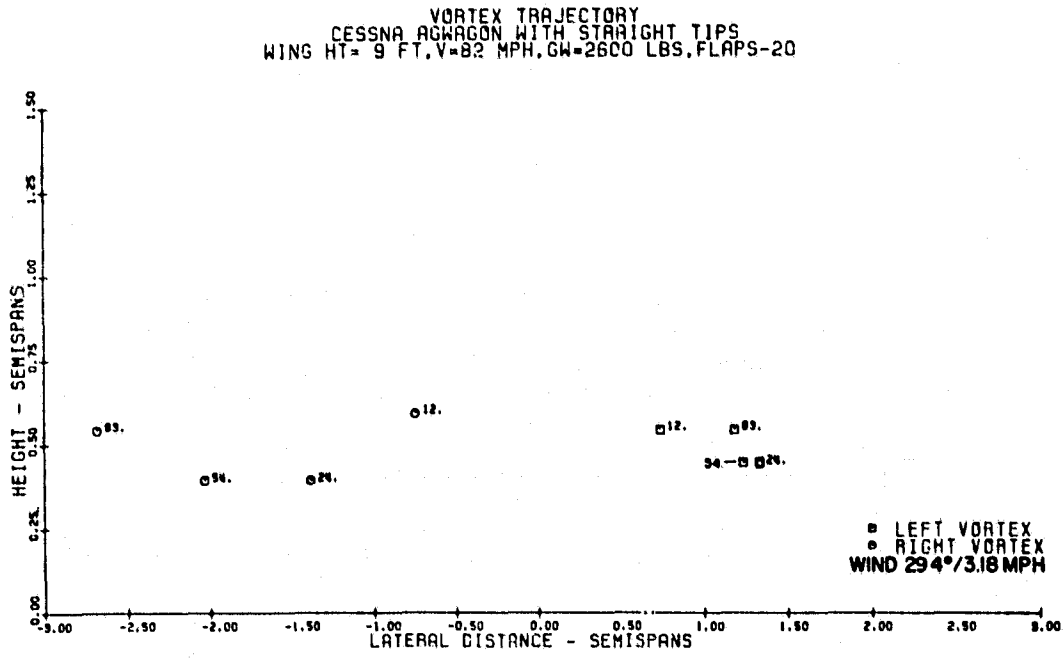

Figure 28. Tip Vortex Trajectory--Full Scale

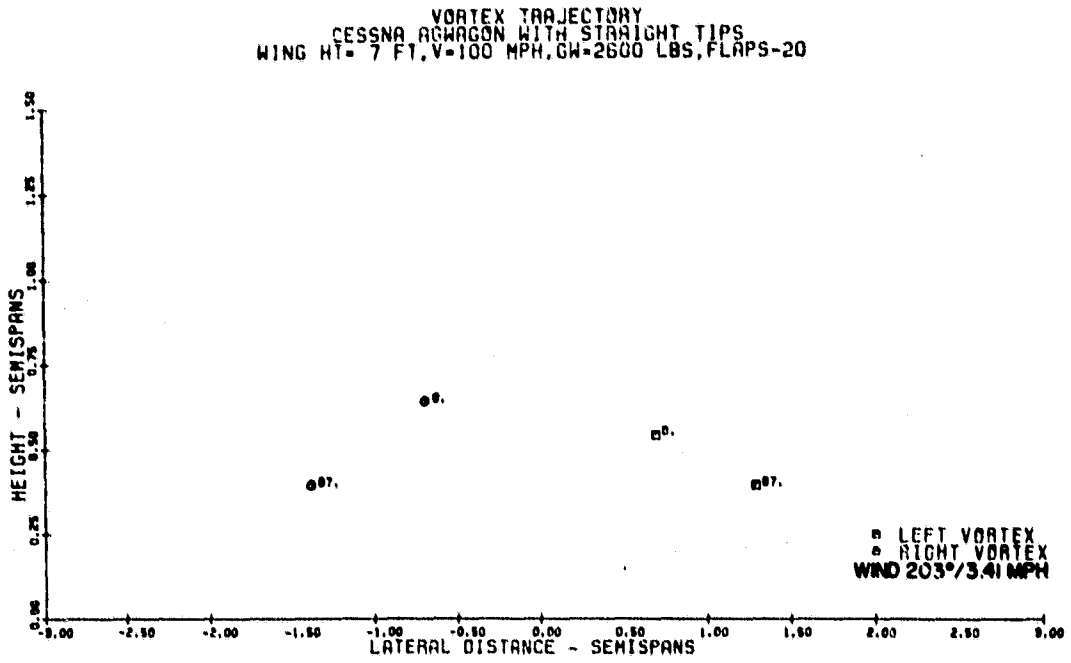

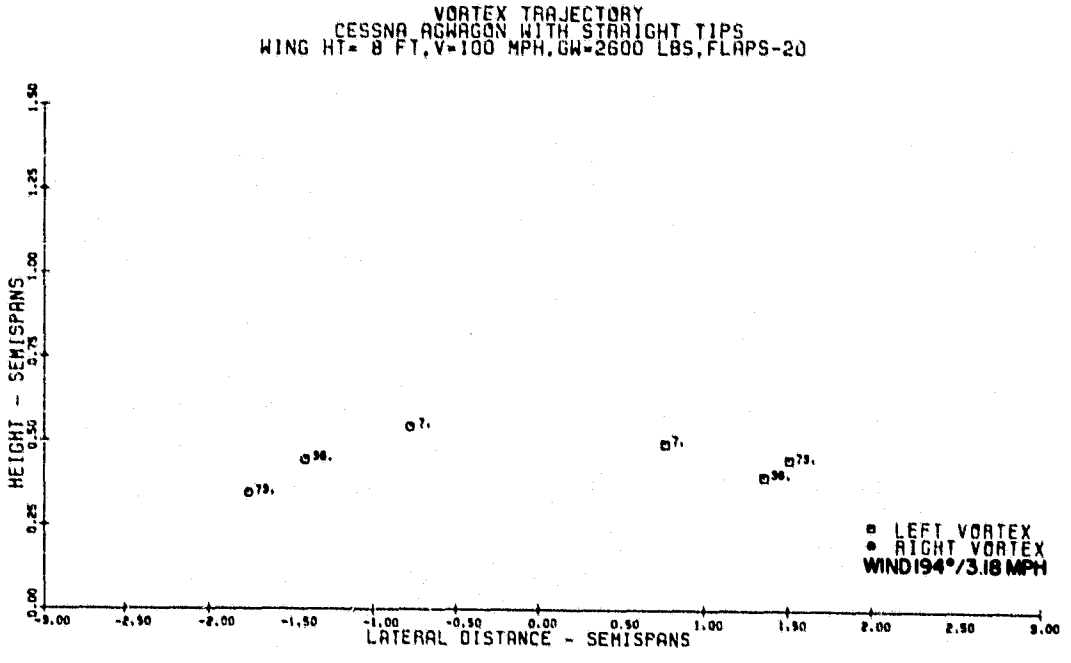

Figure 29. Tip Vortex Trajectory--Full Scale

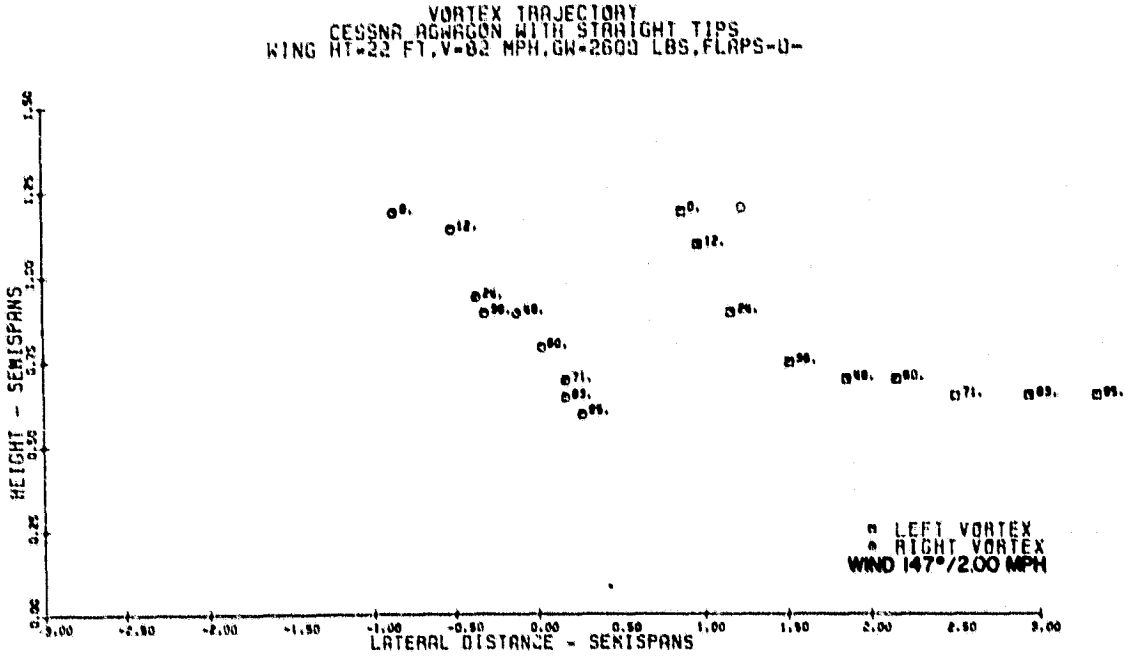

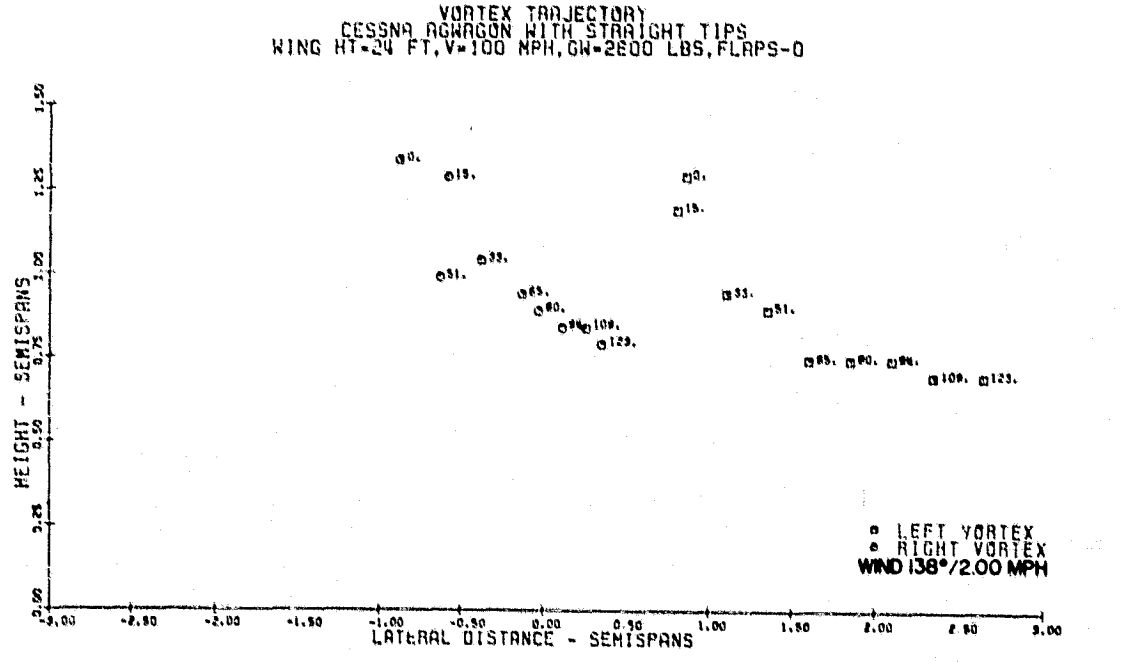

Figure 30. Tip Vortex Trajectory--Full Scale

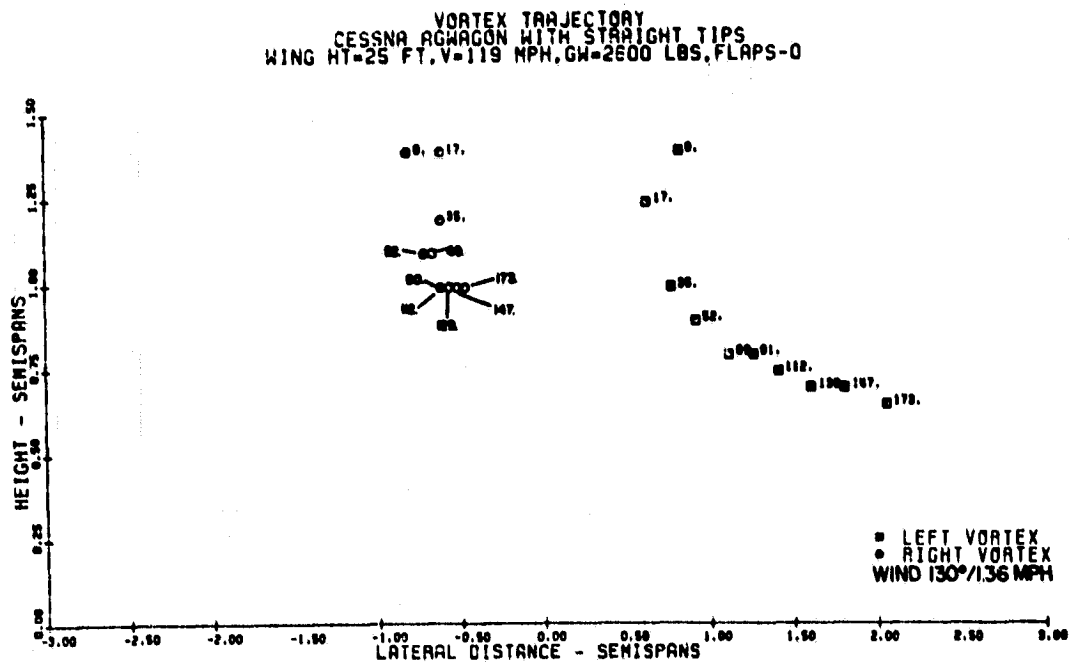

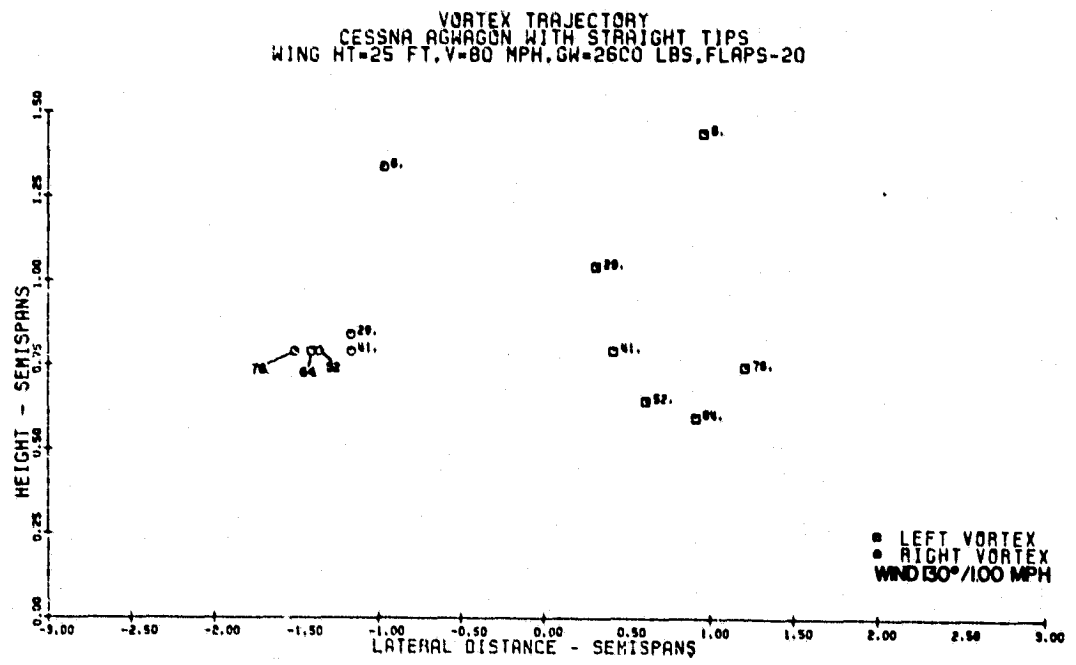

Figure 31. Tip Vortex Trajectory--Full Scale

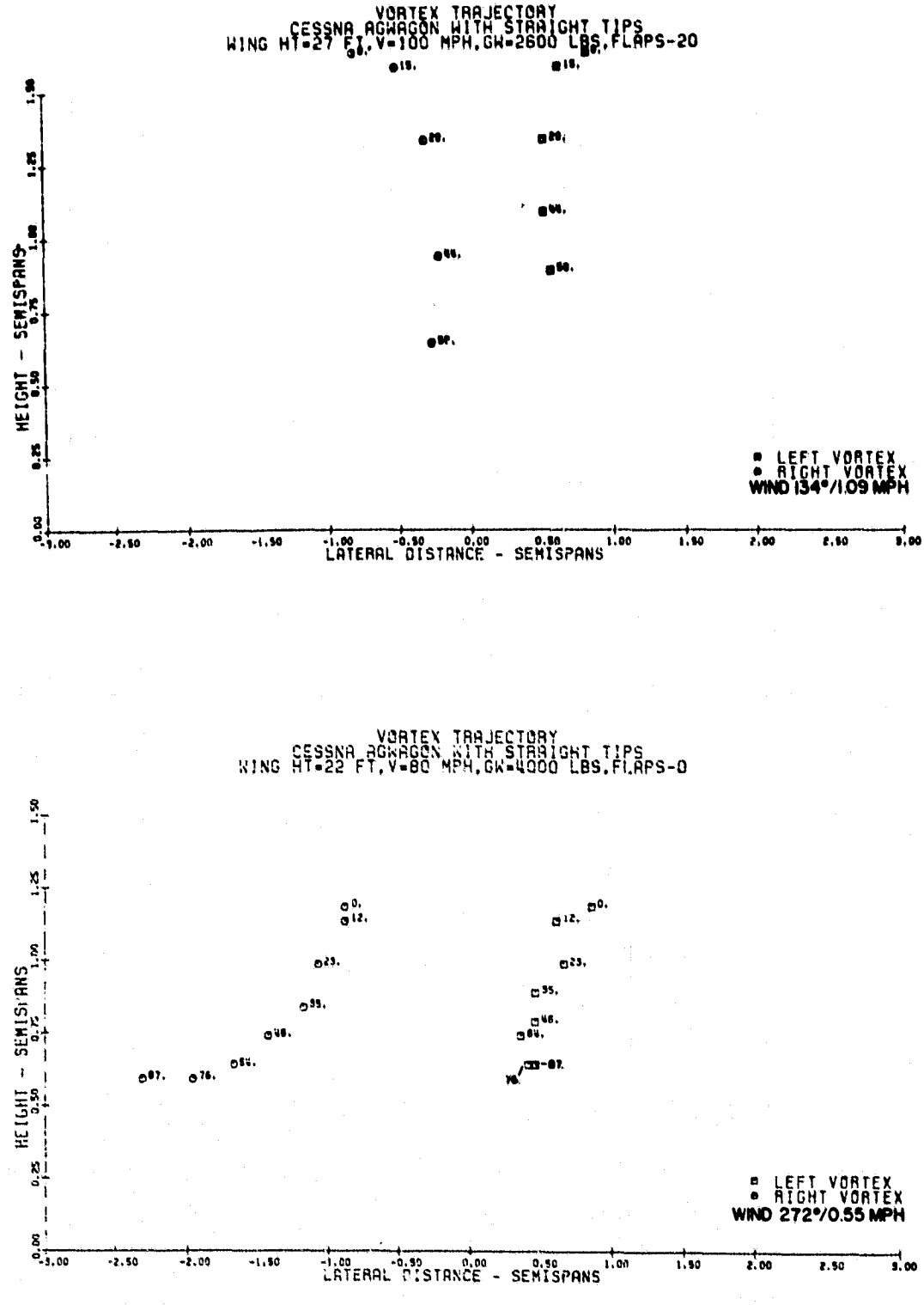

Figure 32. Tip Vortex Trajectory--Full Scale

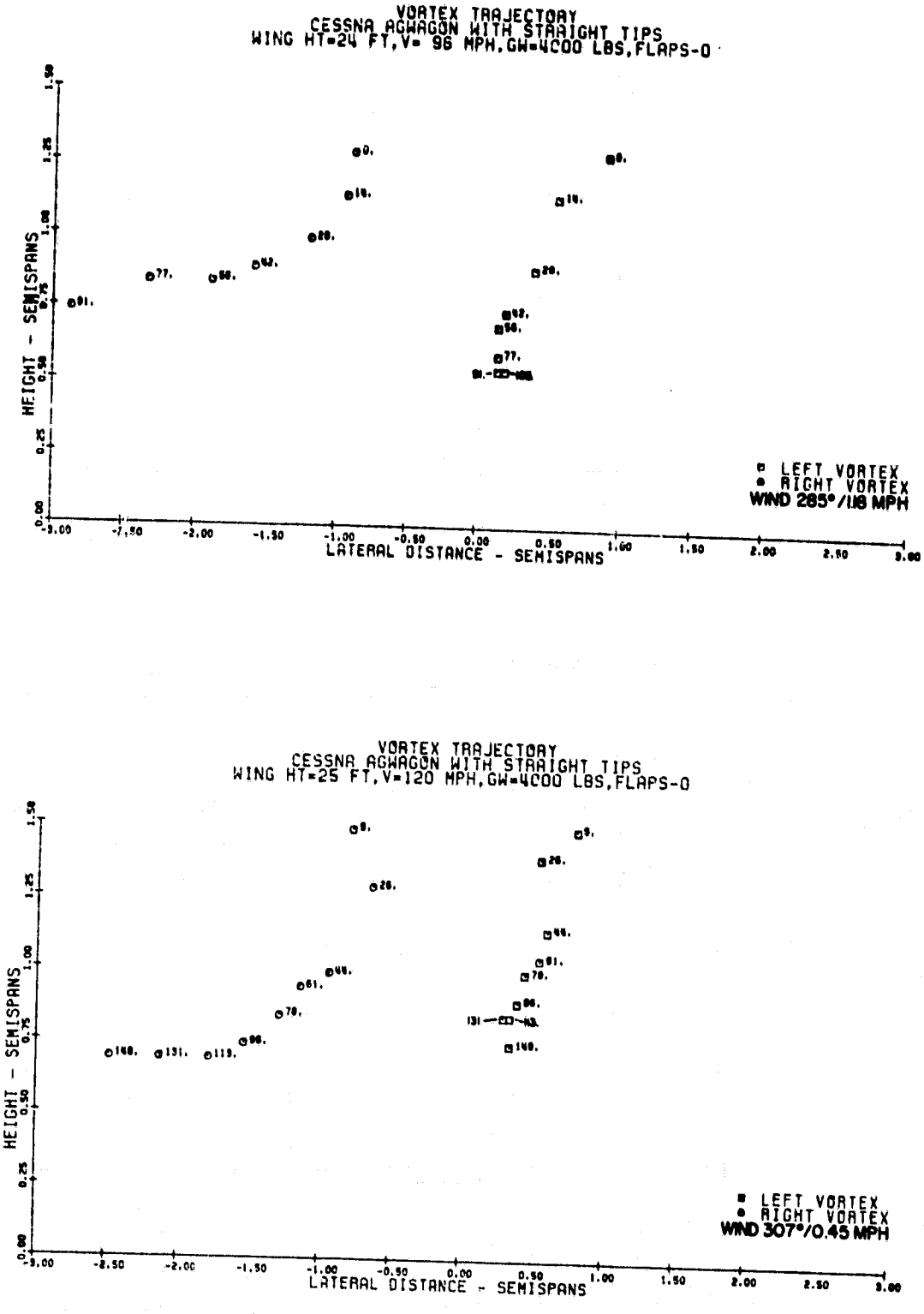

Figure 33. Tip Vortex Trajectory--Full Scale

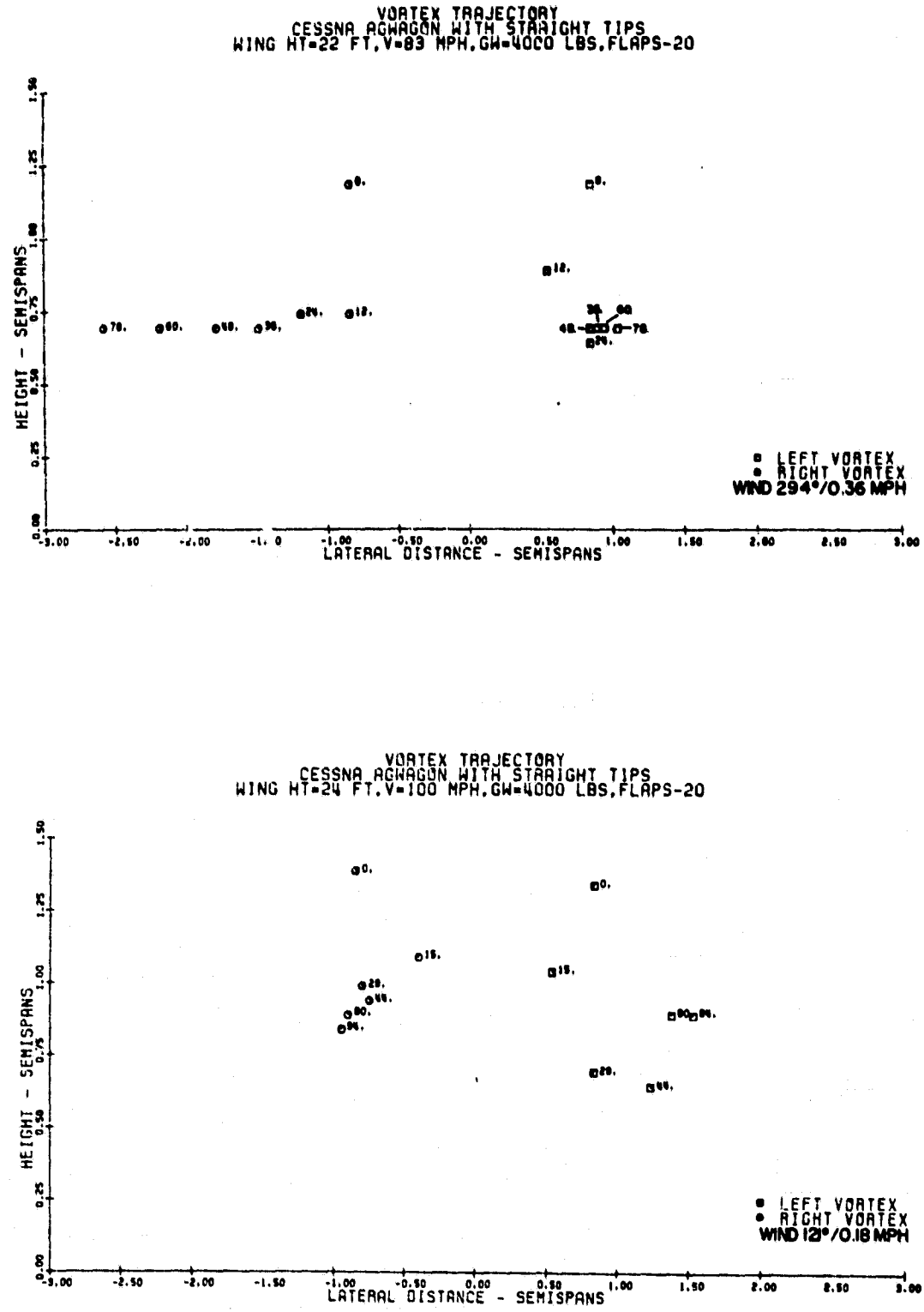

Figure 34. Tip Vortex Trajectory--Full Scale

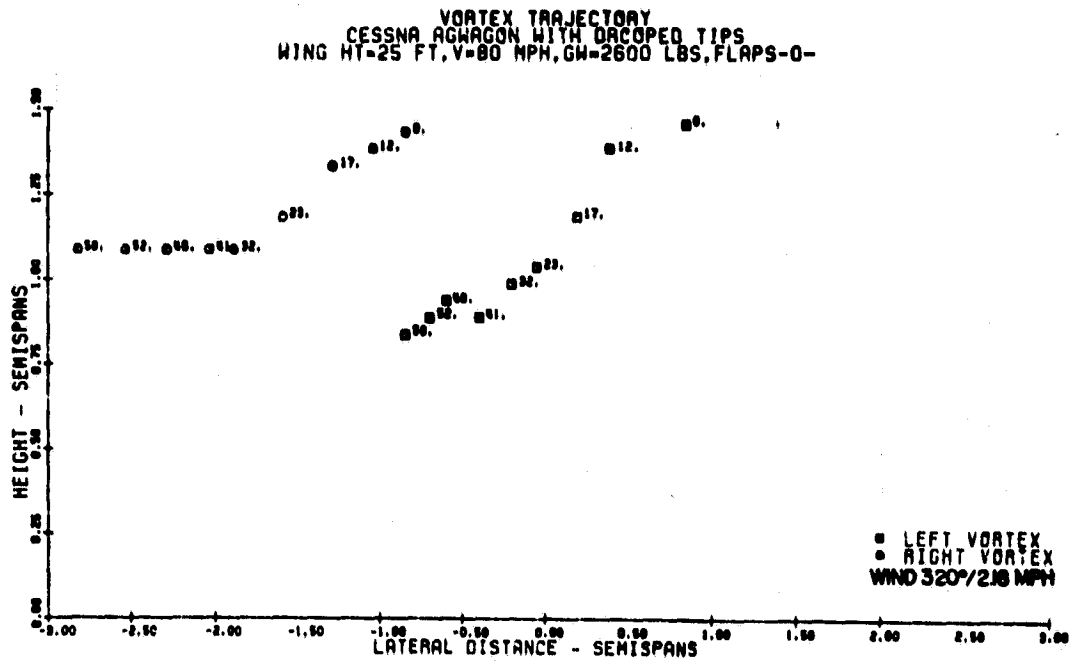

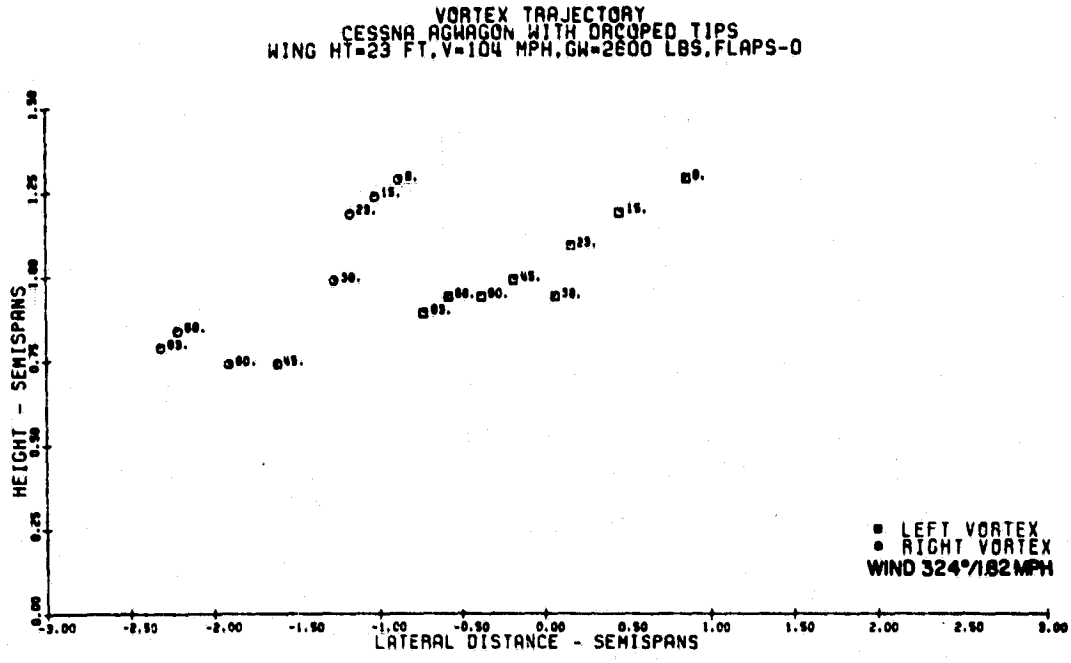

Figure 35. Tip Vortex Trajectory--Full Scale

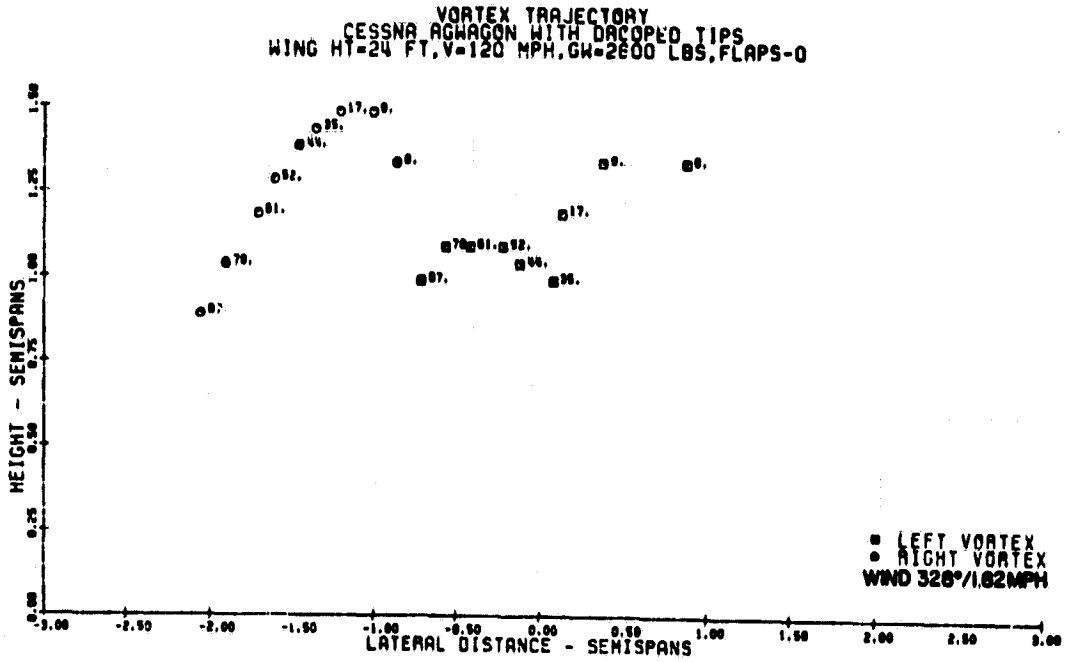

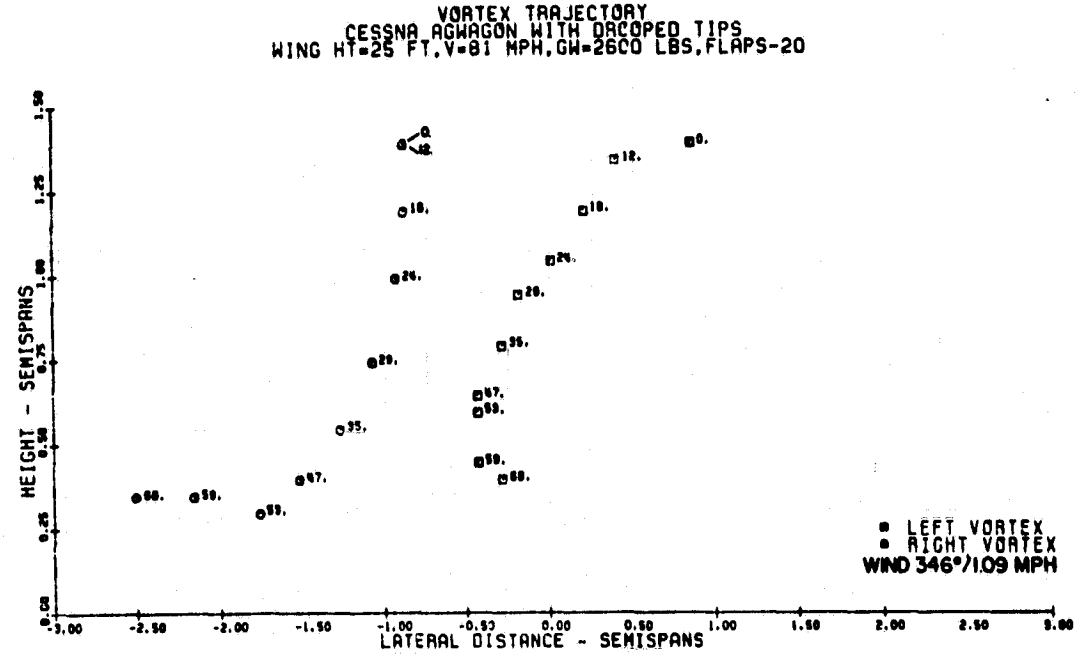

Figure 36. Tip Vortex Trajectory--Full Scale

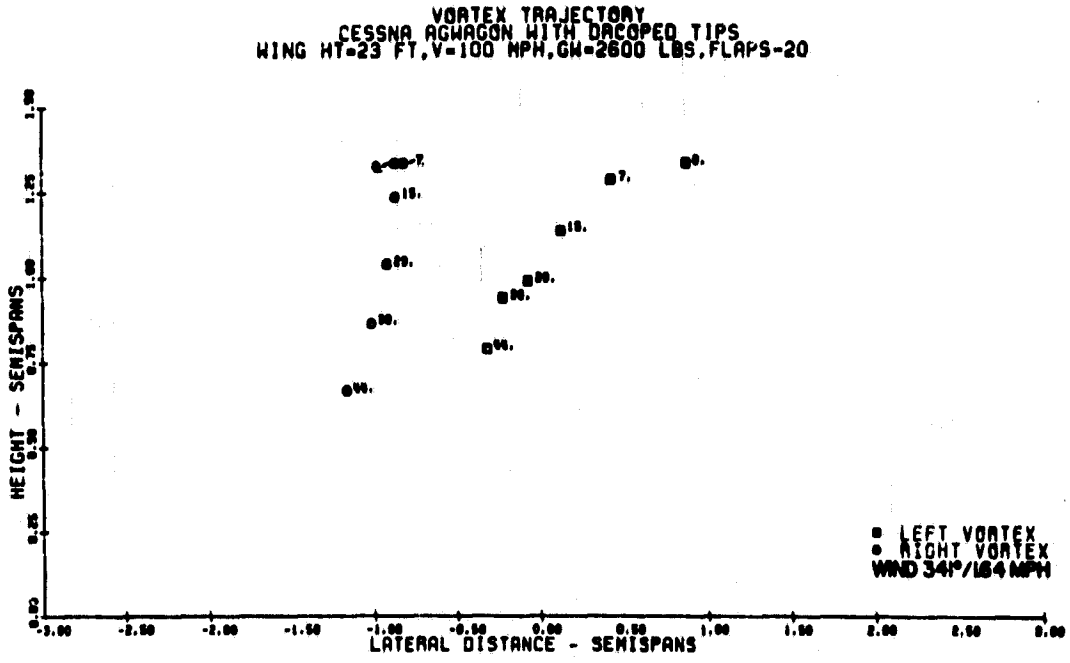

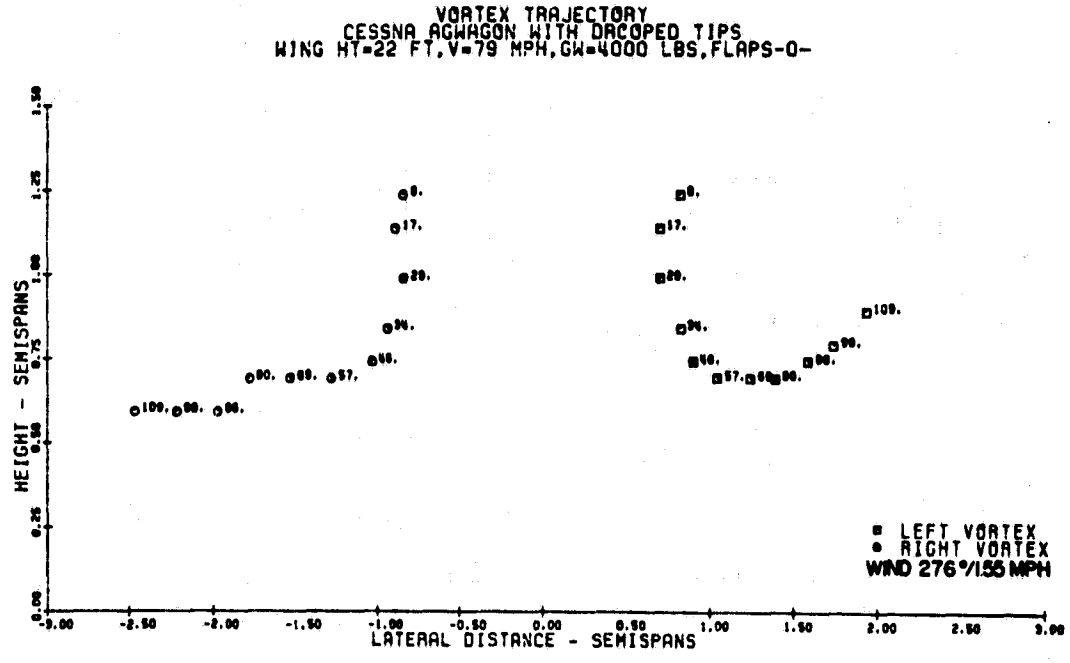

Figure 37. Tip Vortex Trajectory--Full Scale

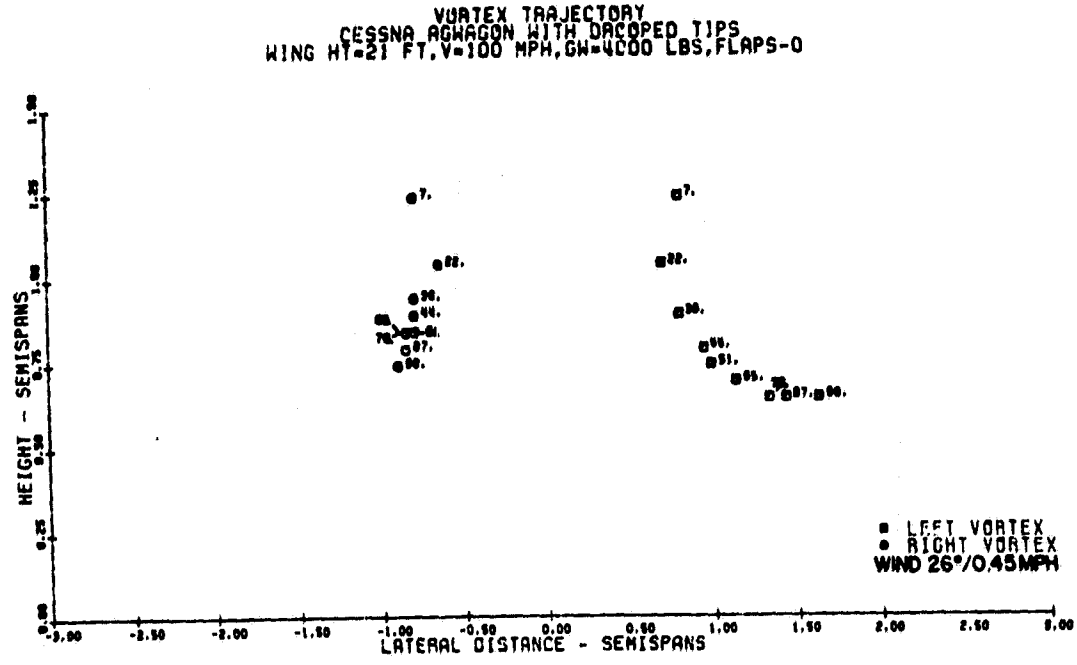

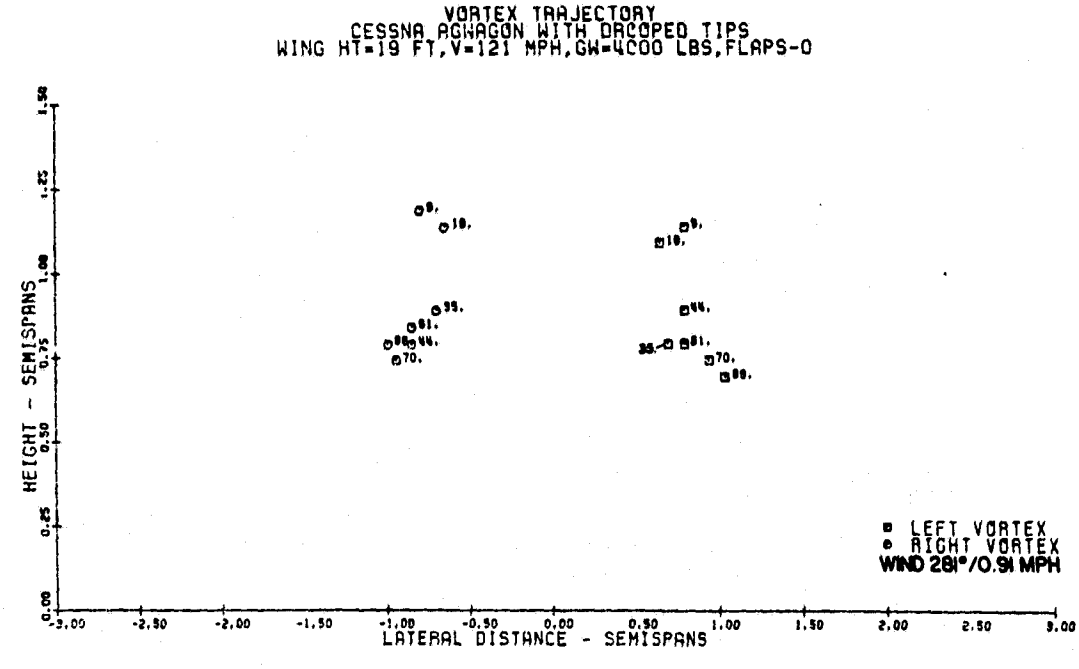

Figure 38. Tip Vortex Trajectory--Full Scale

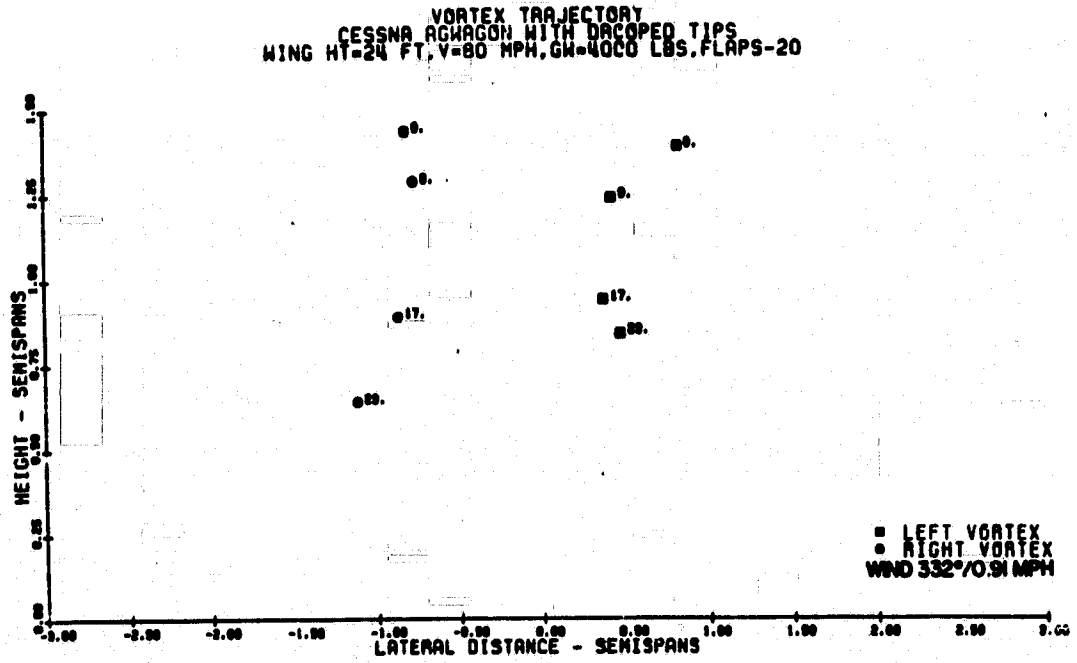

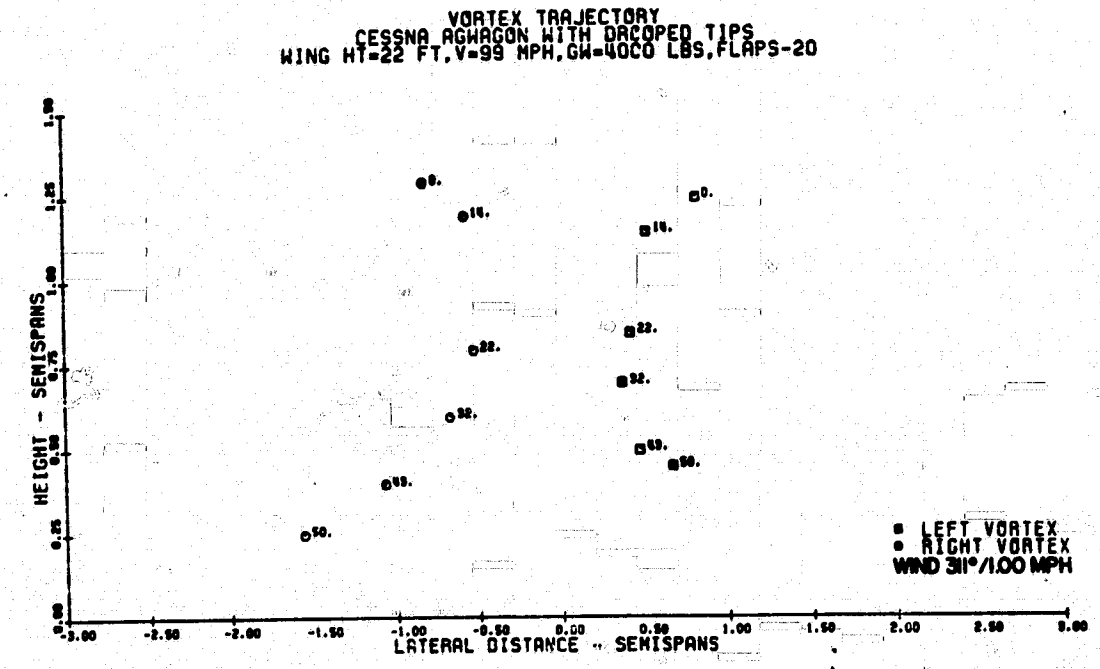

Figure 39. Tip Vortex Trajectory--Full Scale

Figure 40. Scale Model Agwagon

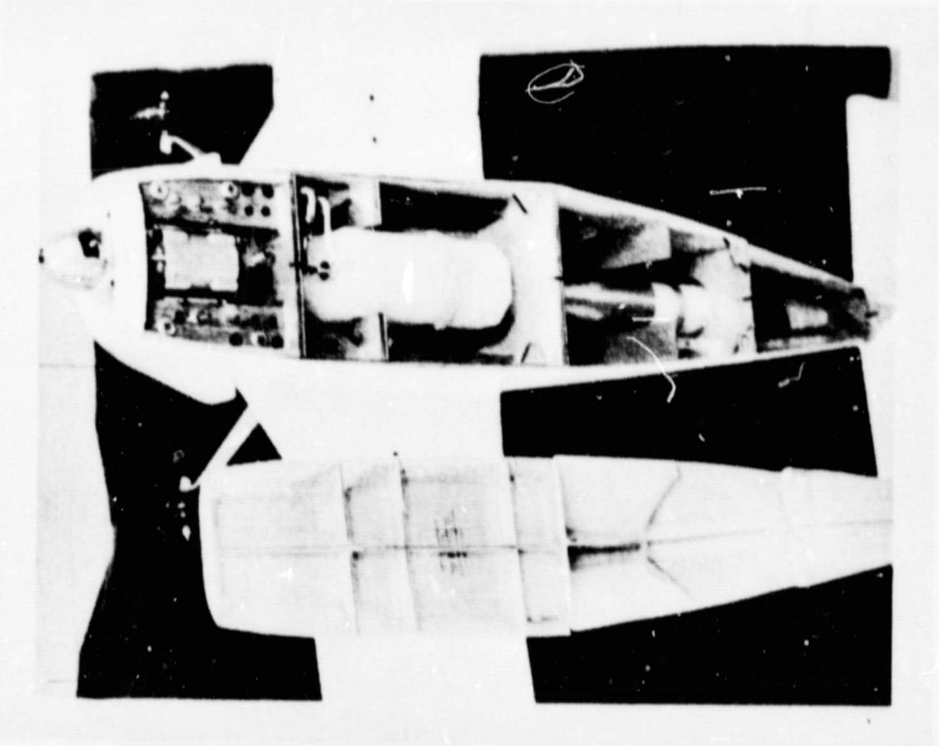

Figure 41. Scale Model Engine Installation

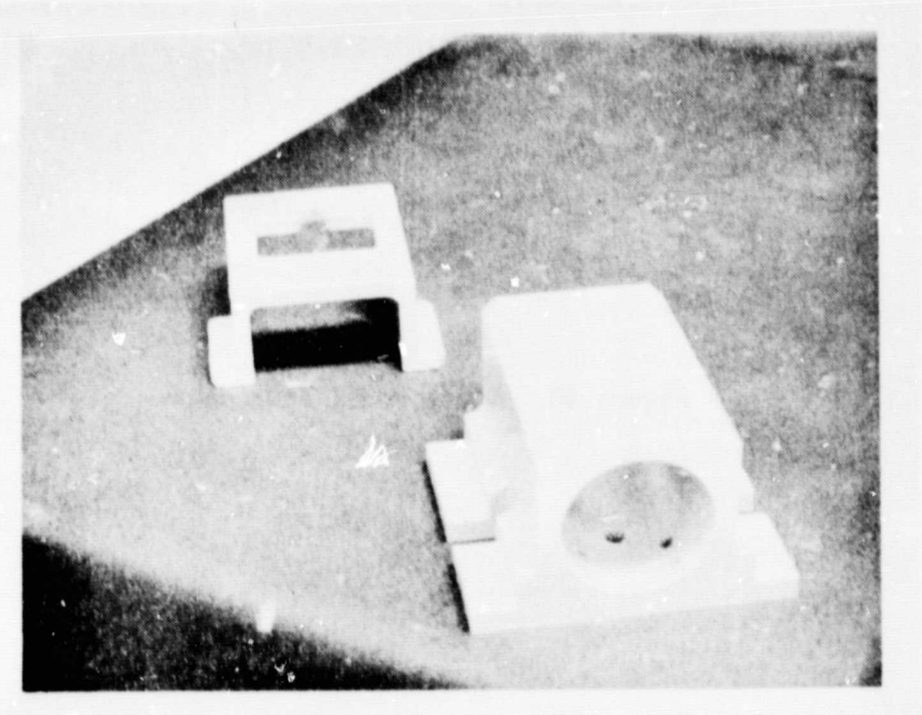

Figure 42. Model Adapter Blocks

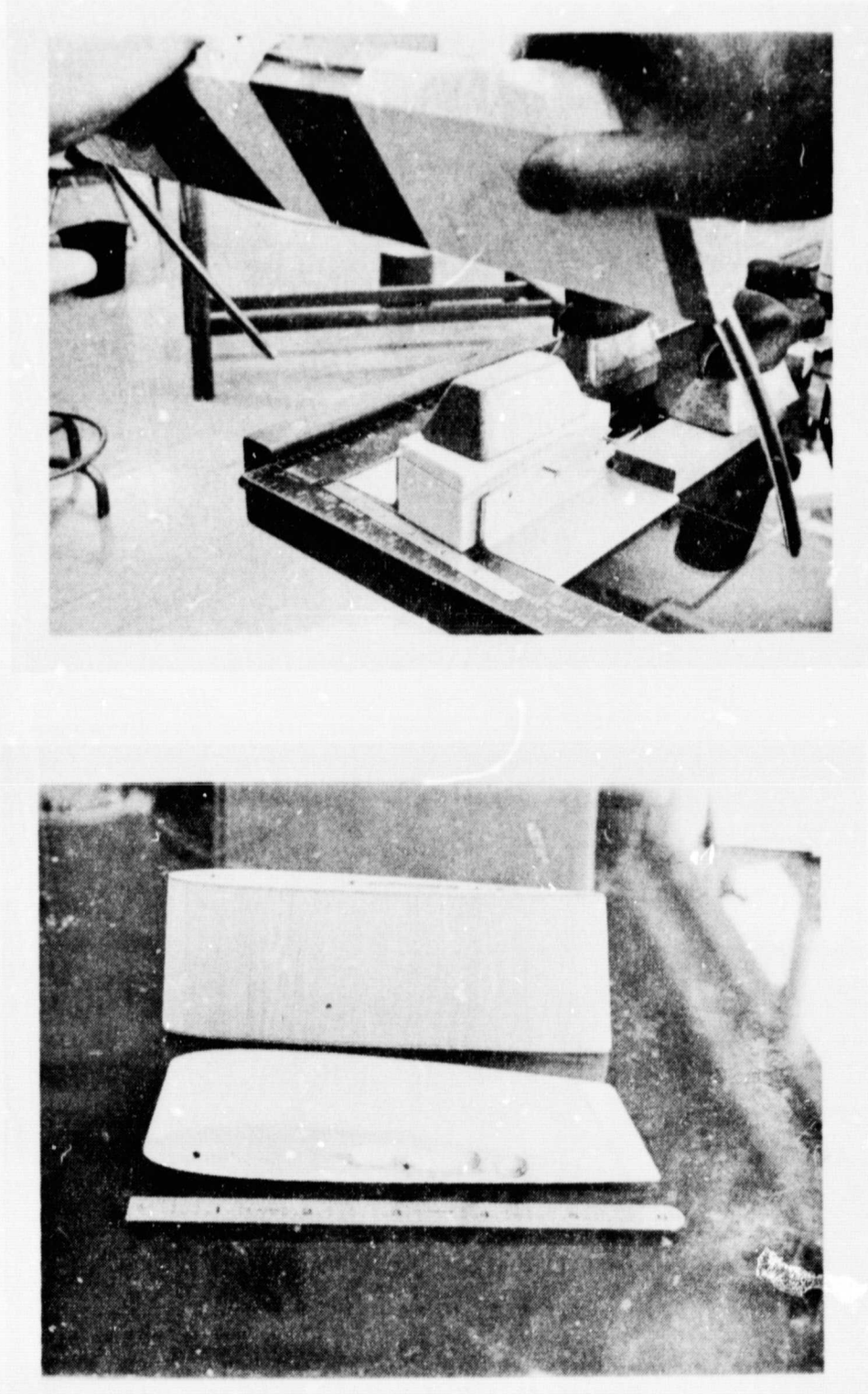

Figure 43. Model Wing Construction

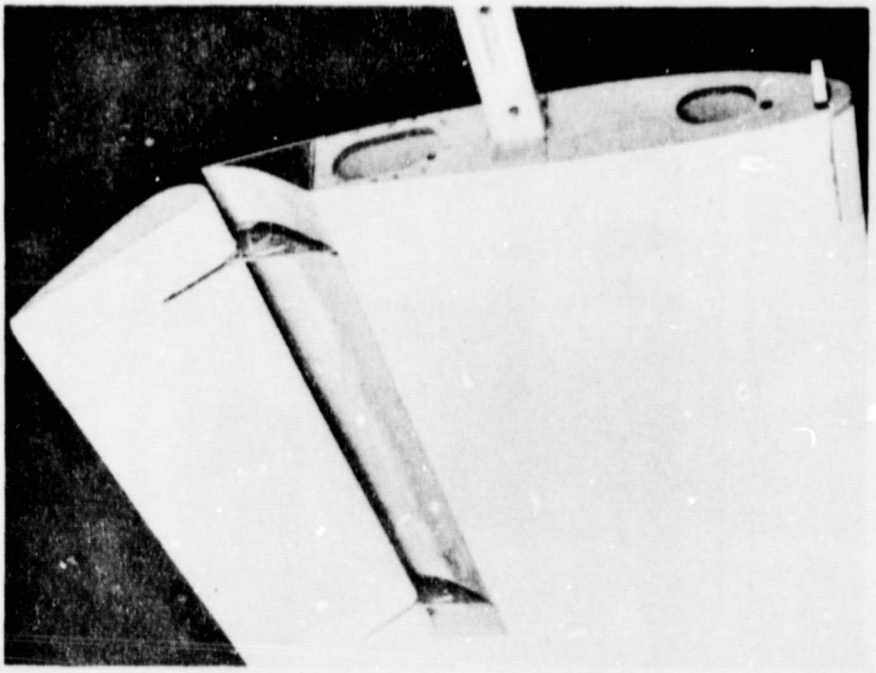

Figure 44. Model Wing with Flaps Extended

Figure 45. Model Support Strut and Boom

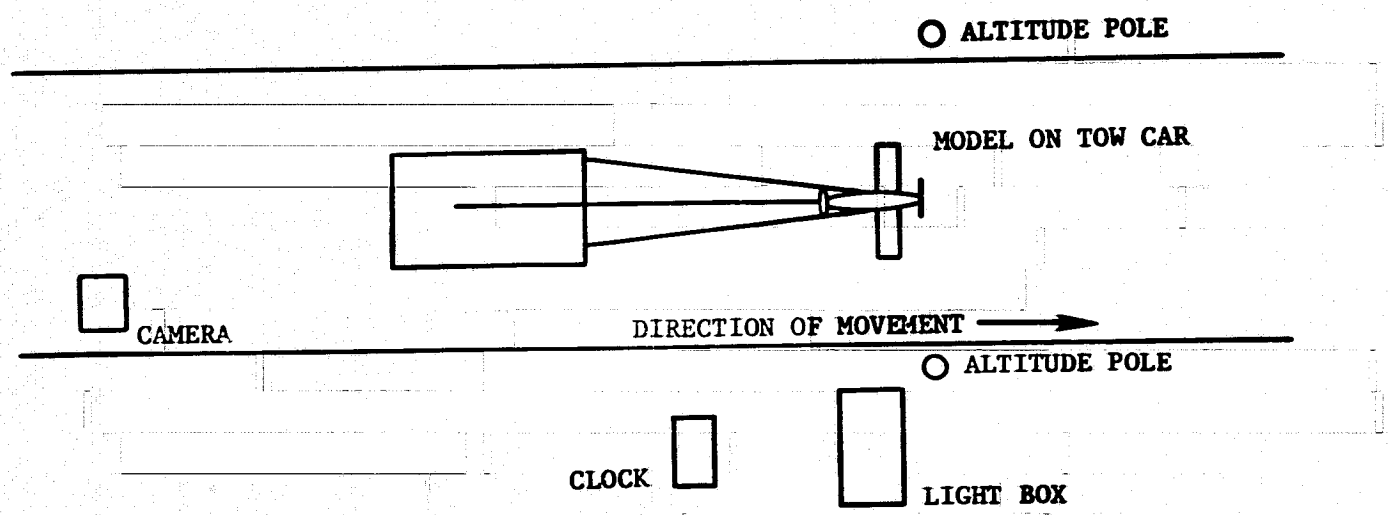

Figure 46. Model Flow Visualization Apparatus

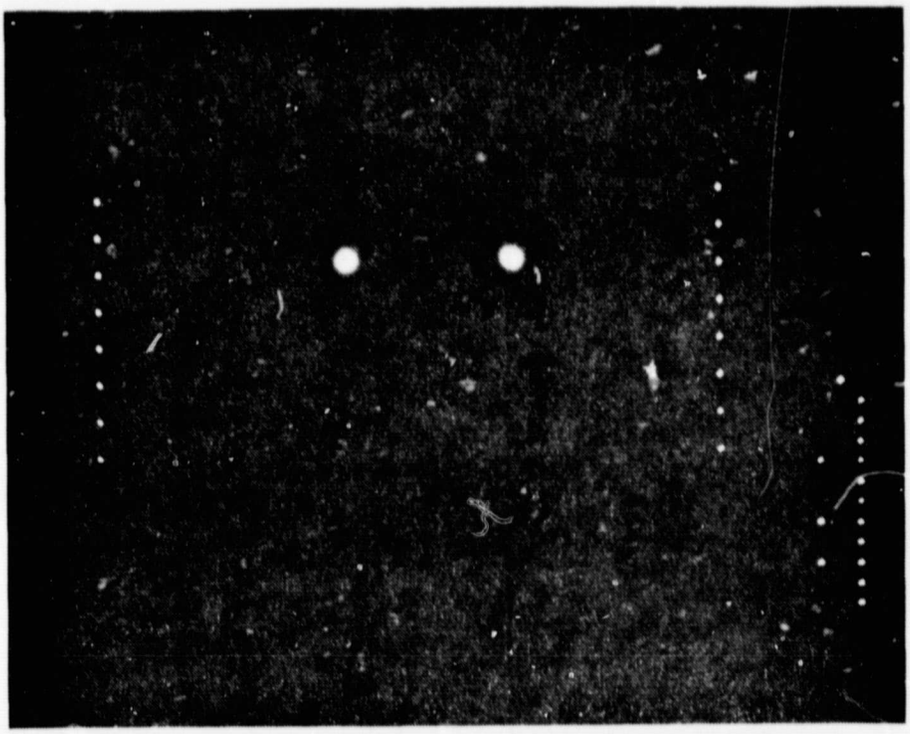

t = 0.0 sec.

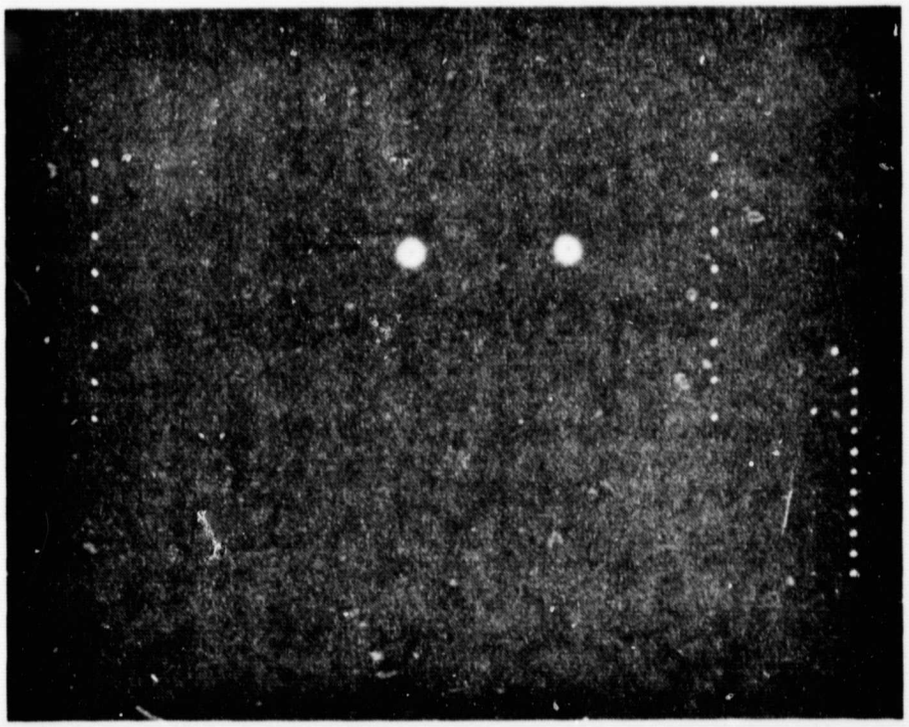

t = 0.6 sec.

Figure 47. Photo Sequence of Model Wing Tip Vortices

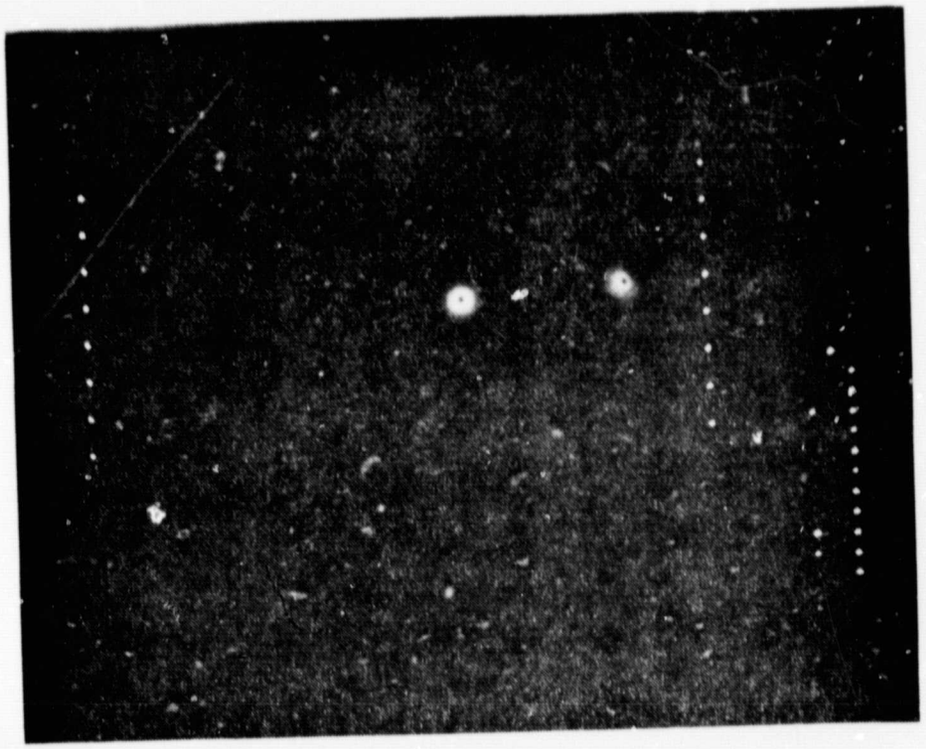

t = 1.2 sec.

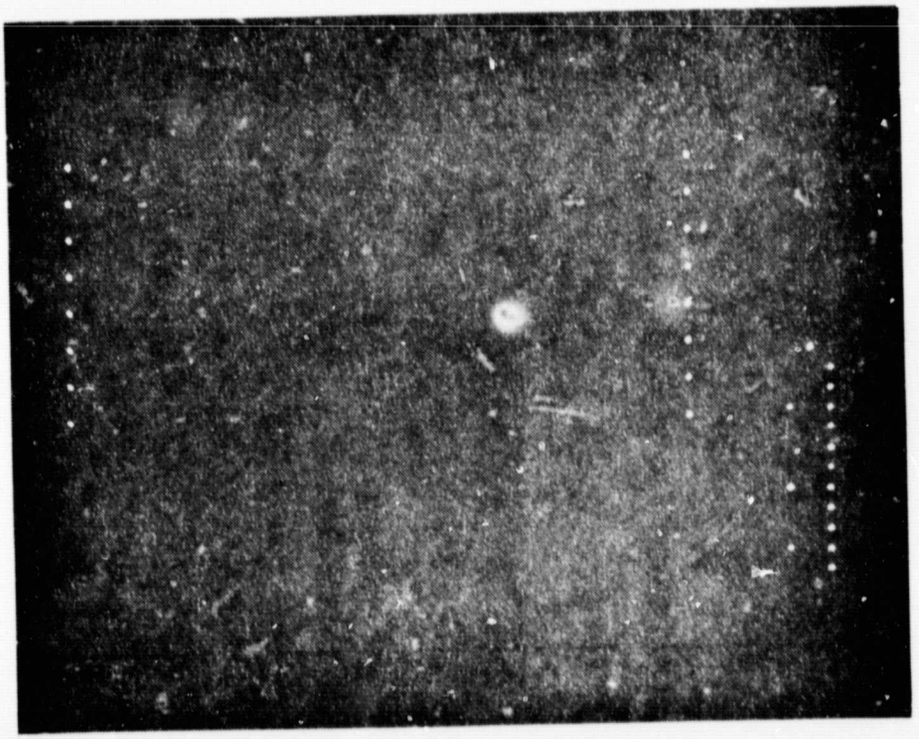

t = 1.8 sec.

Figure 47. Photo Sequence of Model Wing Tip Vortices

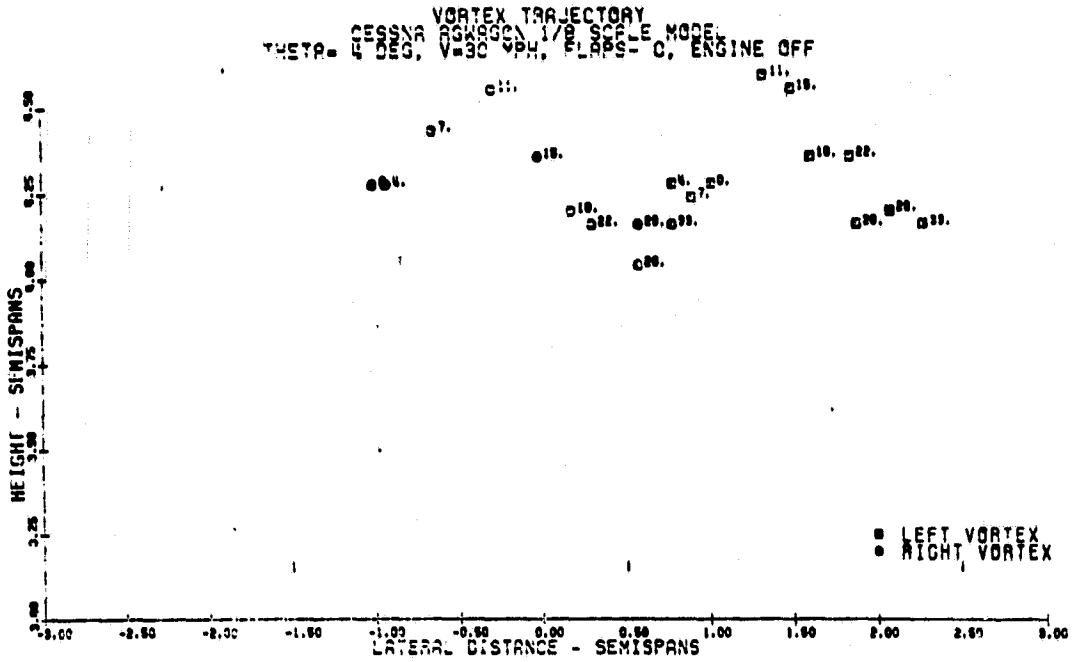

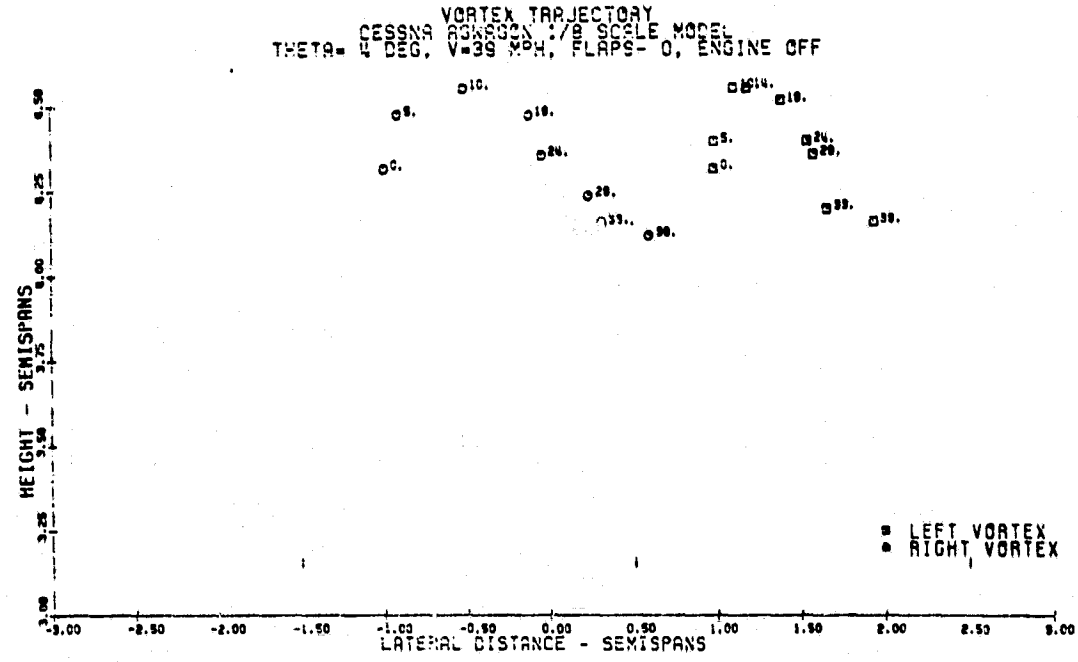

Figure 48. Tip Vortex Trajectory--1/8 Scale

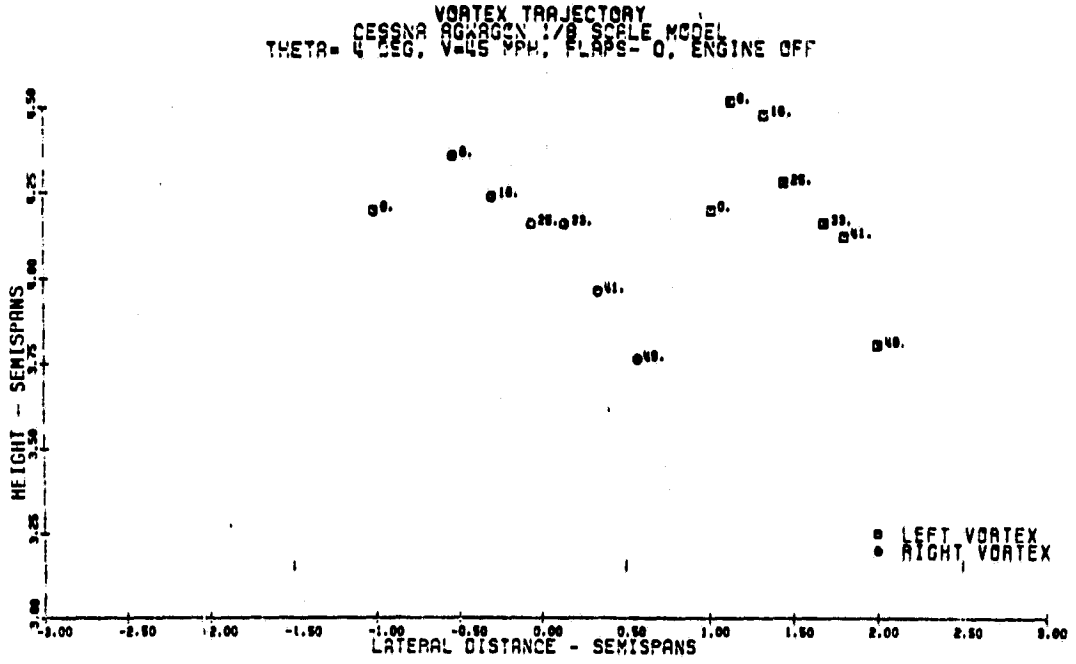

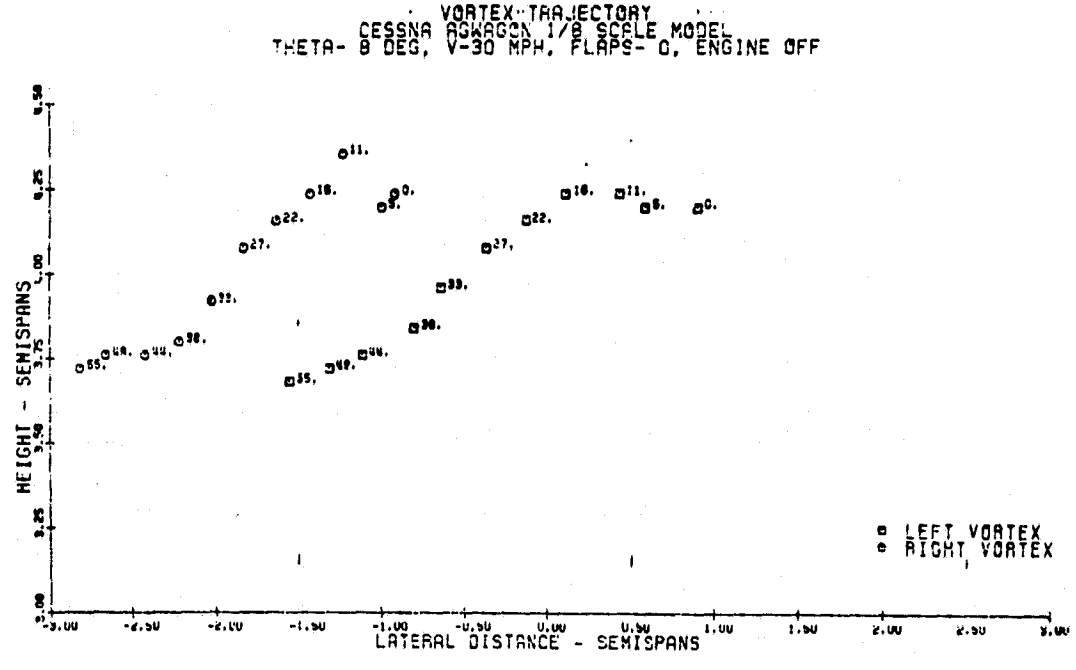

Figure 49. Tip Vortex Trajectory--1/8 Scale

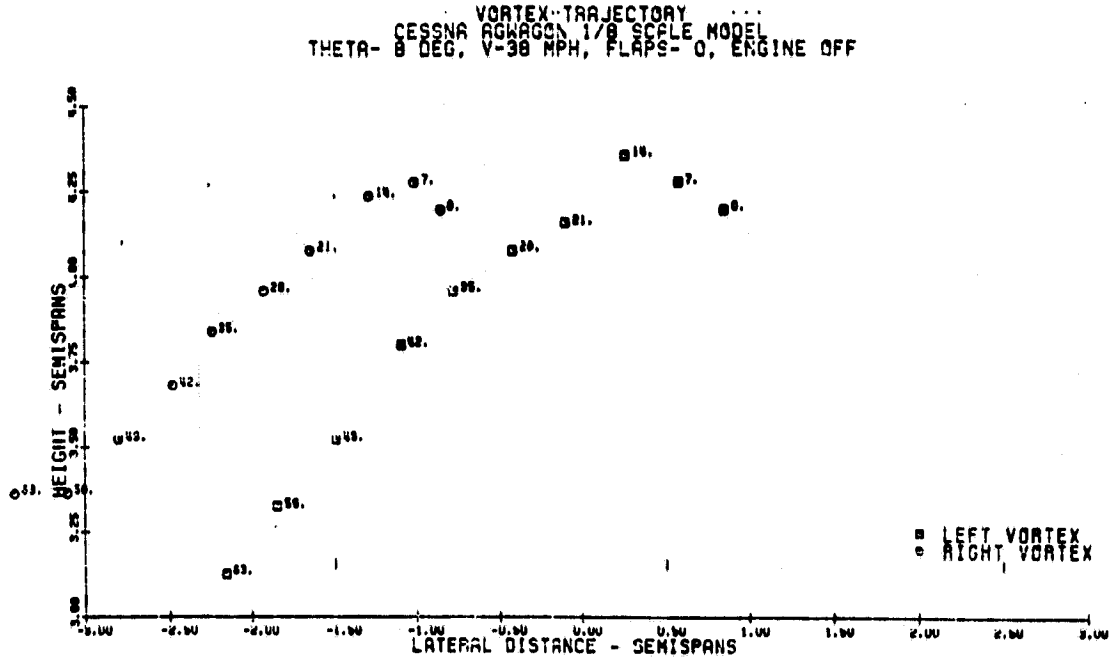

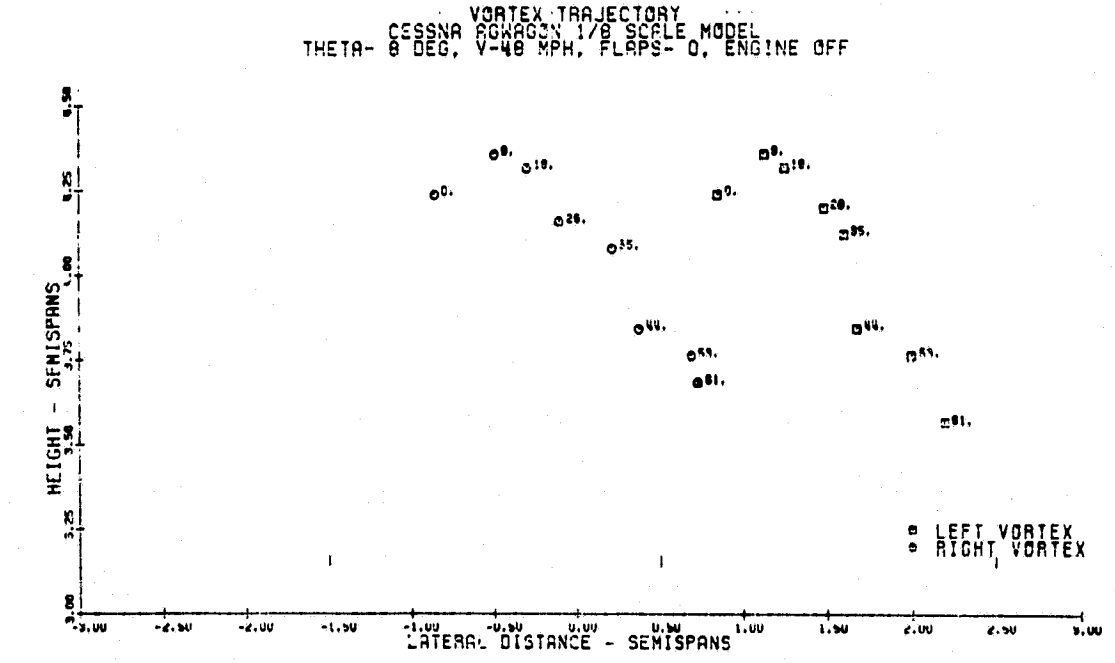

Figure 50. Tip Vortex Trajectory--1/8 Scale

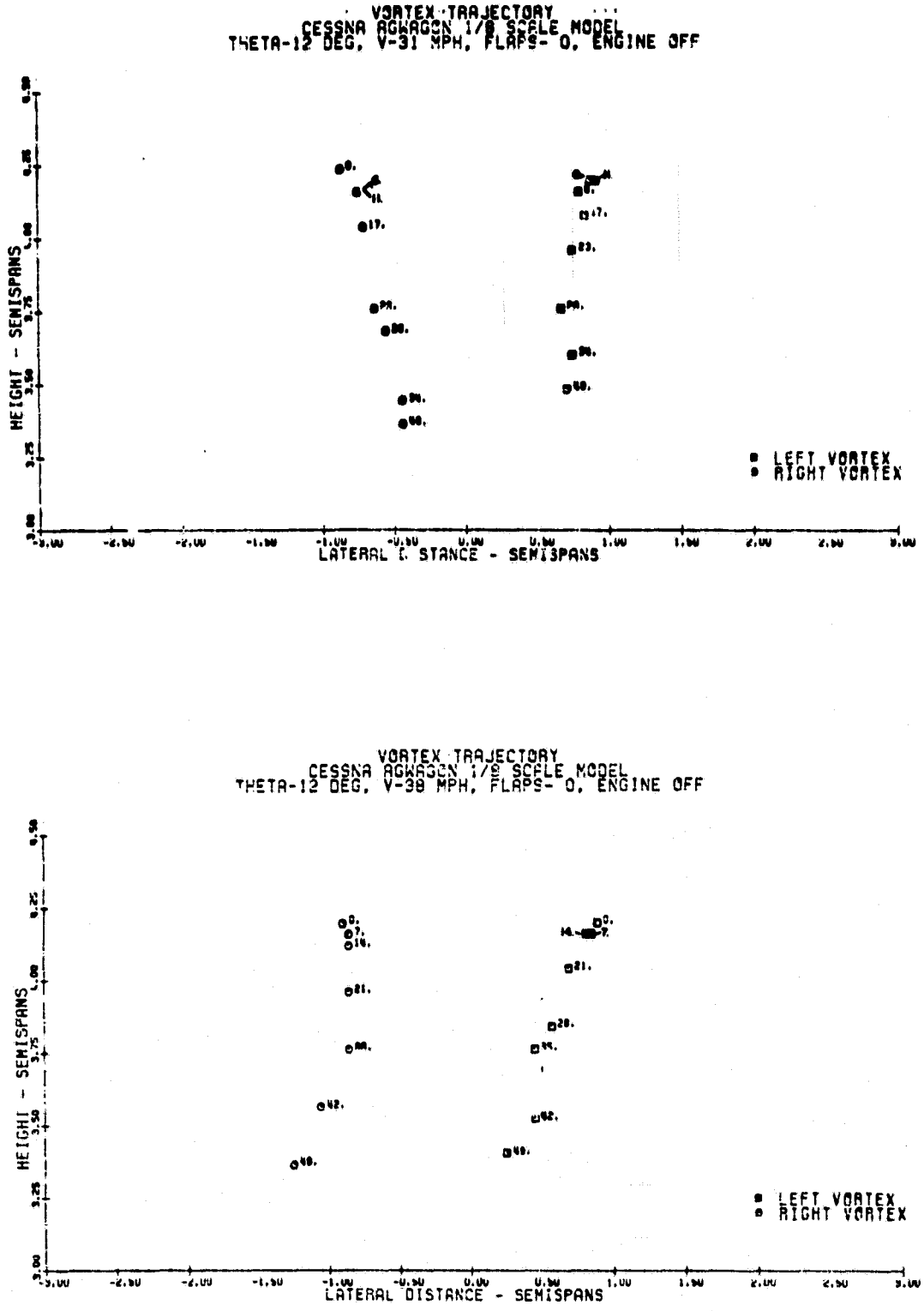

Figure 51. Tip Vortex Trajectory--1/8 Scale

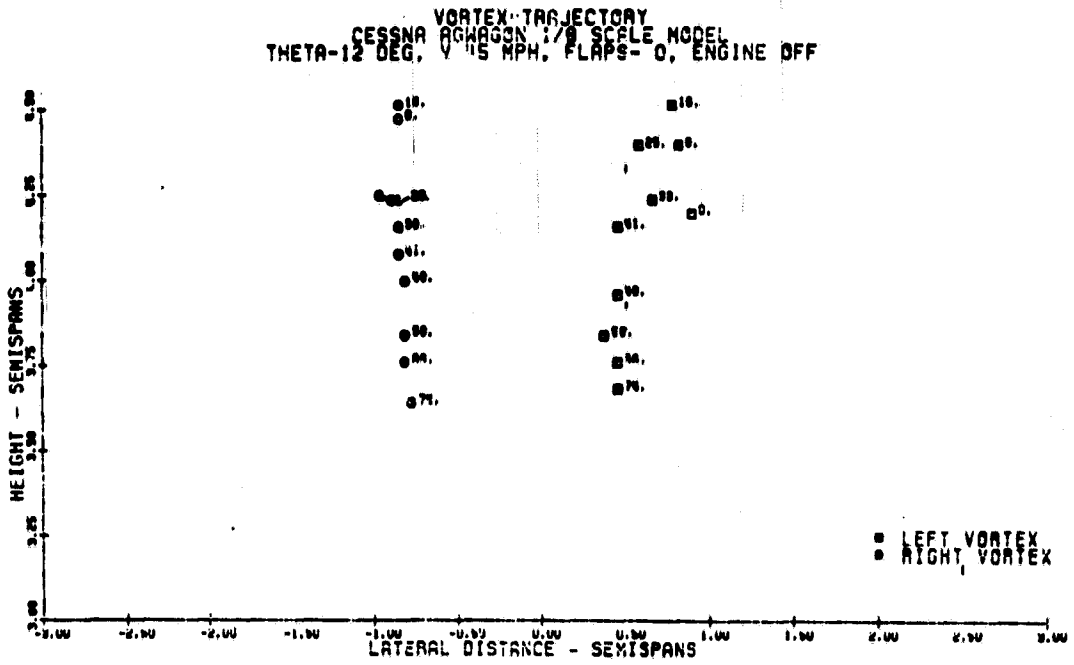

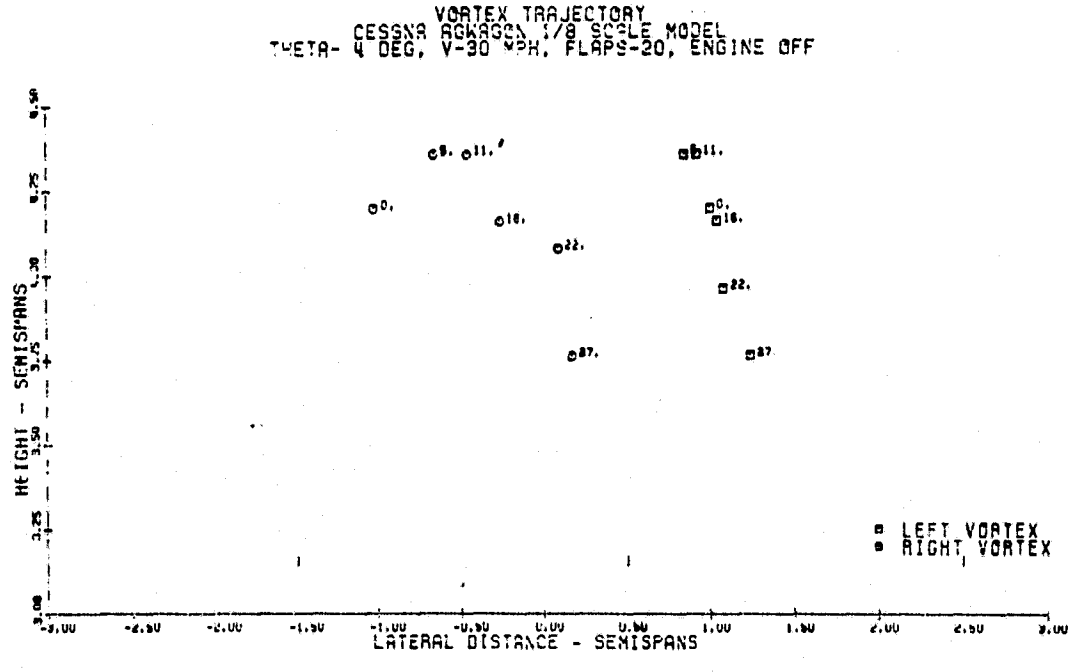

Figure 53. Tip Vortex Trajectory--1/8 Scale

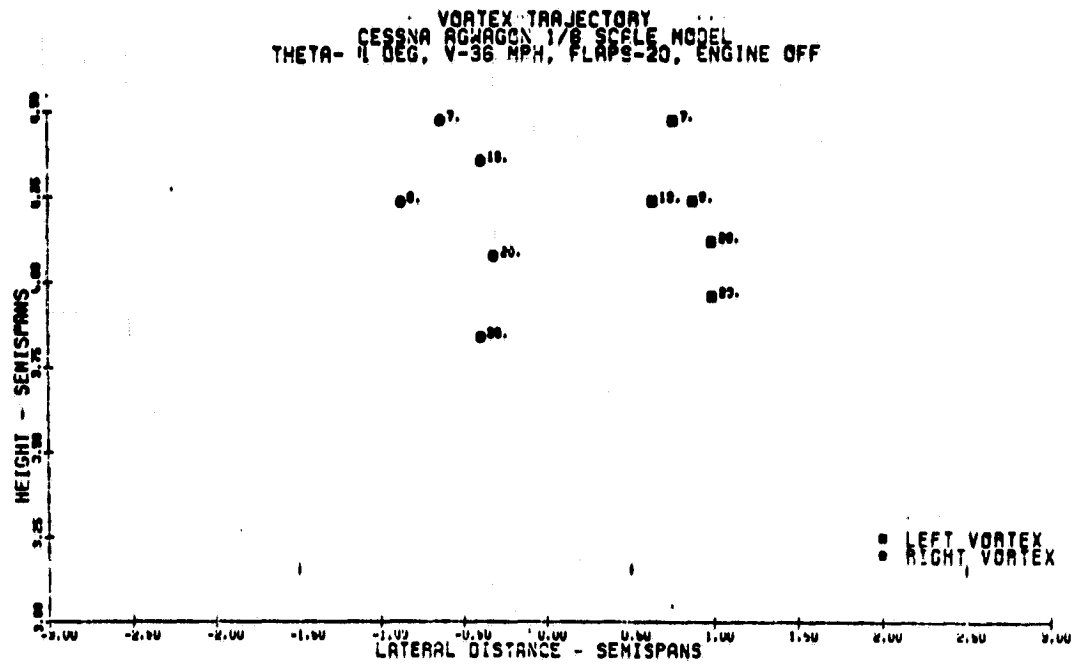

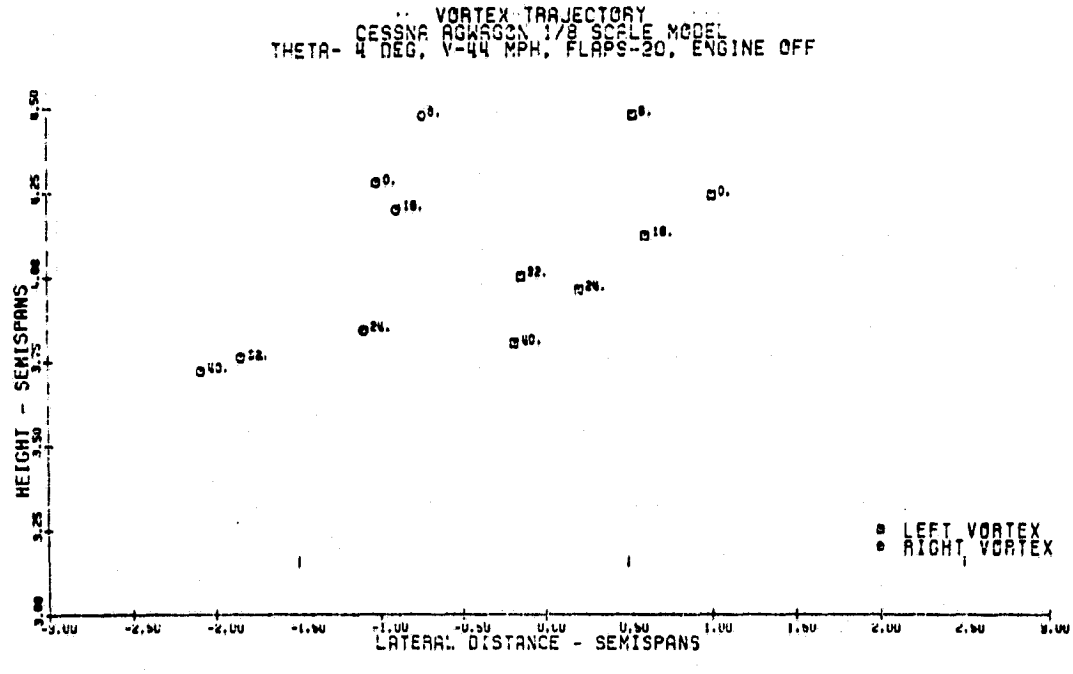

Figure 53. Tip Vortex Trajectory--1/8 Scale

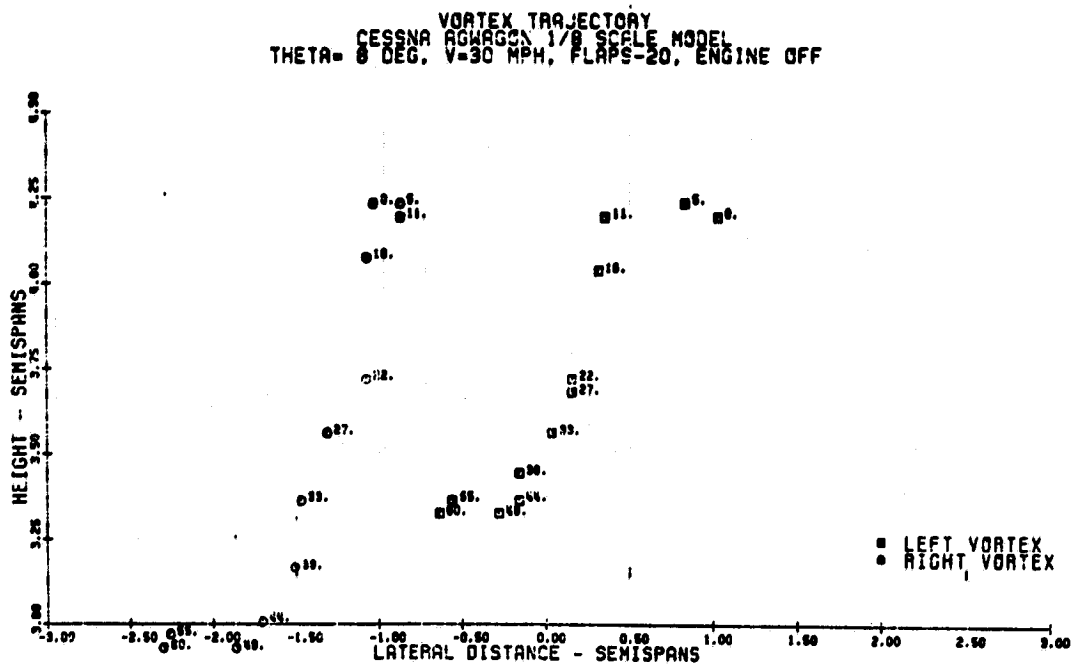

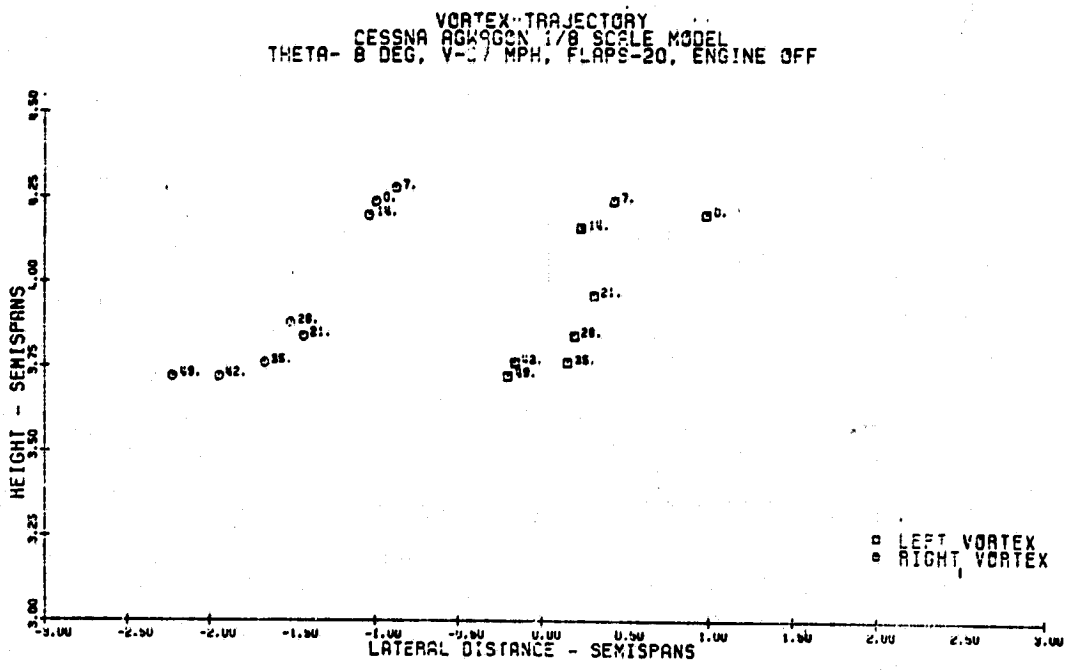

Figure 54. Tip Vortex Trajectory--1/8 Scale

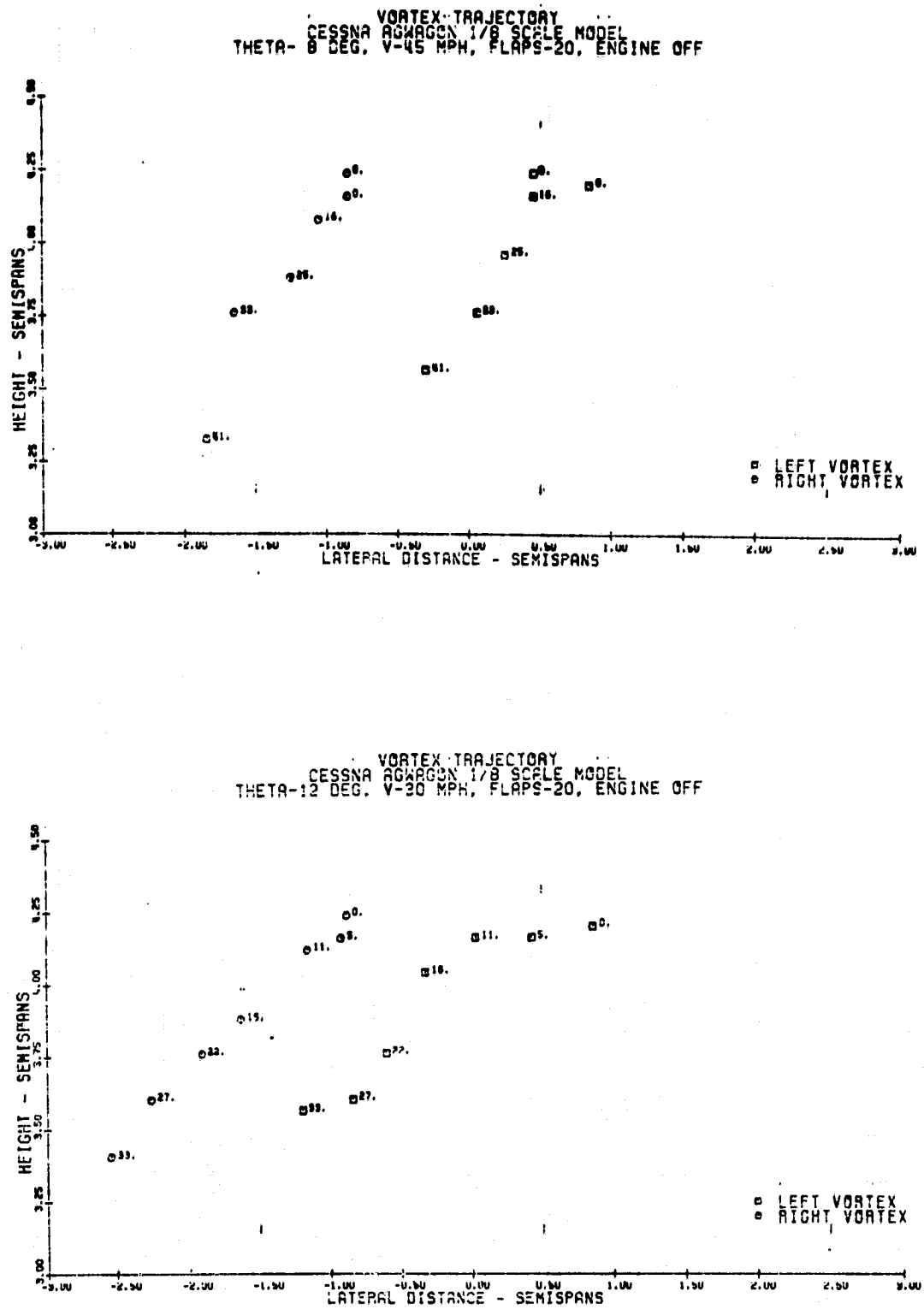

Figure 55. Tip Vortex Trajectory--1/8 Scale

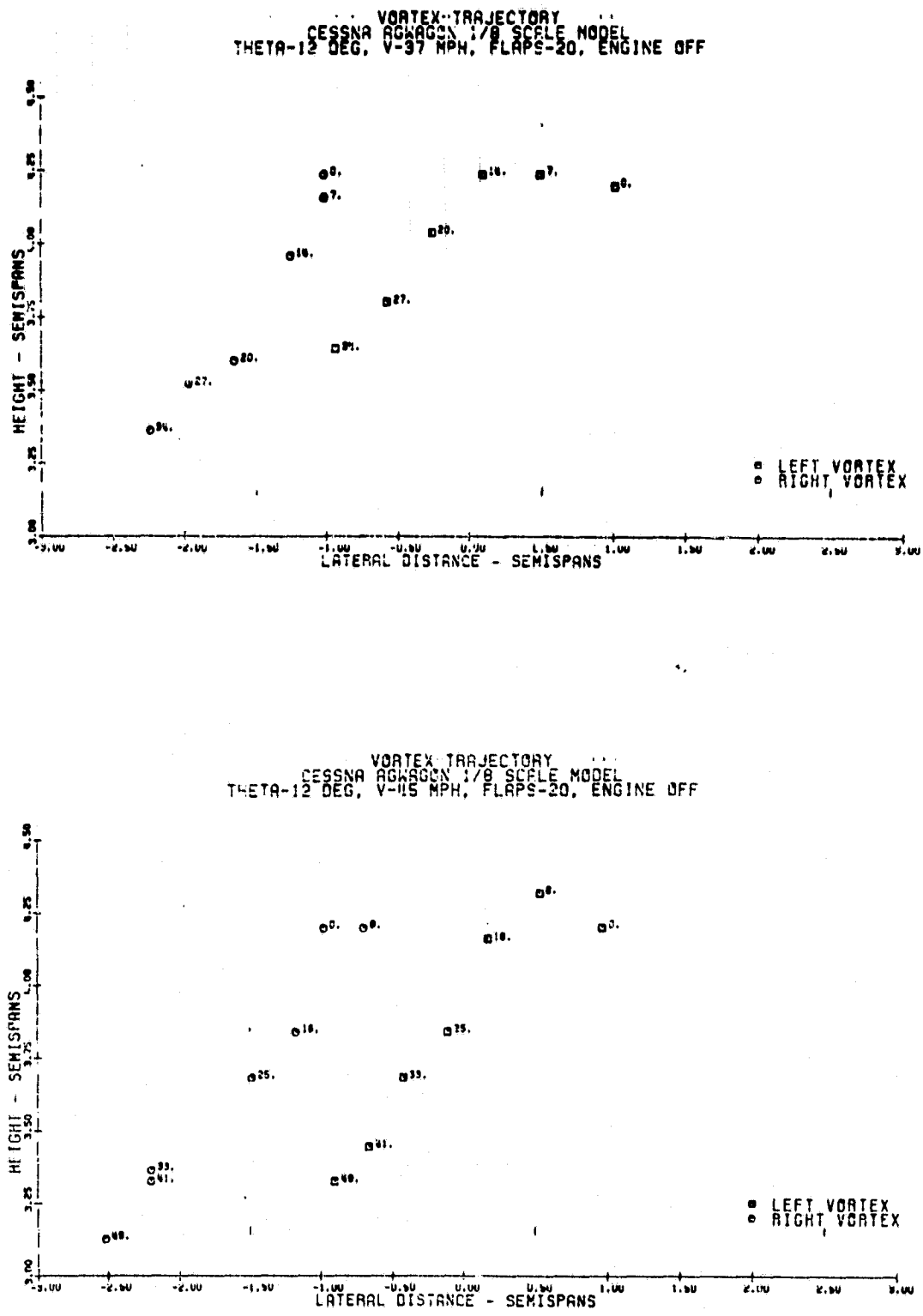

Figure 56. Tip Vortex Trajectory--1/8 Scale

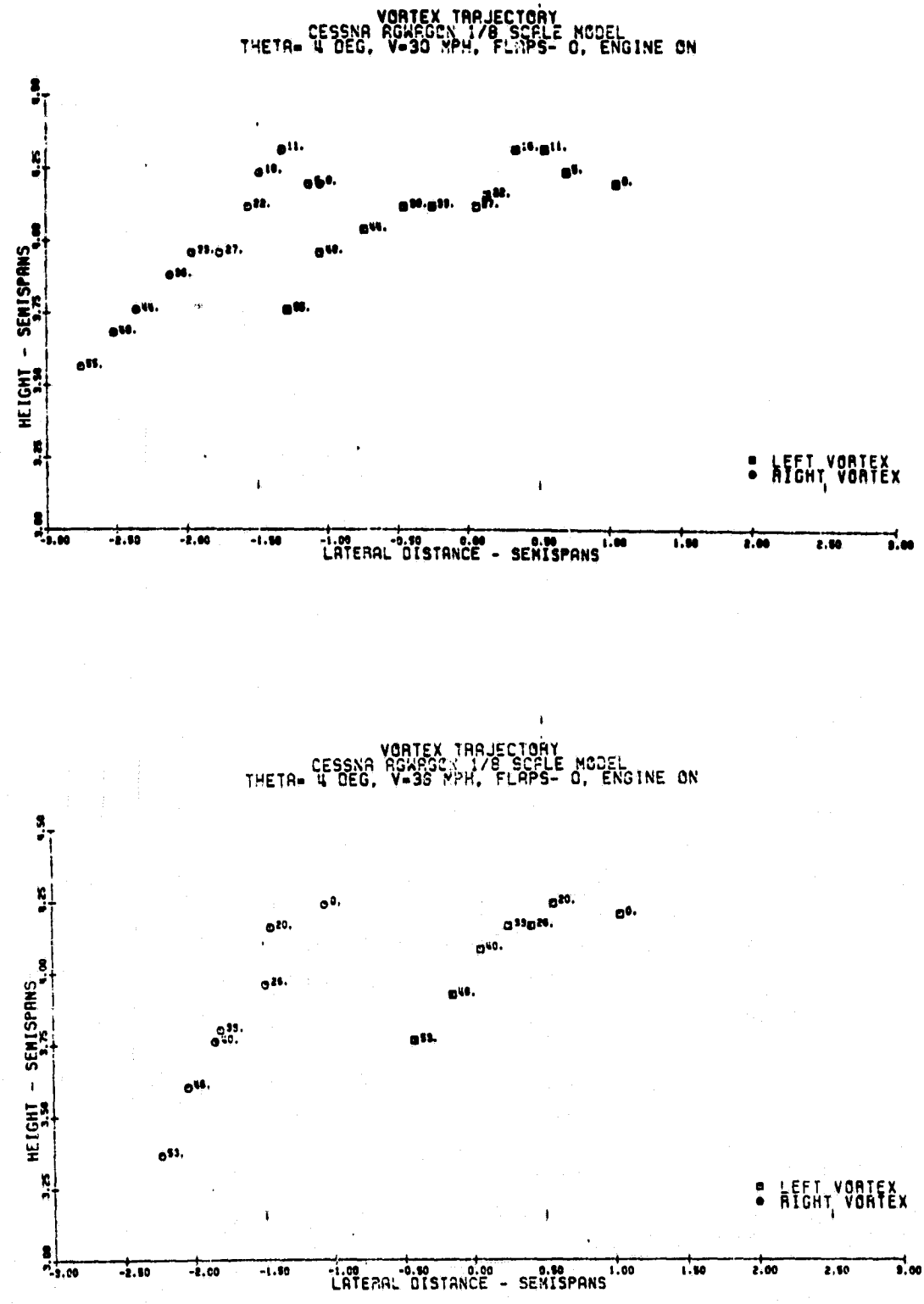

Figure 57. Tip Vortex Trajectory--1/8 Scale

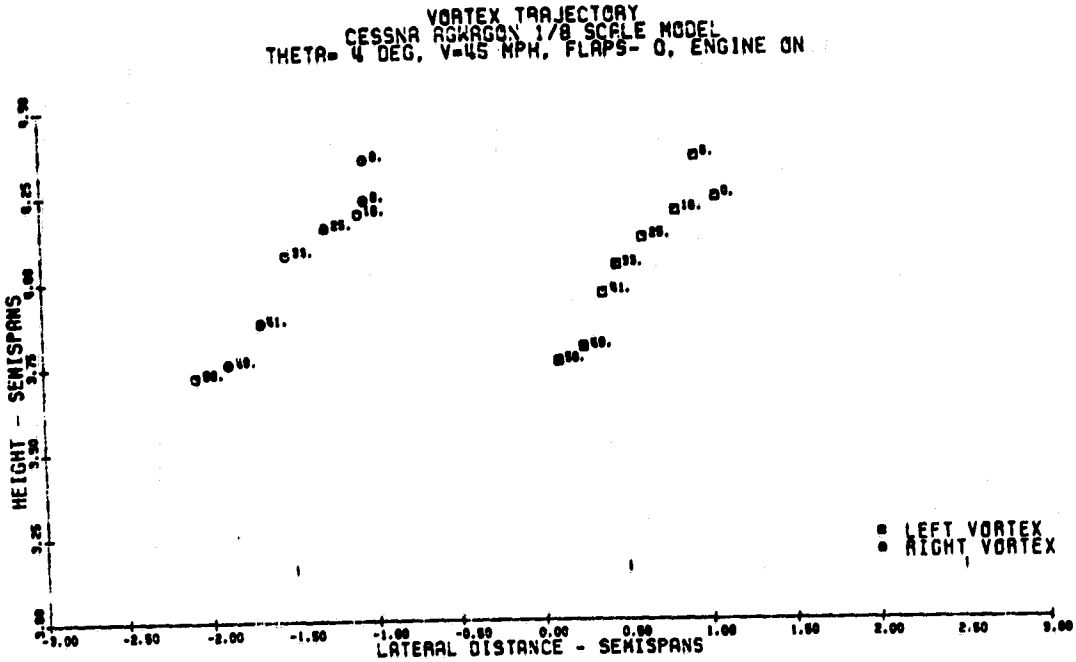

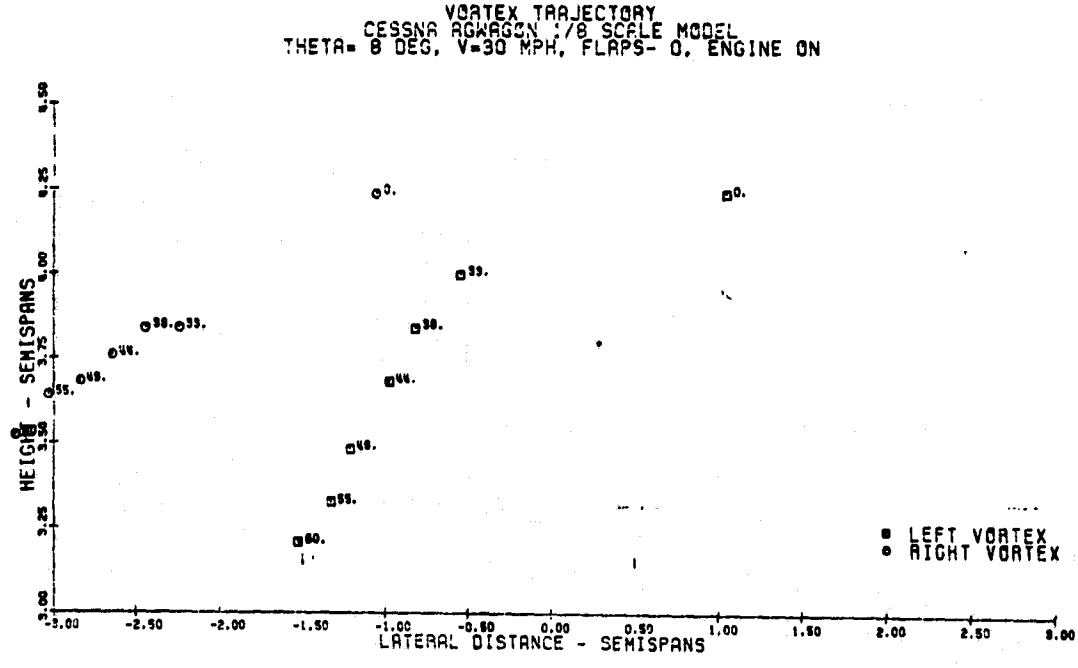

Figure 58. Tip Vortex Trajectory--1/8 Scale

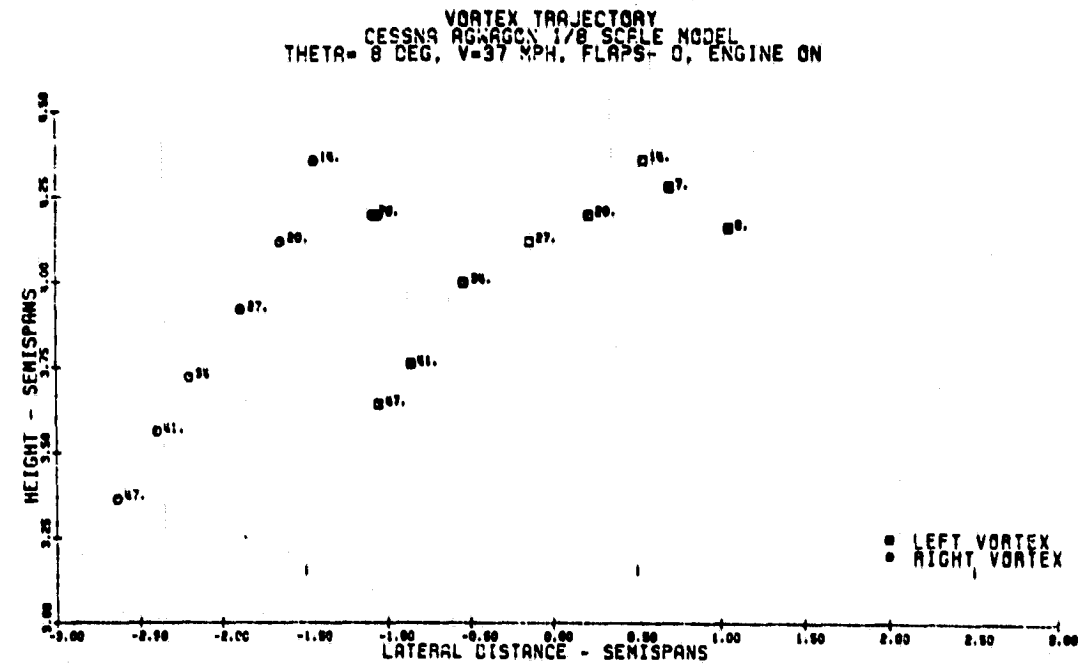

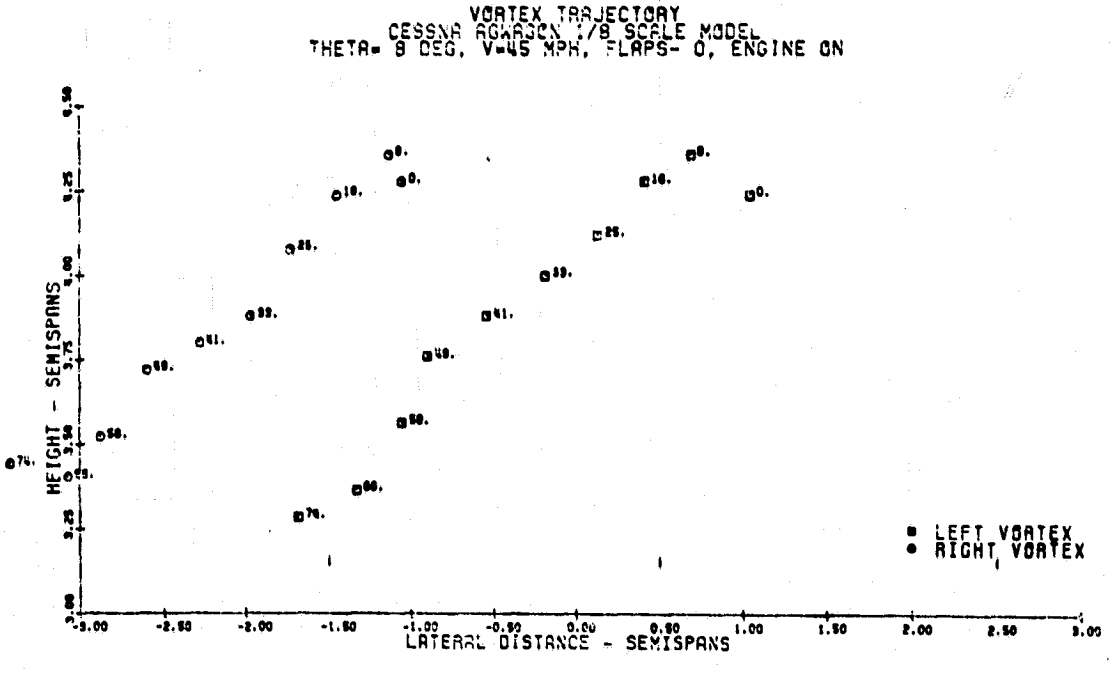

Figure 59. Tip Vortex Trajectory--1/8 Scale

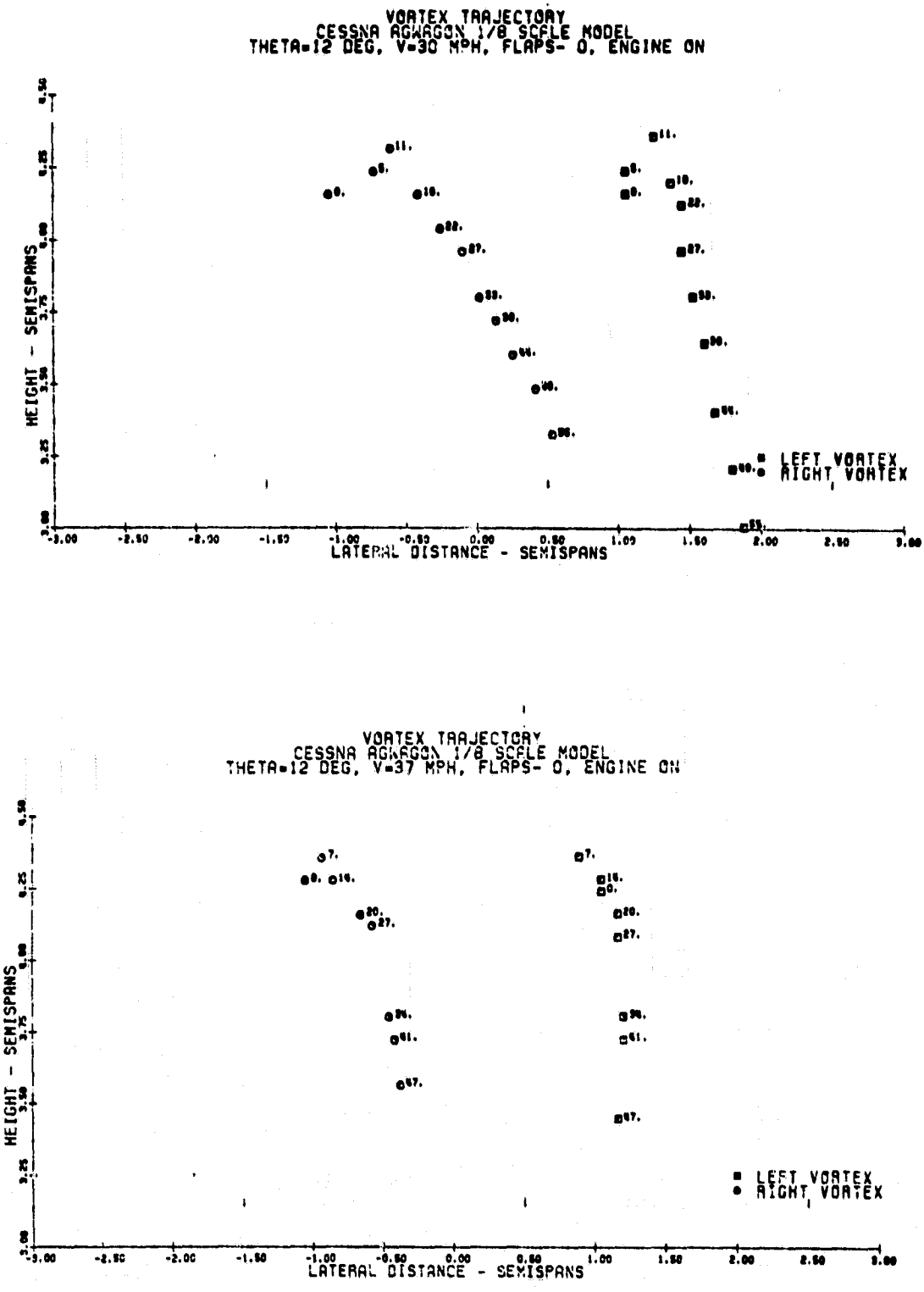

Figure 60. Tip Vortex Trajectory--1/8 Scale

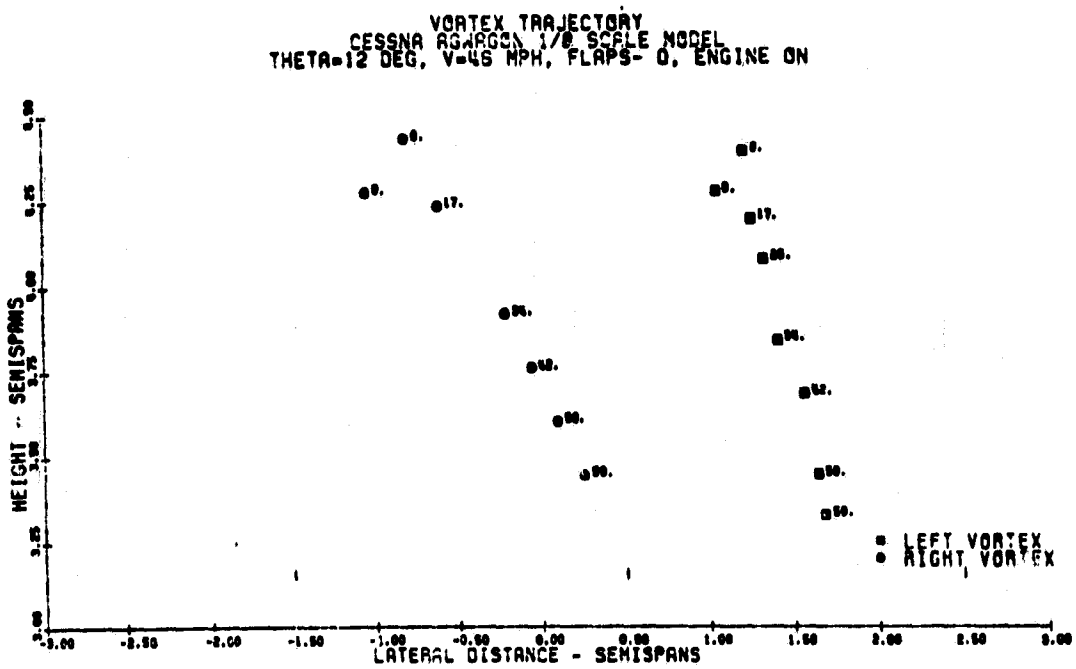

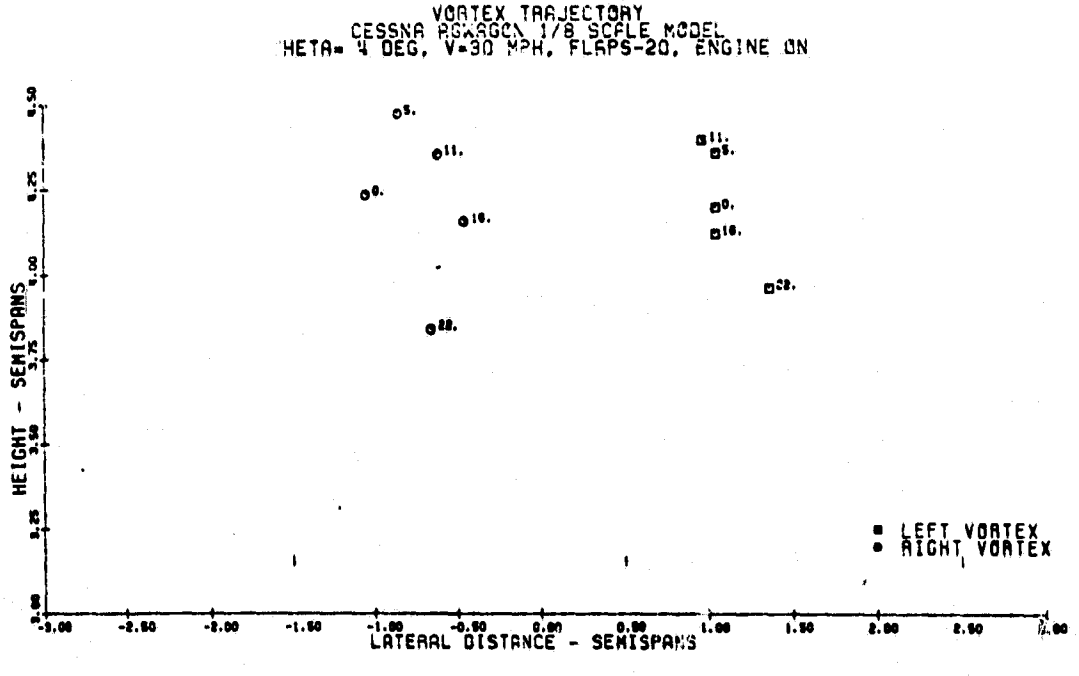

Figure 61. Tip Vortex Trajectory--1/8 Scale

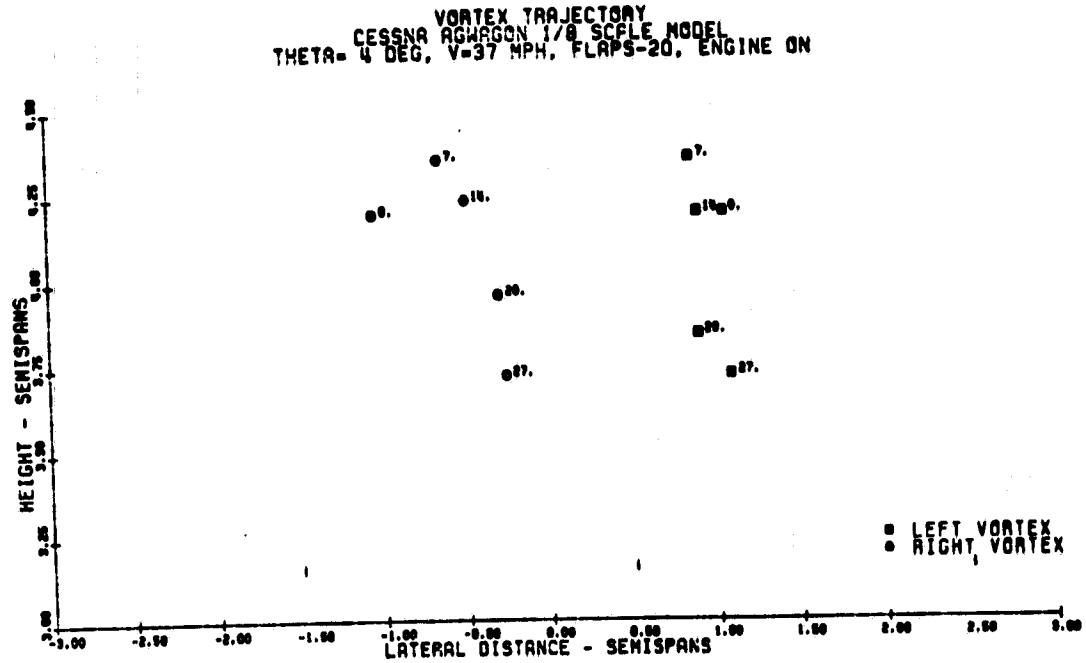

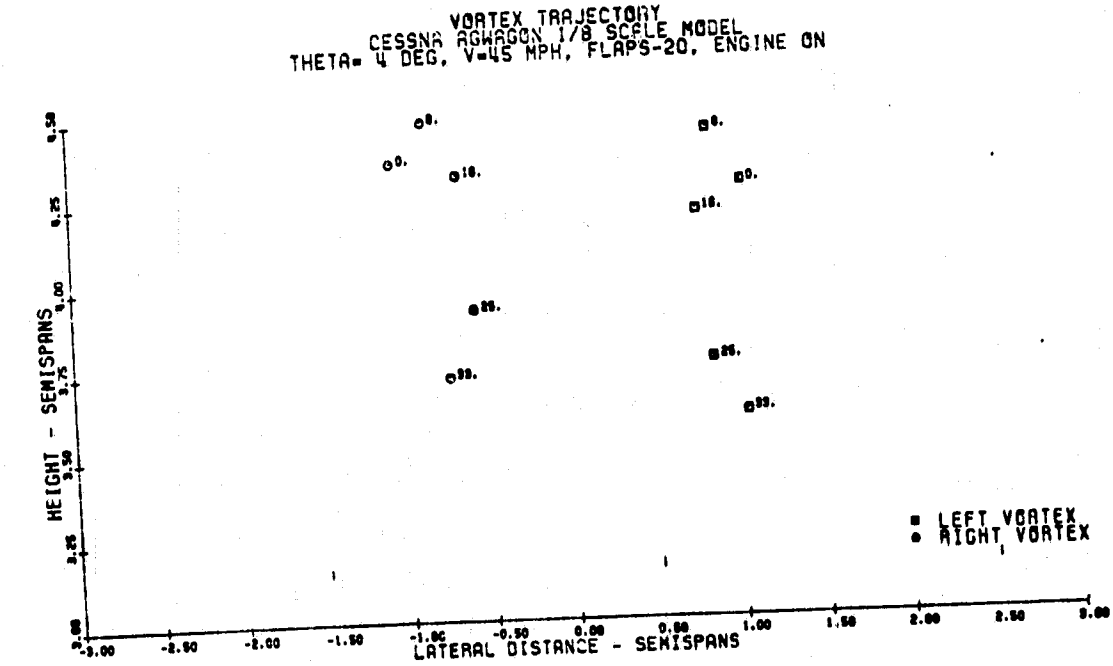

Figure 62. Tip Vortex Trajectory--1/8 Scale

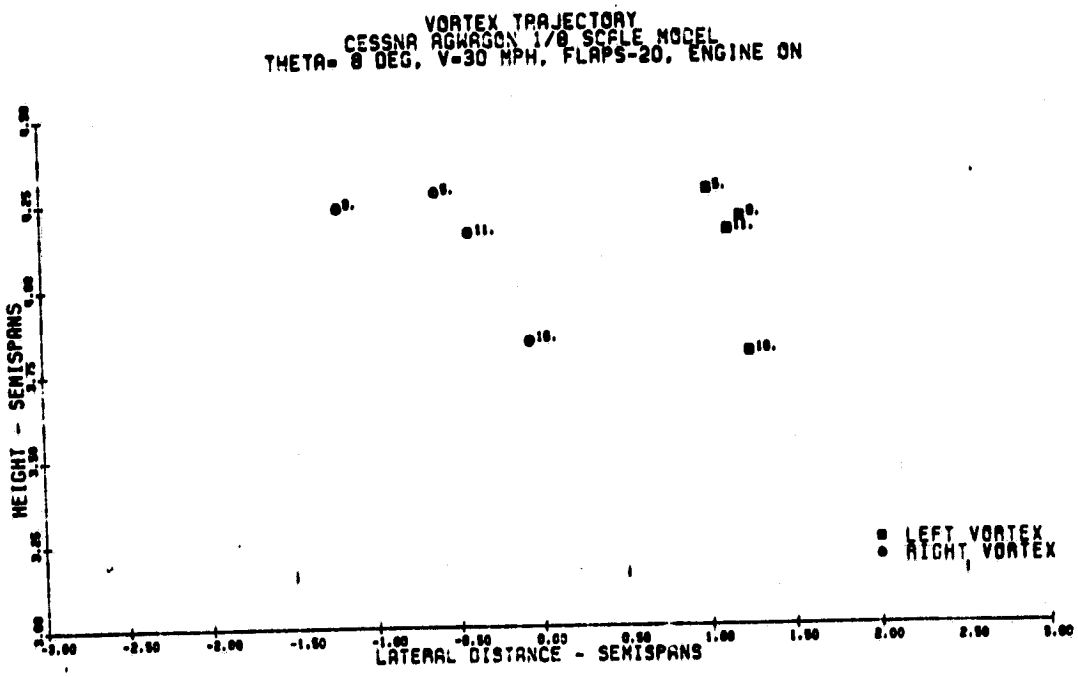

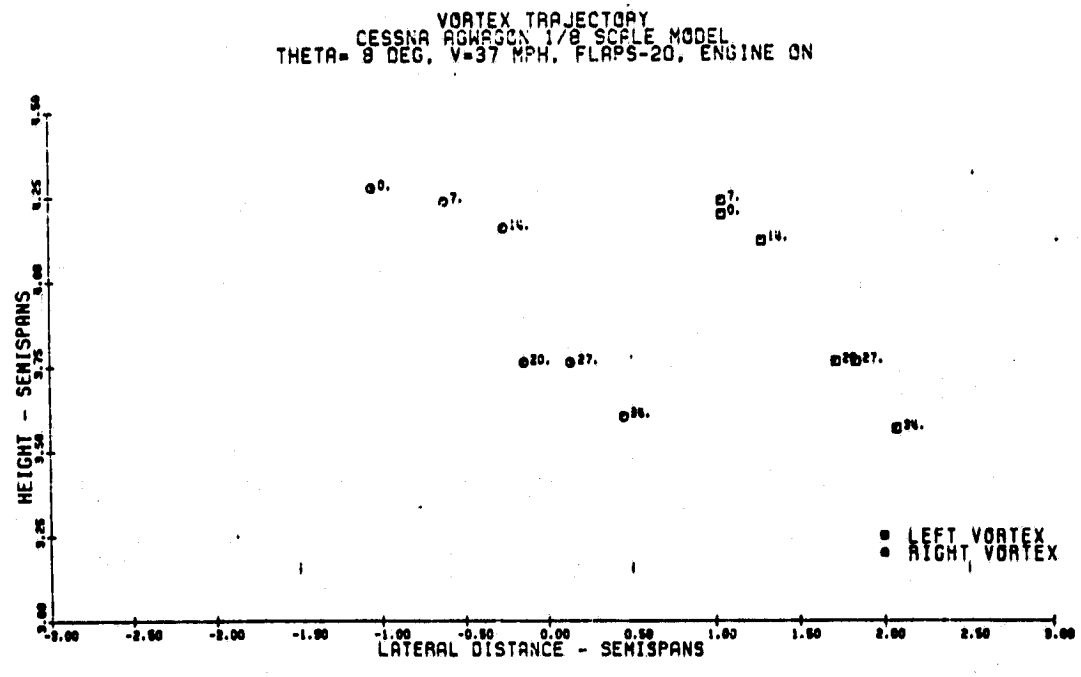

Figure 63. Tip Vortex Trajectory--1/8 Scale

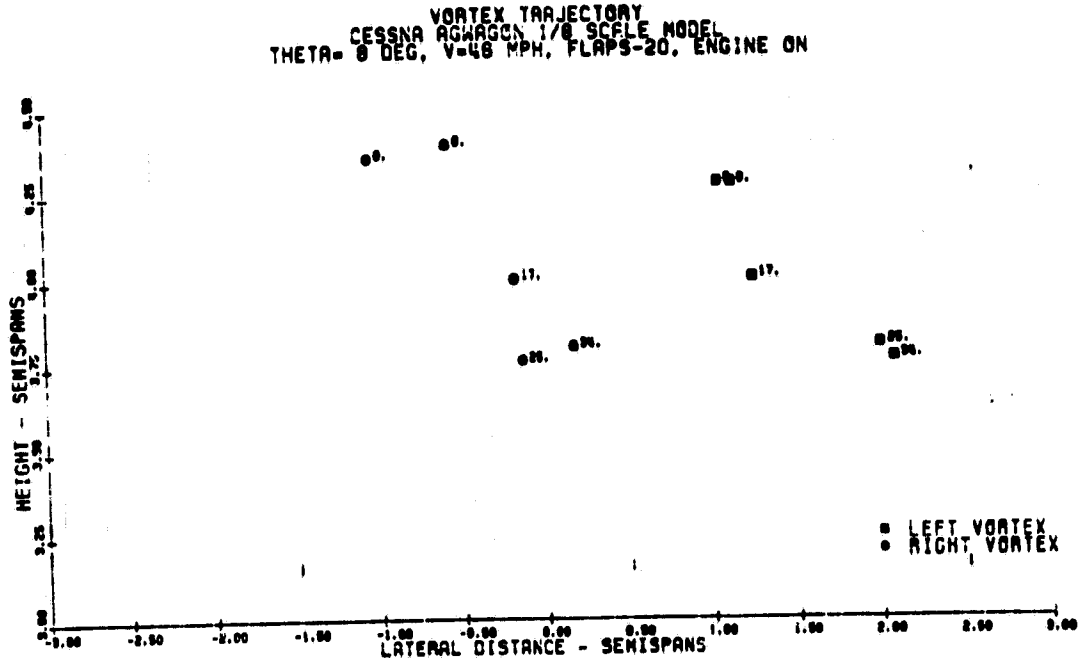

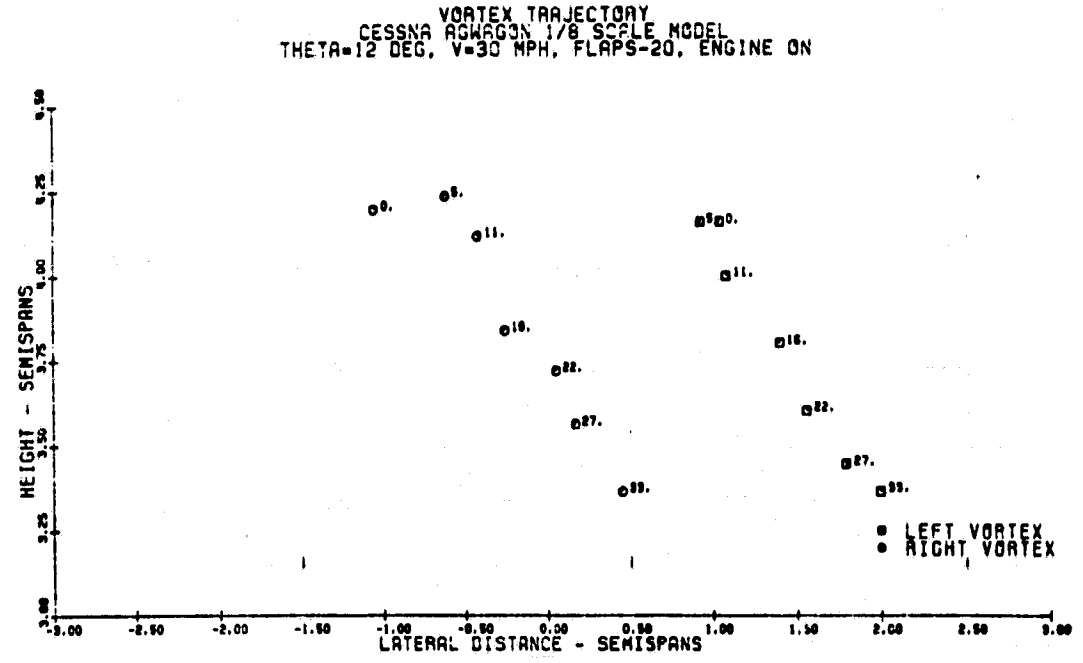

Figure 64. Tip Vortex Trajectory--1/8 Scale

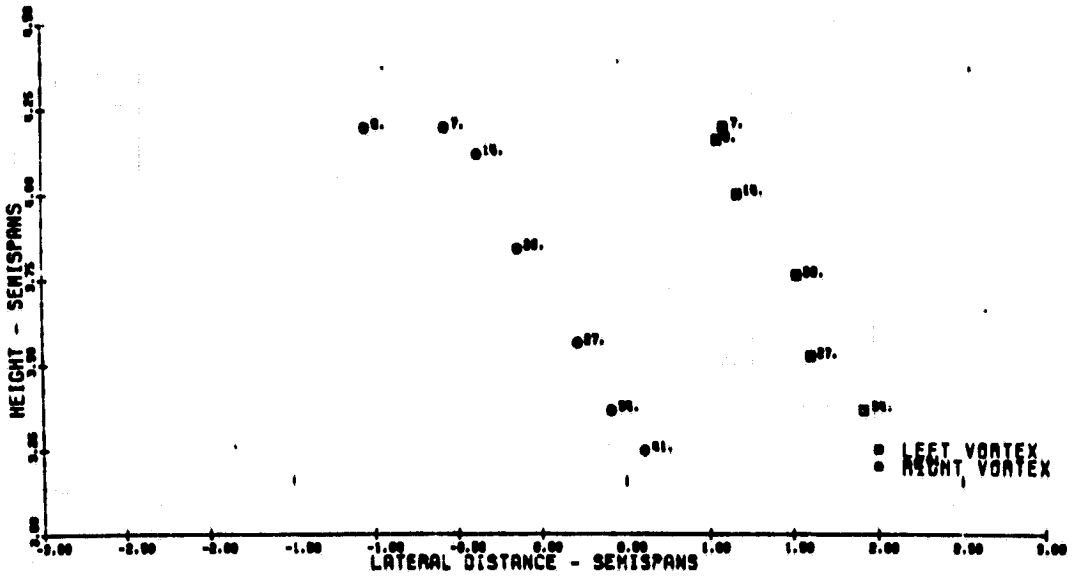

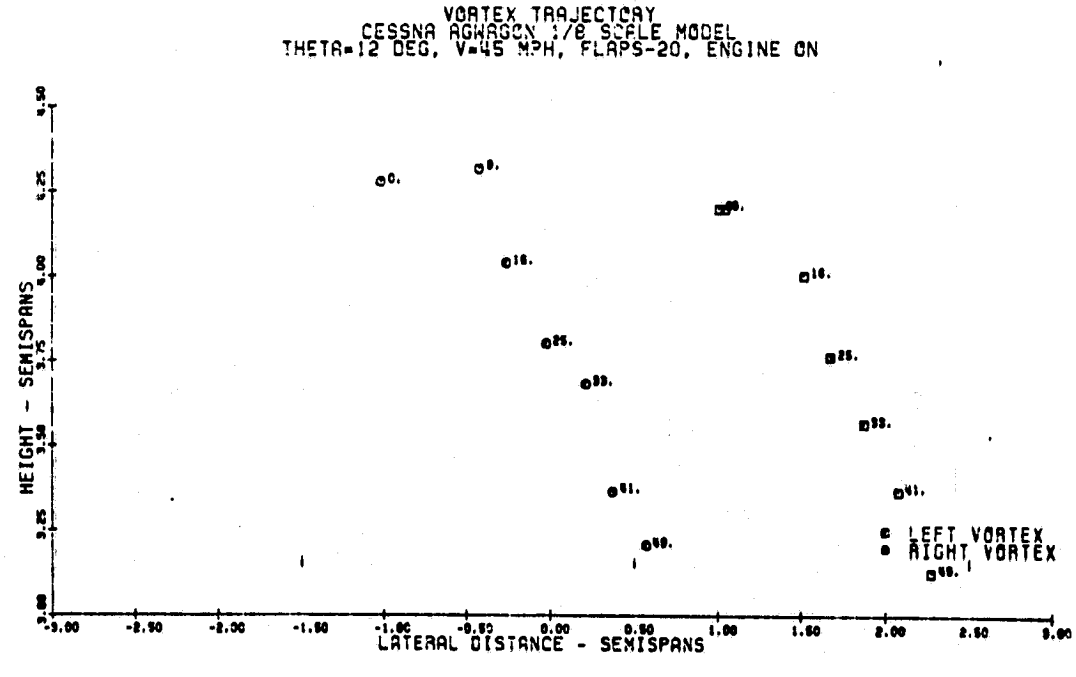

Figure 65. Tip Vortex Trajectory--1/8 Scale

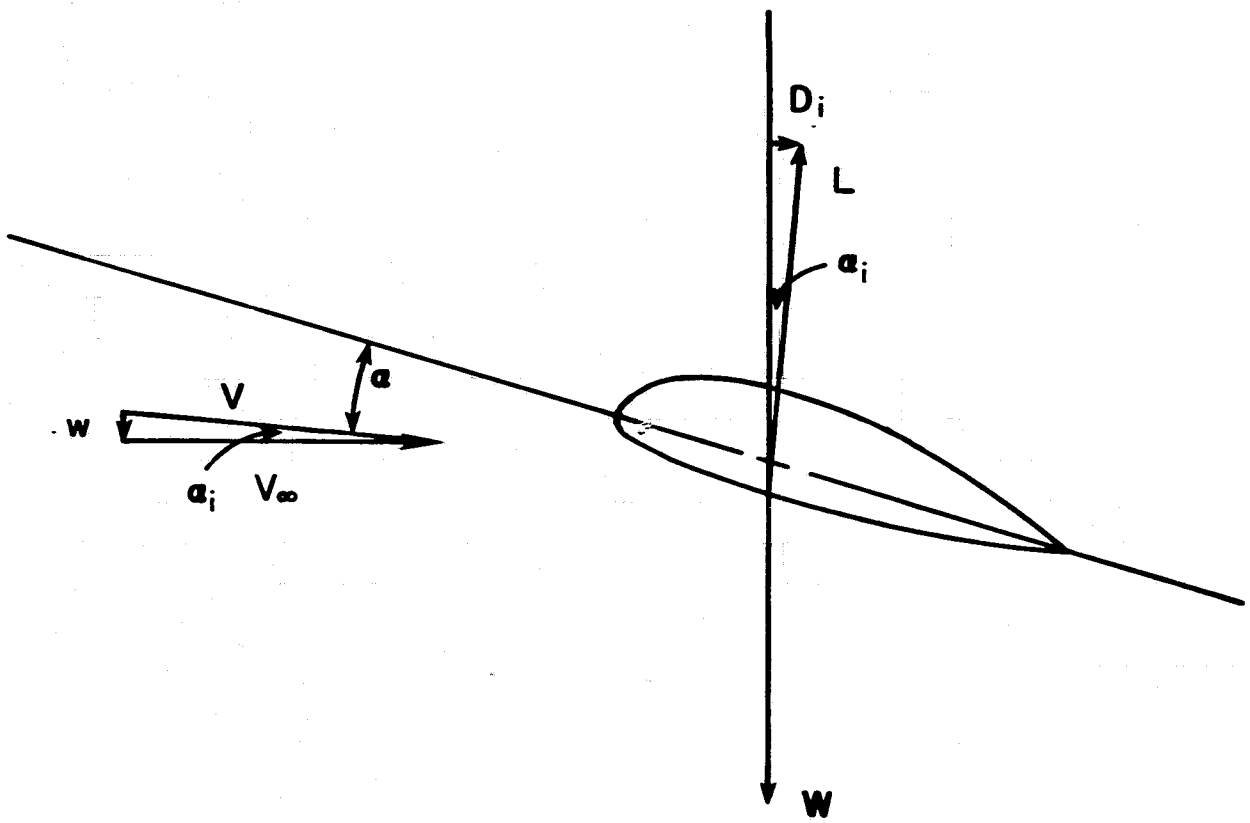

Figure 66. Illustration of Wing Force Vector

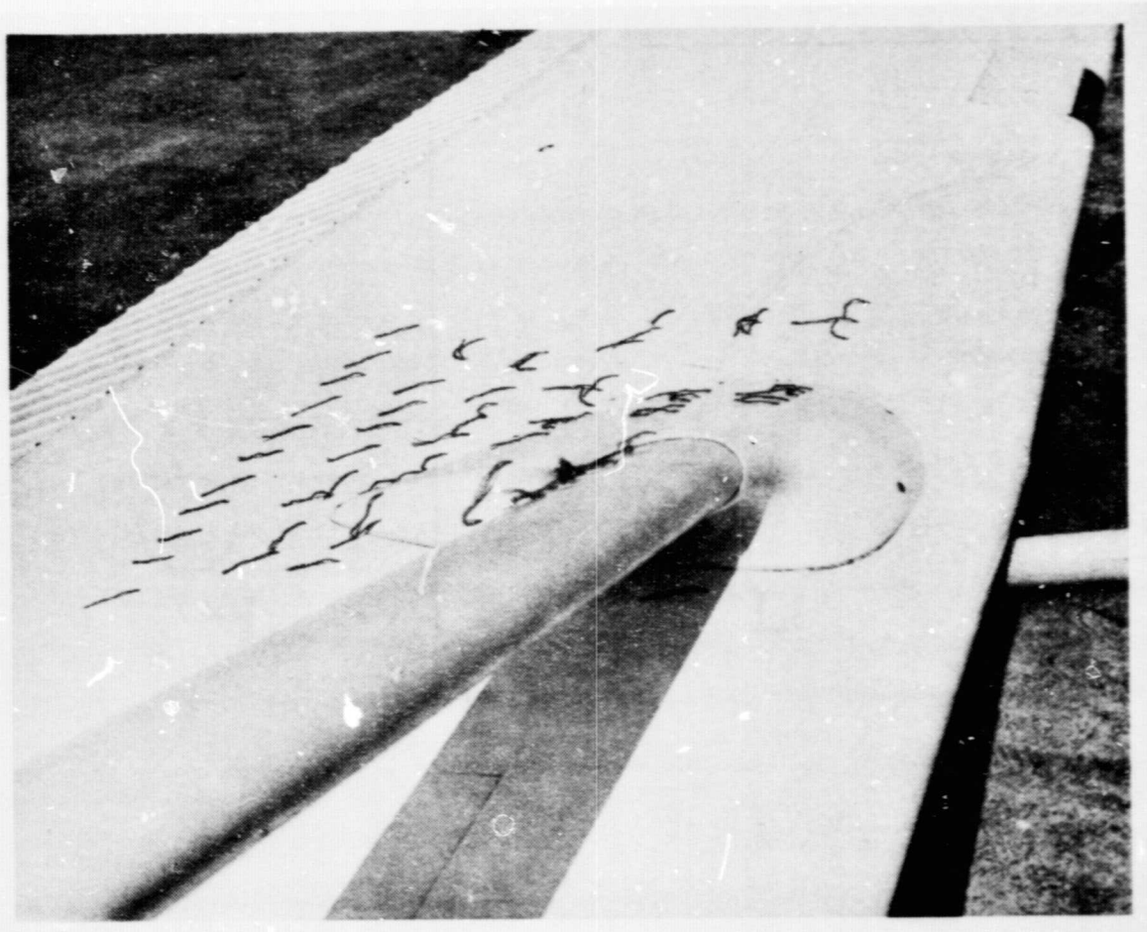

Figure 67. Tufted Wing-Strut Fairing

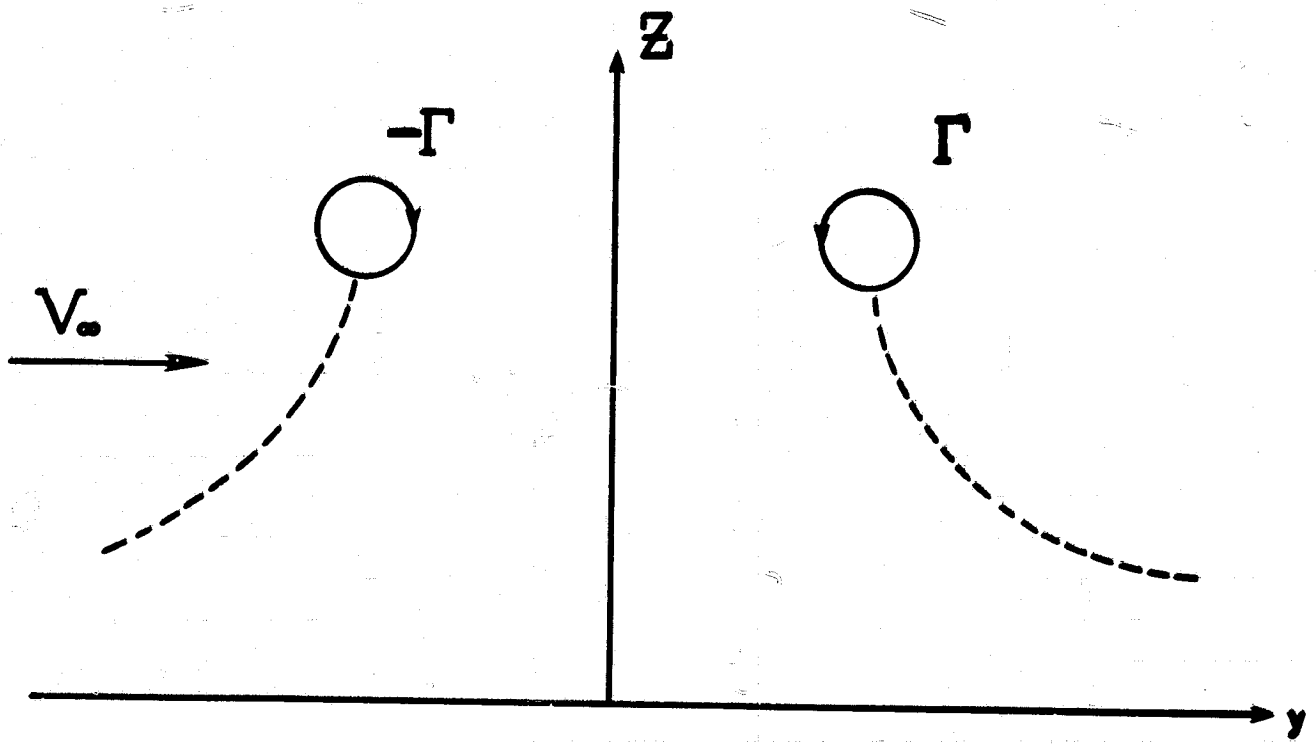

Figure 68. Schematic of Analytical Vortex Model

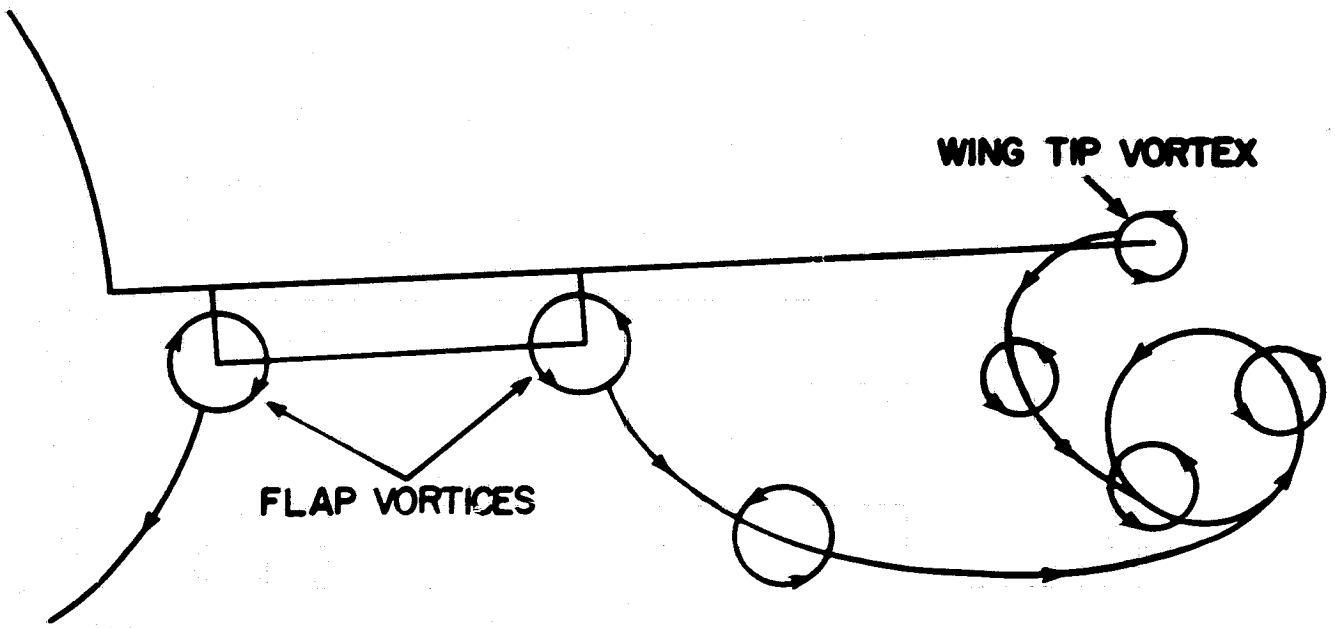

Figure 69. Vortex System Associated with Flapped Wing

t = 0 sec.

t = 2 sec.

Figure 70. Photo Sequence of Flap Vortex System

t = 5 sec.

t = 7 sec.

Figure 70. Photo Sequence of Flap Vortex System

t = 9 sec.

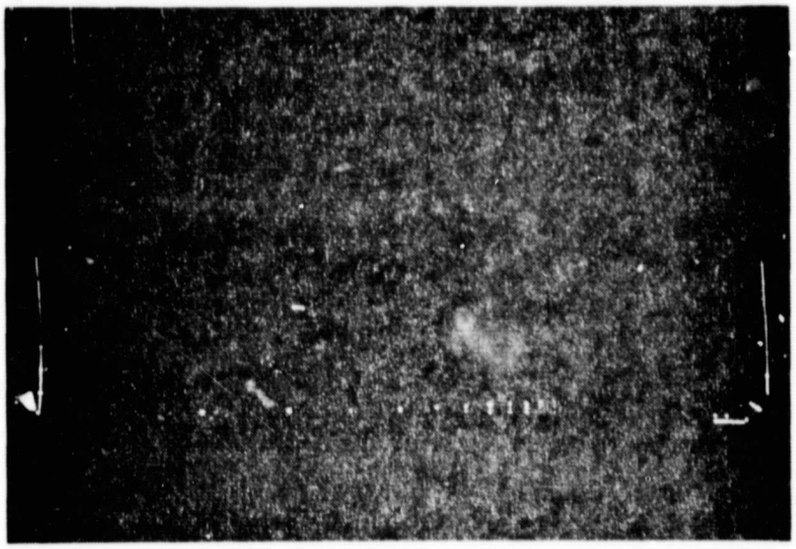

t = 17 sec.

Figure 70. Photo Sequence of Flap Vortex System